Moderate High Temperature is Beneficial or Detrimental Depending on Carbon Availability in the Green Alga *Chlamydomonas reinhardtii*

Ningning Zhang[1,#], Benedikt Venn[2,#], Catherine E. Bailey[1], Ming Xia[1], Erin M. Mattoon[1, 3], Timo Mühlhaus[2], Ru Zhang[1,*]

[1]Donald Danforth Plant Science Center, St. Louis, Missouri 63132, USA;
[2] RPTU Kaiserslautern, Kaiserslautern, 67663, Germany;
[3]Plant and Microbial Biosciences Program, Division of Biology and Biomedical Sciences, Washington University in Saint Louis, St. Louis, MO 63130, USA.

Ningning Zhang: lucy.nnzhang@gmail.com, co-first-author[#]
Benedikt Venn: venn@rptu.de, co-first-author[#]
Ming Xia: celine.xia@wustl.edu, present address[3]
Catherine E. Bailey: cbailey@danforthcenter.org
Erin M. Mattoon: EMattoon@danforthcenter.org
Timo Mühlhaus: timo.muehlhaus@rptu.de
Ru Zhang: rzhang@danforthcenter.org, corresponding author*

Running title: Algal heat responses interact with carbon availability.

Highlight

We revealed the overlooked, dynamic effects of moderate high temperature in algae depending on carbon availabilities and demonstrated the importance of carbon metabolism in thermotolerance of photosynthetic cells.

Abstract

High temperatures impair plant/algal growth and reduce food/biofuel production, but the underlying mechanisms remain elusive. The unicellular green alga *Chlamydomonas reinhardtii* is a superior model to study heat responses in photosynthetic cells due to its fast growth rate, many similarities in cellular processes to land plants, simple and

sequenced genome, and ample genetic/genomics resources. Chlamydomonas grows in light by photosynthesis and/or with supplied carbon source, acetate. The majority published research about Chlamydomonas heat responses used acetate-containing medium. How organic carbon sources affect heat responses is important for algal biofuel/bioproduct industry but understudied. We cultivated Chlamydomonas wild-type cultures under highly controlled conditions in photobioreactors at control of 25°C, moderate high temperature of 35°C, or acute high temperature of 40°C with and without constant acetate supply for 1- or 4-days. Our results showed that 35°C increased algal growth with constant acetate supply but reduced algal biomass and growth without sufficient acetate. The overlooked and dynamic effects of 35°C can be explained by induced carbon metabolisms, including acetate uptake/assimilation, glyoxylate cycle, gluconeogenesis pathways, and glycolysis. Acute high temperature at 40°C for more than 2 days was lethal to algal cultures with and without constant acetate supply. Our research provides insights to understand algal heat responses and help improve thermotolerance in photosynthetic cells.

Key words: moderate high temperature, acute high temperature, heat responses, *Chlamydomonas reinhardtii*, acetate, glyoxylate cycle, gluconeogenesis, glycolysis, photobioreactors

Abbreviations:

Photobioreactors (PBRs), Tris-acetate-phosphate (TAP) medium, Tris-phosphate (TP) medium

Introduction

Many biological processes in photosynthetic cells are sensitive to high temperatures (Mittler *et al.*, 2012; Schroda *et al.*, 2015; Guihur *et al.*, 2022). Global warming increases the intensity, duration, and frequency of high temperatures in the field, reducing plant growth and food/biofuel production (Janni *et al.*, 2020). A recent model revealed high temperature as the primary climatic driver for yield loss in crops from 1981-2017 in US (Ortiz-Bobea *et al.*, 2019). Considering the increasing global temperature and human

population, it is imperative to understand how photosynthetic cells respond to high temperatures and improve plant thermotolerance.

High temperatures in the field have different intensities and durations. For many land plants or algae grown in temperate regions, moderate high temperatures refer to heat slightly above the optimal temperature for growth (at or around 35°C), while acute high temperatures refer to heat at or above 40°C, which significantly reduces or completely halts growth (Zhang *et al.*, 2022*a*). Moderate high temperatures are often long-lasting and frequent in nature with mild effects on photosynthetic cells, while acute high temperatures are often short-term but severely damaging. Most previous heat-stress experiments in plants and algae used acute high temperatures at or above 40°C (Hemme *et al.*, 2014; Rütgers, 2017; Balfagón *et al.*, 2019; Kim *et al.*, 2020; Ji *et al.*, 2021), likely due to the rapid onset and easily quantifiable phenotypes as compared to moderate high temperatures. Although the impact of moderate high temperatures in photosynthetic cells can be difficult to investigate due to comparatively mild phenotypes, moderate high temperatures are physiologically relevant stresses in field conditions and their frequent and long-lasting features could reduce agricultural yield significantly (Delorge *et al.*, 2014; Anderson *et al.*, 2021). Arabidopsis seedlings treated with 5-day heat at 35°C had reduced growth and viability (Song *et al.*, 2021). Additionally, global warming can further increase the frequency and duration of moderate high temperatures in nature. However, the effects of moderate high temperatures in photosynthetic cells are often overlooked and underexplored.

The unicellular green alga *Chlamydomonas reinhardtii* (Chlamydomonas throughout) is a superior model to study heat responses in photosynthetic cells (Schroda *et al.*, 2015). Chlamydomonas can grow in light under photoautotrophic conditions using photosynthesis (Minagawa and Tokutsu, 2015). It can also grow with supplied organic carbon source (acetate) in light (mixotrophic) or dark (heterotrophic) conditions (Sasso *et al.*, 2018), providing a platform to study heat responses under different light/carbon conditions. Additionally, it has a haploid, sequenced, annotated, small genome (111 Mb, 17,741 protein-encoding genes) with simpler gene families and fewer gene duplications

than land plants (Merchant *et al.*, 2007; Karpowicz *et al.*, 2011). Furthermore, several well-established gene editing, cloning, high-throughput, and functional genomic tools are available in Chlamydomonas (Shimogawara *et al.*, 1998; Li *et al.*, 2016, 2019; Greiner *et al.*, 2017; Crozet *et al.*, 2018; Wang *et al.*, 2019; Dhokane *et al.*, 2020; Emrich-Mills *et al.*, 2021).

Algae have great potential for production of biofuels and bioproducts (Scranton *et al.*, 2015; Mathimani and Pugazhendhi, 2019). However, how algal cells respond to high temperatures is under-investigated as compared to land plants (Schroda *et al.*, 2015). Outdoor algal ponds frequently experience moderate high temperatures around 35°C during the summer time (Mata *et al.*, 2010), but the effects of moderate high temperatures on algal growth have been overlooked. Previously published algal heat treatments were often conducted in flasks in pre-warmed water baths at or above 42°C with sharp temperature switches and without control of nutrients (Hemme *et al.*, 2014; Rütgers *et al.*, 2017). While previous research was highly valuable to understand algal heat responses, high temperatures in the field or outdoor ponds often increase gradually. Rapid increases to high temperatures largely reduce algal viability (Zhang *et al.*, 2022*a*); similar effects have also been reported in land plants (Mittler *et al.*, 2012). Acute high temperatures at or above 40°C inhibit algal cell division (Mühlhaus *et al.*, 2011*b*; Hemme *et al.*, 2014; Zachleder *et al.*, 2019; Ivanov *et al.*, 2021), while moderate high temperature at 35°C only transiently inhibits cell division during the first 4-8 hour (h) heat (Zhang *et al.*, 2022*a*). Thus, conducting long-term experiments at moderate high temperatures in flasks can result in overgrown cultures, nutrient depletion, and light limitation, complicating data interpretation.

Consequently, it is advantageous to investigate algal heat responses under highly-controlled conditions in photobioreactors (PBRs) (Zhang *et al.*, 2022*a*; Mattoon *et al.*, 2022), which have several evident strengths: (1) precise temperature regulation with a sterile temperature probe inside each algal culture; (2) controlled heating to mimic the heating speed in nature; (3) the availability of turbidostatic control based on defined parameters (e.g., chlorophyll contents) to enable frequent culture dilutions with constant

125 medium supply; (4) precisely controlled cultivation condition, including temperature, light,
126 nutrient, and air agitation, allowing for reproducible experiments; (5) automatic recording
127 of culture status every minute, e.g. growth conditions and optical densities, enabling
128 quantitative growth rate measurements; (6) being able to simulate nutrient depletion by
129 turning off the turbidostatic control to investigate how nutrient availability affects algal heat
130 responses. Utilization of PBRs for algal cultivation and heat treatments can largely reduce
131 compounding effects during high temperature treatments and improve our understanding
132 of algal heat responses.
133
134 Recently, we conducted systems-wide analyses in wild-type (WT) Chlamydomonas
135 cultures during and after 24-h heat of 35°C and 40°C in PBRs with constant nutrient
136 supply and light in acetate-containing medium (mixotrophic condition) under the
137 turbidostatic control (Zhang *et al.*, 2022*a*). We chose moderate high temperature of 35°C
138 and acute high temperature of 40°C based on the algal growth rates under different
139 temperatures; and the 24-h heat duration allowed us to balance time-course sample
140 collection over a sufficient duration with maintaining culture viability (heat at 40°C for
141 longer time killed algal cells); our experimental conditions enabled us to investigate algal
142 heat responses during and after physiological-relevant high temperatures (Zhang *et al.*,
143 2022*a*). Our results showed that 40°C inhibited algal growth while 35°C increased algal
144 growth with constant acetate supply. The growth inhibition at 40°C could be explained by
145 reduced photosynthesis, impaired respiration, and arrested cell cycle, while these cell
146 parameters had minor changes in algal cultures treated by 35°C. Our proteomics data
147 indicated that several proteins involved in acetate uptake/assimilation, glyoxylate cycle,
148 and gluconeogenesis were up-regulated during 35°C (Zhang *et al.*, 2022*a*).
149 Chlamydomonas uptakes acetate and feeds it into the glyoxylate cycle and
150 gluconeogenesis for starch biosynthesis (Johnson and Alric, 2012, 2013). The main
151 function of glyoxylate cycle is to allow growth when glucose is unavailable and two-carbon
152 compounds, e.g., acetate, are the organic carbon source; glyoxylate cycle is a shunt of
153 the tricarboxylic acid (TCA) cycle in mitochondria but without CO_2 releases to allow for
154 the anabolism of simple carbon compounds in gluconeogenesis, a process to make
155 sugars, e.g., glucose (Johnson and Alric, 2012; Chew *et al.*, 2019; Walker *et al.*, 2021).

156

157 We hypothesized that the increased growth in Chlamydomonas at 35°C with constant
158 acetate supply was attributable to up-regulated acetate metabolisms. The majority of
159 published high temperature research in Chlamydomonas has been conducted in acetate-
160 containing medium (Voß *et al.*, 2010; Mühlhaus *et al.*, 2011*a*; Hemme *et al.*, 2014;
161 Rütgers *et al.*, 2017; Zhang *et al.*, 2022*a*), but the interface between acetate supply and
162 algal heat responses is understudied. To validate our hypothesis and address these
163 unknown questions, we cultivated the same Chlamydomonas WT strain in PBRs as
164 before but heated the cultures at 35°C or 40°C with and without constant acetate supply
165 for 1 or 4 days. Our previous work was conducted at 35°C and 40°C for 24 h with constant
166 acetate supply (Zhang *et al.*, 2022*a*). In this paper, to investigate the effects of carbon
167 availability on algal thermotolerance, we included 3 new different heat treatments at 35°C
168 and 40°C: acetate-depleting condition for 24 h, constant-acetate condition for 4 days, no-
169 acetate condition for 4 days (the last two conditions with turbidostatic control and constant
170 nutrient supply). Our new results confirmed our hypothesis about the role of acetate
171 metabolism in algal thermotolerance and revealed the overlooked effects of moderate
172 high temperature of 35°C on algal growth. Heat of 35°C can be beneficial or detrimental
173 based on acetate availability. Acute high temperature of 40°C is lethal to algal cultures,
174 with and without constant acetate supply. Our research provided insights to understand
175 algal heat responses and help improve thermotolerance in photosynthetic cells.

176

177 **Materials and methods**

178

179 **Algal cultivation**

180 *Chlamydomonas reinhardtii* wild-type strain CC-1690 (also called *21gr*, mating type plus)
181 (Pröschold *et al.*, 2005; Zhang *et al.*, 2022*b*; Sager, 1955-7) was purchased from the
182 Chlamydomonas resource center and used in all experiments. Algal cultures were grown
183 in Tris-acetate-phosphate (TAP, with acetate) or Tris-phosphate (TP, without acetate)
184 medium with revised trace elements (Kropat *et al.*, 2011) in 400 mL photobioreactors
185 (PBRs) (Photon System Instruments, FMT 150/400-RB) as described before (Zhang *et*
186 *al.*, 2022*a*). Each medium type used individual PBRs in independent experiments.

187 Cultures were illuminated with constant 100 μmol photons m^{-2} s^{-1} light (red: blue, 1:1 ratio),
188 and agitated by bubbling with filtered air at a flow rate of 1 L min^{-1}. Algal cultures with
189 targeted cell density around 1-2 x10^6 cells mL^{-1} (~4-6 μg mL^{-1} chlorophyll content) were
190 maintained at 25°C for 4 days with constant nutrient supply through a turbidostatic mode
191 before different temperature treatments. The turbidostatic mode was controlled by OD_{680}
192 (optical density at 680 nm), which is proportional to chlorophyll contents (μg mL^{-1}) and
193 was monitored once per min automatically. When OD_{680} increased to a maximum value
194 slightly above the target value (for target cell density) due to algal growth, OD_{680} signaled
195 the control computer to turn on a turbidostatic pump to add fresh medium to dilute the
196 culture until a minimum OD_{680} slightly below the target value was reached, then the
197 turbidostatic pump was turned off automatically. Because of the small OD range we used,
198 the PBR cultures had exponential growth between dilution events through the
199 turbidostatic mode with constant nutrient supply (Fig. 1A). The OD_{680} data during
200 exponential growth phases in between dilution events was log_2 transformed, and the
201 relative growth rate was calculated using the slope of $log_2(OD_{680})$. The relative growth
202 rate is an inverse of the doubling time of algal cultures. For the treatments without
203 constant nutrient supply (acetate-depleting condition), the turbidostatic pumps were
204 turned off after PBR cultures reached steady growth and at the start of different
205 temperature treatments.
206
207 **High temperature treatments in PBRs**
208 After algal cultures in PBRs reached steady growth with turbidostatic control at 25°C for
209 4 days, PBR temperatures were increased to moderate or acute high temperatures (35°C
210 or 40°C in different PBRs) for the indicated duration with indicated nutrient conditions.
211 PBR temperatures were changed from 25°C to 35°C or 40°C gradually over the course
212 of 30 min with controlled heating speeds. PBR cultures grown under constant 25°C with
213 the same nutrient status and treatment duration served as controls. Algal cultures were
214 harvested from PBRs at different time points during different treatments for various
215 measurements.
216
217 **Algal biomass quantification**

218 Algal cultures (90 mL) were harvested from PBRs, centrifuged to remove supernatants,
219 flash frozen in liquid nitrogen, then stored in a -80°C freezer until analysis. Algal cell
220 pellets were freeze dried for 24 h over liquid nitrogen. The remaining algal dry biomass
221 were weighted and quantified.
222
223 **Acetate quantification assay**
224 Algal cultures were harvested from PBRs (2 mL) and centrifuged to collect 500 μL top
225 clear supernatants to a new tube. The supernatant was stored in a -80°C freezer until
226 analysis. The acetate content in the supernatant was quantified using the Acetate
227 Colorimetric Assay Kit (Sigma, Cat No. MAK086) according to manufacture instructions.
228
229 **Cell imaging using light microscopy**
230 Chlamydomonas cultures harvested at select time points with different temperature
231 treatments were fixed with 0.2% glutaraldehyde (VWR, Cat No. 76177-346). Algal cells
232 were imaged with a Leica DMI6000 B microscope and a 63x (NA1.4) oil-immersion
233 objective.
234
235 **Chlorophyll quantification**
236 Chlorophyll contents in algal cells were quantified as before (Zhang *et al.*, 2022*a*). PBR
237 cultures of 1 mL were harvested in 1.5-mL tubes with 2.5 μL 2% Tween20 (Sigma, P9416-
238 100ML, to help cell pelleting), and centrifuged at 18,407 g at 4°C. After removing
239 supernatant, cell pellets were stored in a -80°C freezer until quantification. Later, cell
240 pellets were thawed, resuspended in 1 mL of HPLC grade methanol (100%, Sigma,
241 34860-4L-R), vortexed for 1 min, incubated in the dark at 4°C for 5 min, and centrifuged
242 at 15,000 g at 4°C for 5 min. Supernatant was pipetted out to a two-sided disposable
243 plastic cuvettes (VWR, 97000-586) for chlorophyll (Chl) quantification at 652 nm and 665
244 nm in a spectrophotometer (IMPLEN Nonophotometer P300) using the following
245 equations: Chl a + Chl b = $22.12*A_{652} + 2.71*A_{665}$ (in μg mL^{-1} algal cultures) (Zhang *et al.*,
246 2022*a*). Chlorophyll concentrations were also normalized to cell densities (Chl pg cell^{-1})

247 or algal cell volume (Chl pg μm^{-3}). Cell density and mean cell volume were measured
248 using a Coulter Counter (Multisizer 3, Beckman Counter, Brea, CA).
249
250 **RNA extraction**

251 PBR cultures of 2 mL were pelleted with Tween-20 (0.005%, v/v) by centrifugation at
252 11,363 x g and 4°C for 2 min, followed by supernatant removal. The cell pellet was flash
253 frozen in liquid nitrogen and then stored in a -80°C freezer until processing. RNA
254 extraction and RT-qPCR analysis were performed as before with minor modifications
255 (Zhang *et al.*, 2022*a*). Total RNA was extracted with TRIzol reagent (Thermo Fisher
256 Scientific, Cat No. 15596026), digested on-column with RNase-free DNase (Qiagen, Cat
257 No. 79256), purified by RNeasy mini-column (Qiagen, Cat No. 74106), and quantified with
258 Qubit™ RNA BR Assay Kit, (Life technology, Cat No. Q10210).
259
260 **RT-qPCR analysis**

261 Total 0.4 µg RNA was reverse transcribed with oligo dT primers using SuperScript® III
262 First-Strand Synthesis System (Life technology, Cat No. 18080-051) following
263 manufacturer instructions. Quantitative real-time PCR (RT-qPCR) analysis was
264 performed using a CFX384 Real-Time System (C 1000 Touch Thermal Cycler, Bio-Rad,
265 Hercules, California) using SensiFAST SYBR No-ROS kit (Bioline, BIO-98020) following
266 this set-up: (1) 95°C (2 min); (2) 40 cycles of 95°C (5 s), 60°C (10 s), and 72°C (15 s); (3)
267 final melt curve at 60°C (5 s), followed by continuous temperature ramping from 60°C to
268 99°C at a rate of 0.5°C s^{-1}. Melting curves and qPCR products were tested to ensure
269 there were no primer dimers or unspecific PCR products. All RT-qPCR products were
270 sequenced for confirmation. Primers and gene IDs for RT-qPCR were included in
271 Supplementary Table 1. *CBLP* (*β-subunit-like polypeptide*, Cre06.g278222), (Schloss,
272 1990; Xie *et al.*, 2013) and *EIF1A* (*Eukaryotic translation initiation factor 1A,*
273 Cre02.g103550) (Strenkert *et al.*, 2019) had stable expression among all time points, and
274 were used as reference genes for RT-qPCR normalization. The relative gene expressions
275 were calculated relative to the pre-heat time point by using the $2^{-\Delta\Delta CT}$ method (Livak and
276 Schmittgen, 2001; Hellemans *et al.*, 2007; Remans *et al.*, 2014). Three biological

replicates were included for each time point and treatment. RT-qPCR was used to verify some selected transcripts and compared with the results of RNA-seq for samples harvested under the acetate-depleting conditions (Supplemental Fig. 2). RNA-seq for samples harvested under the constant-acetate conditions were verified by RT-qPCR previously (Zhang *et al.*, 2022*a*).

RNA-seq analysis

Raw sequencing data for the constant-acetate experiments at 35°C and 40°C were obtained from (Zhang *et al.*, 2022*a*). Raw sequencing data for the constant-acetate experiment at 25°C and acetate-depleting experiments at 25°C, 35°C, and 40°C were collected in this study. All raw sequencing data were processed using the same pipeline as described below.

RNA libraries were prepared and sequenced by the Joint Genome Institute (JGI, Community Science Program) using the NovaSeq platform generating 151-nt paired-end reads. Plate-based RNA sample preparation was performed on the PerkinElmer Sciclone NGS robotic liquid handling system using Illumina's TruSeq Stranded mRNA HT sample prep kit utilizing poly-A selection of mRNA following the protocol outlined by Illumina in their user guide: https://support.illumina.com/sequencing/sequencing_kits/truseq-stranded-mrna.html, and with the following conditions: total RNA starting material was 1000 ng per sample and 8 cycles of PCR was used for library amplification. The prepared libraries were quantified using KAPA Biosystems' next-generation sequencing library qPCR kit and ran on a Roche LightCycler 480 real-time PCR instrument. Sequencing of the flowcell was performed on the Illumina NovaSeq sequencer using NovaSeq XP V1.5 reagent kits, S4 flowcell, following a 2x151 indexed run recipe.

Samples were quality control filtered using the JGI BBDuk and BBMap pipelines (BBDuk 2022). Samples were quality assessed using FastQC (Andrews) and mapped to the *Chlamydomonas reinhardtii* v5.6 genome (Merchant *et al.*, 2007) using HISAT2 version 2.2.0 (Kim, Langmead, and Salzberg 2015). Reads per feature were counted via featureCounts (Liao, Smyth, and Shi 2014). The count matrix was combined with existing

308 data (Zhang *et al.*, 2022*a*), resulting in a 16,403x101 count matrix (Supplemental Dataset
309 4, 5). The normalization of the count matrix was conducted using the median of ratios
310 method (Love, Huber, and Anders 2014). Prior to imputation of two missing time points in
311 the constant-acetate-25°C condition (see details below), transcripts were filtered to have
312 nonzero counts in at least 90% of the samples.
313
314 Under constant 25°C, acetate, and light with turbidostatic control (constant-acetate-25°C),
315 the algal growth rates and cell physiologies stay constant (Fig. 5). We had RNA-seq data
316 for 8 time points (pre-heat, 0, 0.5, 1, 2, 24, 26, and 48 h) under constant-acetate-25°C
317 and these samples were highly correlated with each other (with Pearson correlation ≥
318 0.993) (Supplemental Fig. 1). RNA samples for the time points of 4 and 8 h under the
319 constant-acetate-25°C condition were unavailable; thus RNA-seq data for the 4 and 8 h
320 under the constant-acetate-25°C condition were imputed from other extra time points (0,
321 0.5, 1, 26, 48 h) of the same condition. For the time points of 4 and 8 h under the constant-
322 acetate-25°C condition, each transcript triplicates were sampled randomly using the 5
323 extra time points under the same condition mentioned above. It was ensured that both
324 missing time points were not imputed with the same count data. The final count matrix
325 consists of 14,893 transcripts in 90 samples (5 time points measured at 6 conditions as
326 triplicates). The natural logarithm was determined for all normalized counts before
327 averaging triplicates. Pearson correlation coefficients were calculated for all sample pairs.
328
329 The count data were tested for differential expression using DESeq2 v1.38.3 (Love,
330 Huber, and Anders 2014). DESeq2 applies a Benjamini Hochberg correction for multiple
331 testing. The design matrix was constructed to test for global kinetic differences between
332 the three different temperatures and both growth media over time. The following tests
333 were performed (Supplemental Dataset 1, 3, 5): (A) acetate-depleting 25°C vs acetate-
334 depleting 35°C; (B) acetate-depleting 25°C vs acetate-depleting 40°C; (C) constant-
335 acetate 25°C vs constant-acetate 35°C; (D) constant-acetate 25°C vs constant-acetate
336 40°C; (E) temperature effect: (constant-acetate 35°C and acetate-depleting 35°C) vs
337 (constant-acetate 40°C and acetate-depleting 40°C); (F) medium effect: (constant-

338 acetate 35°C and constant-acetate 40°C) vs (acetate-depleting 35°C and acetate-
339 depleting 40°C); (G) acetate-depleting 25°C vs constant-acetate 25°C.
340
341 Functional descriptions were determined for each transcript (Merchant *et al.*, 2007;
342 Usadel *et al.*, 2009; Venn and Mühlhaus, 2022). Transcripts were grouped according to
343 their functional description. Time courses of normalized transcript counts were visualized
344 as $\log_2$(fold change). An ANOVA was performed for each transcript at each treatment to
345 elucidate whether a transcript underwent a relevant change during its time course (Venn
346 et al., 2022a). Heatmaps (Supplemental Dataset 1) and functional sets figures
347 (Supplemental Dataset 2) were created using Plotly.NETv4.0.0 (Schneider *et al.*, 2022).
348
349 Ontology enrichment was performed using extended MapMan annotations (e.g.
350 "PS.lightreaction.LHC" became "PS.Lightreaction.LHC", "PS.Lightreaction" and "PS")
351 (Supplemental Dataset 3). The measured and filtered transcripts served as background.
352 If a transcript showed significant differential expression in the respective comparison
353 (FDR < 0.05), it was considered as significant for its annotations. Enrichment p values
354 were determined using hypergeometric tests. Multiple testing correction was performed
355 using the Benjamini-Hochberg method (Benjamini and Hochberg, 1995; Venn *et al.*,
356 2022).
357
358 **Results**
359 To investigate how the availability of organic carbon source affected algal heat responses,
360 we first cultivated WT Chlamydomonas cells (CC-1690, *21gr*) in PBRs in Tris-acetate-
361 phosphate (TAP, acetate as carbon source) medium at 25°C with constant nutrient supply
362 through turbidostatic control (providing frequent fresh medium and culture dilution) (Fig.
363 1A). After algal cultures reached steady growth rates in PBRs, the turbidostatic control
364 was turned off and cultures were switched to 35°C, or 40°C, or stayed at 25°C for 24 h
365 without constant acetate supply, defined as the acetate-depleting condition. This
366 experiment allowed us to quantify acetate consumption under different temperatures,
367 which could not be performed in cultures with turbidostatic control or frequent medium
368 dilution. It also enabled us to investigate algal heat responses under the acetate-depleting

369 condition, similar to shaker cultures, which were used by most previous algal heat
370 experiments in the published literatures (Hemme *et al.*, 2014; Rütgers *et al.*, 2017). Under
371 the acetate-depleting condition, algal cultures were harvested at different time points to
372 analyze cell physiologies, biomass, and transcriptome (Fig. 1B). Algal dry biomass
373 quantification showed that cultures treated with 35°C had increased biomass at 8-h heat
374 but decreased biomass at 24-h heat as compared to 25°C (Fig. 1C). Acetate quantification
375 in the supernatant of algal cultures showed that 35°C-treated cultures had increased
376 acetate consumption and depleted acetate faster than 25°C or 40°C (Fig. 1D).
377
378 We hypothesized the transiently increased and then decreased algal biomass in 35°C-
379 treated cultures was due to increased acetate uptake/usage followed by acetate
380 starvation in the end under the acetate-depleting condition (Fig. 1). Chlamydomonas
381 uptakes acetate and feeds it into the glyoxylate and gluconeogenesis cycles to produce
382 starch, which can be used in glycolysis to generate ATP (Johnson and Alric, 2012, 2013)
383 (Fig. 2A). To verify this hypothesis, we performed RNA-seq analysis and investigated key
384 transcripts involved in the acetate uptake/assimilation, glyoxylate, gluconeogenesis, and
385 glycolysis cycles under the acetate-depleting condition by comparing with the constant-
386 acetate condition (Fig. 2B-P). Under the acetate-depleting condition, almost all these
387 transcripts related to acetate uptake/metabolism were up-regulated under 35°C as
388 compared to 25°C. Similar 35°C effects on these transcripts were held under the constant-
389 acetate condition, although the up-regulation of these transcripts were stronger and lasted
390 longer at 35°C under the constant-acetate condition than the acetate-depleting condition.
391 In contrast, these transcripts related to acetate uptake/metabolism were down-regulated
392 under 40°C as compared to 25°C under both the acetate-depleting and constant-acetate
393 conditions. Our RT-qPCR results of selected transcripts showed similar trends as our
394 RNA-seq data (Supplemental Fig. 2). These results showed that the 35°C promoted
395 acetate metabolism, from acetate uptake/assimilation to glyoxylate, gluconeogenesis,
396 and glycolysis cycles; however, these acetate metabolism pathways were reduced under
397 40°C.
398

399 Besides the acetate metabolism pathways mentioned above, we also checked transcripts
400 related to other processes that are often affected by high temperatures (Supplemental
401 Fig. 3, 4). Chlamydomonas has 2 heat shock transcription factors, HSF1 and HSF2; HSF1
402 is the master heat regulator but the function of HSF2 is unclear (Schulz-Raffelt *et al.*,
403 2007). The transcripts of both *HSF*s were induced by heat, with higher induction at 40°C
404 than 35°C under the same acetate condition or higher induction under the acetate-
405 depleting than constant-acetate condition at the same high temperature (Supplemental
406 Fig. 3A, B). Heat shock proteins (HSPs) are the hallmarks of heat responses and HSPs
407 function as chaperones to help refold denatured proteins, fold nascent polypeptides, and
408 prevent denatured protein aggregates (Altschuler and Mascarenhas, 1982; Schroda *et*
409 *al.*, 2015; Haq *et al.*, 2019). Based on molecular mass, HSPs are grouped to large HSPs
410 (HSP100/90/70/60, >50 kDa) and small HSPs (10-43 kDa) (Jee, 2016; Bourgine and
411 Guihur, 2021). Under the acetate-depleting condition, many transcripts related to large
412 HSPs, *HSP60/70/90s*, were down-regulated at 24 h of 25°C and 35°C; such down-
413 regulation of *HSP60/70/90s* was absent at 24 h of 25°C and 35°C under the constant-
414 acetate condition or 24 h of 40°C under both acetate conditions (Supplemental Fig. 4A-
415 C). Additionally, transcripts of *HSP100* and most of the *small HSPs* did not have such
416 down-regulation at 24 h of 25°C and 35°C under the acetate-depleting condition
417 (Supplemental Fig. 4D, E). Almost all transcripts related to *HSPs* we examined, including
418 *HSP60/70/90/100s* and *small HSPs*, were up-regulated at 2 h of 40°C, with similar
419 induction fold change under either the acetate-depleting or constant-acetate condition
420 (Supplemental Fig. 4A-E). It suggested the early induction of these *HSPs* under 40°C
421 were temperature-dependent (present at 40°C while much less so under 35°C) but
422 acetate-availability-independent. Alternatively, the acetate-availability may not differ that
423 much at 2 h of the acetate-depleting and constant-acetate condition (Fig. 1D).
424
425 The global transcriptome changes related to light reaction and Calvin-Benson cycle of
426 photosynthesis suggested more disturbance of these transcripts under the acetate-
427 depleting than the constant-acetate conditions at the same temperatures, and more
428 disturbance of these transcripts at 40°C than 35°C under the same acetate conditions
429 (Supplemental Fig. 4F-M). Chlamydomonas employs a cellular structure, pyrenoid, to

430 concentrate CO_2 for improved carbon fixation efficiency, called carbon concentrating
431 mechanisms (CCM) (Meyer *et al.*, 2017; Hennacy and Jonikas, 2020). Under the acetate-
432 depleting conditions, several transcripts related to CCM were up-regulated at 24 h under
433 25°C and 35°C, but not under the same temperature of the constant-acetate condition,
434 suggesting the induction of CCM when acetate was depleted, and cell densities increased
435 at 24 h of 25°C and 35°C under the acetate-depleting condition (Supplemental Fig. 4N).
436 Such induction of the CCM transcripts was absent at 40°C under either acetate condition,
437 which may correlate with the altered pyrenoid structures at 40°C (Zhang *et al.*, 2022*a*).
438 Transcripts related to photoprotection had larger induction at 24 h under all three
439 temperatures of the acetate-depleting than the constant-acetate conditions at the same
440 temperature, indicating compromised photosynthesis and the need for photoprotection
441 when acetate was depleted (Supplemental Fig. 4O).
442
443 The compromised photosynthesis under high temperatures lead to increased
444 accumulation of reactive oxygen species (ROS) (Pospíšil, 2016; Janni *et al.*, 2020;
445 Niemeyer *et al.*, 2021). Some transcripts related to ROS scavenging were down-regulated
446 at 24 h of 25°C and 35°C under the acetate-depleting condition but much less so under
447 the constant-acetate condition at the same temperatures (Supplemental Fig. 4R-V). This
448 may be related to the increased cell density and reduced light/oxidative stress at 24 h of
449 25°C and 35°C under the acetate-depleting condition. Such down-regulation of transcripts
450 related to ROS scavenging was not present at 24 h of 40°C under the acetate-depleting
451 condition. This may suggest relatively increased ROS accumulation and ROS scavenging
452 activity at 40°C than 25°C and 35°C under the acetate-depleting conditions. Additionally,
453 transcripts related to ROS scavenging had very similar transcriptional changes at 40°C
454 under either the acetate-depleting or constant-acetate condition, suggesting 40°C had
455 more dominant effects on the ROS accumulation and ROS scavenging activities than
456 acetate.
457
458 Transcripts related to cell cycle and cell wall had similar transcriptional patterns under
459 each of the six conditions (Supplemental Fig. 4W, X). Under diurnal cycles, cell wall genes
460 were up-regulated following the up-regulation of cell cycle genes and cell walls form

461 around daughter cells during cell division (Zones *et al.*, 2015). These transcripts were
462 down-regulated at 24 h of 25°C under the acetate-depleting condition, suggesting the
463 transition to cell cycle arrest due to acetate-depletion. The reduction of these transcripts
464 was larger and more prolonged under 40°C than 35°C, consistent with complete and
465 transient inhibition of cell cycle under 40°C and 35°C, respectively (Hemme *et al.*, 2014;
466 Zhang *et al.*, 2022*a*). At 24 h of 40°C and 35°C, these transcripts were more reduced
467 under the acetate-depletion condition than the constant-acetate condition.
468
469 Almost all transcripts mentioned above had little changes at 25°C during all time points
470 of the constant-acetate condition, validating the steady growth and constant cell status
471 under the turbidostatic control with constant nutrient/light but without heat treatments in
472 our algal cultures grown in PBRs (Supplemental Fig. 4).
473
474 We performed statistical analysis to investigate global transcript kinetic differences
475 between different conditions (Supplemental Dataset 1, 3). We then applied ontology
476 enrichments analysis for transcripts that were significantly expressed in a defined
477 comparison to identify differentially regulated biological processes (Supplemental Fig. 5,
478 Supplemental Dataset 3). The top enriched function group that differed at 25°C and 35°C
479 under both acetate-depleting and constant-acetate condition is the nucleus-encoded
480 ribosomal proteins that are involved in chloroplast protein synthesis (Supplemental Fig.
481 5A, C). More than half of the ribosomal related transcripts were down-regulated at 4 h
482 heat of 35°C as compared to 25°C under both acetate conditions (Supplemental Fig. 4Y,
483 Z), suggesting 35°C may compromise chloroplast function. The top enriched function
484 group that differs between 25°C and 40°C under the acetate-depleting condition is the
485 mitochondrial electron transport (Supplemental Fig. 5B). Many transcripts related to
486 mitochondrial electron transport were down-regulated at 2 h heat of 40°C as compared
487 to 25°C under the acetate-depleting condition (Supplemental Fig. 4AA, AB). When
488 comparing 35°C and 40°C regardless the acetate availability, the top enriched function
489 group is also the mitochondrial electron transport (Supplemental Fig. 5E). The results
490 suggested that mitochondrial electron transport was more sensitive to 40°C than 25°C
491 and 35°C. Under the constant-acetate condition, 40°C affected RNA processes the most

492 as compared to 25ºC (Supplemental Fig. 5D, 4AC, AD). When comparing the acetate-
493 depleting and constant-acetate conditions regardless the high temperatures, the top two
494 enriched groups are phosphate transport and mitogen-activated protein kinase (MAP
495 kinase) cascades signaling (Supplemental Fig. 5F). MAP kinase signaling pathways has
496 important roles in plant growth and stress responses and involve protein
497 phosphorylation/dephosphorylation (Bigeard and Hirt, 2018; Jagodzik *et al.*, 2018; Zhang
498 and Zhang, 2022). The biggest differences in transcripts related to the MAP kinase
499 signaling pathways between the acetate-depleting and constant-acetate conditions were
500 at the 24 h time point at 25ºC and 35ºC when the acetate was depleted (Supplemental
501 Fig. 4AF), suggesting potential roles of the MAP kinase signaling pathways in nutrient
502 sensing and growth regulation. When comparing the acetate-depleting and constant-
503 acetate conditions at 25ºC, the top enriched function groups are dominantly related to cell
504 motility (Supplemental Fig. 5G). More than half of the transcripts related to cell motility at
505 25ºC were down-regulated at 24 h under the acetate-depleting condition but not the
506 constant-acetate condition (Supplemental Fig. 4AG, AH). Microscopic images showed
507 that cells had flagella at 24 h of 25ºC under the acetate-depleting condition (Supplemental
508 Fig. 6). Thus, the down-regulation of transcripts related to cell motility may suggest the
509 transition from motile to non-motile phase when the acetate was depleted. Cell motility
510 needs energy and ciliary beating frequency corelates with the cytosolic ATP concentration
511 in Chlamydomonas (Takano *et al.*, 2021).
512
513 To further understand our transcriptome data and the effects of acetate, we compared
514 cell physiologies at different temperatures between the acetate-depleting and constant-
515 acetate conditions (Fig. 3). Under the acetate-depleting condition without medium dilution,
516 cell density increased over time at 25ºC and 35ºC but no changes at 40ºC because of
517 cell cycle arrest at 40ºC (Fig. 3A). Cell density was lower at 35ºC than 25ºC at 8 h and 24
518 h time points, suggesting reduced growth rates at 35ºC at the end of the acetate-depleting
519 condition. Algal cells treated at 35ºC had transiently increased then decreased cell size
520 while 40ºC-treated algal cells had steadily increased cell size due to heat-inhibited cell
521 division (Fig. 3B). Under the acetate-depleting condition, chlorophyll content per culture
522 volume (mL) had no significant differences between 25ºC and 40ºC but was significantly

523 higher at 8-h of 35°C than 25°C (Fig. 3C), consistent with the increased biomass at the
524 8-h of 35°C (Fig. 1C). Chlorophyll content normalized to cell density revealed constant
525 chlorophyll per cell during 25°C, but transiently and constantly increased cellular
526 chlorophyll during 35°C and 40°C, respectively (Fig. 3D). Chlorophyll content normalized
527 to cell volume showed the increased cellular chlorophyll during 40°C and 35°C could not
528 be completely explained by increased cell volume (Fig. 3E).
529
530 Based on our previously published data, we summarized cell parameters in algal cultures
531 grown in the same PBRs but under the constant-acetate condition through turbidostatic
532 control for 24 h (Zhang *et al.*, 2022*a*) (Fig. 4F-J). Cell parameters at different time points
533 during 25°C had little or no changes as compared to the pre-heat time points,
534 demonstrating the steady algal growth and effectiveness of the turbidostatic control with
535 constant acetate supply. Under the constant acetate condition, the smaller changes of
536 cell density and chlorophyll per mL culture as compared to the acetate-depleting
537 conditions were due to the turbidostatic control and frequent dilution of the culture (Fig.
538 3F and 3H). The changes of cell volume and chlorophyll content per cell during 35°C and
539 40°C had the similar trends under both the acetate-depleting and constant-acetate
540 condition, but the increase of these parameters was larger under 40°C in cultures with
541 the constant-acetate than the acetate-depleting condition (Fig. 3B, D, G, I). This was
542 supported by the fold changes of cell parameters by comparing the data under the
543 acetate-depleting and constant-acetate conditions (Fig. 3K-O).
544
545 In addition to the cellular parameters mentioned above using time-course harvesting, we
546 next utilized non-disruptive methods to quantify algal growth under different temperatures.
547 The acetate-depleting condition without turbidostatic control allowed us to have a large
548 range of cell densities under different temperature treatments to investigate the optical
549 density (OD) vs cell density relationship and validate automatic culture monitoring under
550 different temperature treatments. OD_{680} (optical density at 680 nm) monitors chlorophyll
551 content per mL culture (Chapman *et al.*, 2015; Xiao *et al.*, 2015; Young *et al.*, 2022).
552 OD_{750} (optical density at 750 nm) monitors light scattering and is thought to be
553 proportional to cell density or cell volume (Chioccioli *et al.*, 2014; Young *et al.*, 2022). Our

PBRs can measure OD_{680} and OD_{720}, but no OD_{750}. However, OD_{720} serves as a proximity for OD_{750} for light scattering. Thus, we investigated the dynamic changes of OD_{680} and OD_{720} relative to chlorophyll content, cell density, and cell volume before and during heat treatments under the acetate-depleting condition, in medium starting with acetate but without constant acetate supply (Fig. 4). The change of OD_{680} and OD_{720} (Fig. 4A, B) mimicked the change of chlorophyll content per mL algal culture for all three temperature treatments (Fig. 3C). But the change of OD_{720} (Fig. 4B) mimicked the change of cell density for 25°C and 35°C but not 40°C (Fig. 3A). Combining all data from different temperature treatments and time points, both OD_{680} and OD_{720} were linearly proportional to chlorophyll content per mL algal culture (Fig. 4C, D), but they were much less proportional to cell volume or cell density (Fig. 4E-J). Our results showed that OD_{680} and OD_{720} can be used to accurately estimate chlorophyll content in algal cultures with different heat treatments, thus they can be used to estimate algal relative growth rates based on chlorophyll accumulation during an exponential growth phase between dilution events with turbidostatic control in PBRs (Zhang *et al.*, 2022*a*) (See methods for details). The relative growth rates calculated from both OD_{680} and OD_{720} yielded similar results. Because OD_{680} had larger values and higher signal/noise ratios than OD_{720}, we used OD_{680} to estimate relative growth rates of PBR cultures over several days under the turbidostatic controls with and without acetate supply to investigate how acetate affected algal heat responses at 35°C and 40°C in long-term (Fig. 5-9). This research goal could not be achieved without turbidostatic controls because our acetate-depleting experiment revealed that acetate was fully depleted in 24 h during all three temperature treatments of 25°C, 35°C and 40°C without constant acetate supply (Fig. 1D).

To investigate the effects of acetate on long-term heating, after algal cultures reached steady growth at 25°C in PBRs with turbidostatic control, we conducted all three temperature treatments with continuously turbidostatic control and constant acetate supply for 4 days (Fig. 5). Without heat treatments, algal growth rates and cell parameters stayed constant at 25°C, demonstrating the effectiveness of our turbidostatic control for steady algal growth (Fig. 5). At 35°C with constant acetate supply, the relative growth rates increased first, but the increase was reduced to a smaller degree after 2-day heating

585 at 35ºC and stabilized thereafter (Fig. 5A). At 40ºC, the relative growth rates decreased
586 steadily, and the cultures died after 2-day heating at 40ºC, suggesting algal cells could
587 not acclimate to long-term constant heat at 40ºC, even with constant acetate supply. Cells
588 treated with 40ºC had more than 4-fold increase of cell volume as compared to the pre-
589 heat condition, followed by reduced cellular chlorophyll and cell death (Fig. 5C-F). The
590 turbidostatic mode by OD_{680} tightly controlled the chlorophyll contents in unit of ug per mL
591 culture in PBRs during the treatments of 25ºC and 35ºC (Fig. 5D), but not 40ºC due to
592 the cell cycle arrest and overwhelmingly increased chlorophyll per cell, and eventually
593 cell death under 40ºC (Fig. 5B and E).
594
595 To further test the effects of acetate on algal heat responses, we conducted a different
596 sets of experiments using algal cultures grown in PBRs, under the turbidostatic control
597 with constant nutrient supply but in photoautotrophic medium (no acetate), with different
598 temperature treatments for 4 days (Fig. 6). Without heat treatments, algal growth rates
599 and cell parameters stayed constant at 25ºC, demonstrating the effectiveness of our
600 turbidostatic control for steady algal growth under photoautotrophic conditions. Without
601 acetate but with constant medium supply, algal growth had gradual decreased growth
602 rates during 35ºC (Fig. 6A), unlike the increased growth rates during 35ºC with constant
603 medium and acetate supply (Fig. 5A), strongly supporting the role of acetate in algal heat
604 tolerance. Without acetate, algal cells with 35ºC treatment had increased cell volume and
605 chlorophyll contents (Fig. 6B-F). Our microscopic images showed that the dramatically
606 increased cell volume during 35ºC was due to the formation of palmelloids (Fig. 7).
607 Palmelloids are clumps of non-motile cells, which often results from a failure of hatching
608 or release from the mother cell wall under stressful conditions (Harris, 2009). It is reported
609 that Chlamydomonas cells aggregated to form palmelloids after 3 min acute heat shock
610 at 50ºC in the acetate-containing medium (de Carpentier *et al.*, 2022). The dramatically
611 increased cell volume due to palmelloids did not occur in the constant-acetate-35ºC
612 condition (Fig. 5C), suggesting 35ºC was more stressful without acetate than with acetate.
613 The reduction of growth rates during 40ºC was comparable with and without acetate (Fig.
614 5A and 6A).
615

616 To better compare algal growth and cell physiologies under the turbidostatic control with
617 and without acetate, we normalized the data with heat treatments to the constant 25°C
618 with the same medium type (Fig. 8). Algal cells treated with 35°C without acetate had
619 similar pattern of cell density and cell volume as algal cells treated with 40°C with acetate
620 (Fig. 8B, C), supporting 35°C was more stressful without acetate than with acetate. The
621 normalized data also revealed the increased chlorophyll per mL culture, per cell, and per
622 cell volume during 35°C without acetate (Fig. 8D-F).
623
624 Our PBRs could also monitor photosystem II (PSII) operating efficiency using chlorophyll
625 fluorescence measurement automatically (Fig. 9). Heat at 40°C reduces PSII operating
626 efficiency dramatically, with more reduction without acetate than with acetate during the
627 first two days of heating (Fig. 9B, C, D). The acetate effects on PSII operating efficiency
628 disappeared in algal cells treated by 40°C for more than 2 days (Fig. 9D). The reduction
629 of PSII operating efficiency during 35°C was much smaller than during 40°C, with higher
630 PSII operating efficiency in 35°C-treated algal cells with acetate than without acetate (Fig.
631 9D).
632
633 **Discussion**
634 By performing algal cultivation under highly controlled conditions in PBRs with and without
635 a constant organic carbon source, acetate, we investigated how the availability of acetate
636 affected the growth of Chlamydomonas under moderate (35°C) and acuate high
637 temperatures (40°C) (Fig. 10).
638
639 **Heat of 35°C was beneficial or detrimental depending on carbon availability**
640 Under the turbidostatic control without nutrient limitation, moderate high temperature of
641 35°C increased algal growth rates with constant acetate supply (Fig. 5A), but decreased
642 agal growth rates without acetate in photoautotrophic medium (Fig. 6A), confirming the
643 important role of acetate in heat tolerance. The increased heat tolerance to 35°C with
644 acetate is not strain-dependent because the acetate effects were similar in two different
645 algal strains: CC-1690 (this study) and CC-5325 (Mattoon *et al.*, 2022). In medium starting
646 with acetate but without constant acetate supply (the acetate-depleting condition), algal

647 biomass increased first but then decreased at 35°C compared to 25°C, which can be
648 explained by increased acetate uptake/usage initially followed by acetate
649 depletion/starvation by the end of the 24-h 35°C treatments (Fig. 1C, D).
650
651 Under the acetate-depleting condition, besides acetate, other nutrients may also be
652 depleted gradually during 24 h. We checked known transcription factors and regulators
653 responding to starvation of other nutrients, including *nitrogen starvation responsive*
654 *regulator 1 (NRR1)* (Boyle *et al.*, 2012), *sulfur starvation responsive regulator 2.1*
655 *(SNRK2.1)* (González-Ballester *et al.*, 2010), *phosphorus starvation response 1 (PSR1)*
656 (Bajhaiya *et al.*, 2016), *copper deficiency response regulator 1 (CRR1)* (Sommer *et al.*,
657 2010), and *iron deficiency response regulator (MAPK3)* (Fei *et al.*, 2017). If these
658 nutrients were depleted, the corresponding transcription factors and regulators would be
659 up-regulated. Most of these nutrient-deficiency transcription factors and regulators had
660 minimal or no induction at 24 h of the acetate-depleting condition (Supplemental Fig. 3C-
661 G). One exception is the *NRR1*, which was up-regulated at 25°C or 35°C but was down-
662 regulated under 40°C at 24 h of the acetate-depleting condition (Supplemental Fig. 3C).
663 The results suggested minimal or no limitation of sulfur, phosphorus, copper, and iron
664 during the acetate-depleting condition, but some nitrogen deficiency at 24 h of the
665 acetate-depleting condition. One of the responses to nitrogen deficiency is reduction of
666 chlorophyll (Schmollinger *et al.*, 2014). During our acetate-depleting condition, most
667 transcripts involved in chlorophyll biosynthesis were stable (Supplemental Fig. 4Q).
668 Additionally, there was no change of the chlorophyll per cell or per cell volume at 24 h of
669 25°C as compared to the pre-heat time point which did not have acetate-limitation; these
670 parameters were higher under 35°C and 40°C than 25°C at 24 h of the acetate-depleting
671 condition (Fig. 3D, E). Collectively, the results indicated that the nitrogen limitation may
672 have just started at 24 h of the acetate-depleting condition, thus would not impact the cell
673 physiology too much. Finally, our results from the 4-day constant-acetate and no-acetate
674 conditions under the turbidostatic control strongly pointed to the effects of acetate on algal
675 heat tolerance but not other nutrients (Fig. 5, 6). Thus, the acetate effects are the focus
676 of our research.
677

678 Chlamydomonas uptakes acetate and feeds it into the glyoxylate cycle and
679 gluconeogenesis for starch biosynthesis and starch is broken down through glycolysis to
680 make cellular energy (Johnson and Alric, 2012, 2013) (Fig. 2A). The dynamic effects of
681 35°C on algal growth under different acetate conditions can be explained by the 35°C-
682 induced carbon metabolisms, including the up-regulation of transcripts related to acetate
683 uptake/assimilation, glyoxylate cycle and gluconeogenesis pathways, and glycolysis (Fig.
684 2). The up-regulation of these transcripts lasted longer with higher induction under the
685 constant-acetate than the acetate-depleting condition (Fig. 2). Energy produced from
686 glycolysis can be used for energy-requiring cellular activities to increase thermotolerance
687 (Olas *et al.*, 2021), e.g., production of heat shock proteins and repair pathways related to
688 photosynthesis (Murata and Nishiyama, 2018; Bourgine and Guihur, 2021). Pyruvate
689 kinase catalyzes the final step of glycolysis and it converts phosphoenolpyruvate and one
690 ADP to pyruvate and one ATP (Baud *et al.*, 2007; Wulfert *et al.*, 2020). Chlamydomonas
691 mutants deficient in pyruvate kinase were heat-sensitive under 35°C in acetate-containing
692 medium (Mattoon *et al.*, 2022), supporting the important roles of glycolysis in
693 thermotolerance of 35°C. Although ATP production mainly comes from mitochondrial
694 respiration, the ATP production from glycolysis can be important under stressful
695 conditions where energy availability is limited (van Dongen *et al.*, 2011). Under low
696 oxygen conditions, plants increase activity of pyruvate kinases to produce more ATP (van
697 Dongen *et al.*, 2011). Heat-treated barley leaves utilized glycolysis as an alternative
698 energy source for thermotolerance based on proteomics analysis (Rollins *et al.*, 2013).
699
700 Additionally, acetate may protect photosynthesis from heat-induced photoinhibition.
701 Acetate is proposed to protect PSII against photoinhibition by replacing the bicarbonate
702 associated to the non-heme iron at the acceptor side of PSII, changing the environment
703 of plastoquinone, and affecting PSII charge recombination (Roach *et al.*, 2013). Our PSII
704 efficiency data supported this hypothesis because PSII efficiency was higher with acetate
705 than without acetate during 25°C, 35°C or 40°C treatments (Fig. 9D). Chlamydomonas
706 grown in acetate-containing medium produced less singlet O_2 (one kind of ROS) than
707 those grown in non-acetate-containing, photoautotrophic medium (Roach *et al.*, 2013).
708 Furthermore, experimental and modeling analysis suggested that acetate promoted cyclic

electron flow (CEF) around photosystem I (PSI); reducing equivalents produced during the acetate metabolism reduce plastoquinone pools and increase CEF activity (Johnson and Alric, 2012; Lucker and Kramer, 2013; Chapman *et al.*, 2015). CEF cycles photosynthetic electrons around PSI, producing only ATP but no NADPH and providing extra ATP needed for photosynthesis and other cellular activities (Munekage *et al.*, 2004; Baker *et al.*, 2007). CEF balances the ATP/NADPH ratio, contributes to the generation of transthylakoid proton motive force, and protects both PSI and PSII from photo-oxidative damage (Johnson, 2011; Yamori and Shikanai, 2016). The increased acetate uptake under 35°C (Fig. 1D) was coupled with induced CEF activity measured by P700 oxidation/reduction in Chlamydomonas (Zhang *et al.*, 2022*a*). Our transcriptome analysis also showed up-regulation of transcripts related to PSI and CEF at 2h of 35°C treatments under either the acetate-depleting or constant-acetate condition, consistent with heat-induced CEF in the presence of acetate (Supplemental Fig. 4J, P).

The effects of acetate on the improved heat tolerance under the moderate high temperature may also be related to the accumulation of thermoprotective metabolites (osmolytes, including amino acids, sugars, and sugar alcohols) (Guihur *et al.*, 2022) or compatible solutes (Hemme *et al.*, 2014; Schroda *et al.*, 2015). Compatible solutes accumulate from the catabolism of large molecules upon the onset of heat to stabilize membranes and prevent protein unfolding/aggregation (Schroda *et al.*, 2015). In Chlamydomonas, these compatible solutes include glycerophos-phoglycerol (GPG), trehalose, β_alanine, isoleucine, asparagine, glutamine, and guanosine (Hemme *et al.*, 2014). The elevated acetate metabolism at 35°C with constant acetate supply may increase the accumulation of these thermoprotective metabolites. This is an understudied but exciting area. Future metabolite analysis may provide more information about this.

With constant acetate supply, 35°C is beneficial, increasing carbon metabolisms and energy production, thus improving thermotolerance and growth (Fig. 5). If algal cells can be cultivated under sterile conditions with constant organic carbon supply, 35°C could be used to promote algal growth and increase biofuel/bioproduct generation under mixotrophic conditions in light. Culture temperature of 35°C in closed, outdoor algal ponds

740 may not be difficult to reach with natural sunlight heating in the summertime of the
741 moderate climate regions and year-round in the tropical regions.
742
743 Without constant acetate supply, 35°C is detrimental. Under the acetate-depleting
744 condition, the 35°C-elevated carbon metabolism without sufficient carbon input may
745 deplete cellular carbon reserves. This was not sustainable in the long term and eventually
746 reduced biomass accumulation (Fig. 1C). With constant acetate supply, heat at 35°C
747 transiently arrested the cell cycle, which recovered after 8 h at 35°C (Fig. 3G). In
748 photoautotrophic medium without acetate, 35°C reduced algal growth rates and inhibited
749 cell division (stressed cells aggregated to form palmelloids) (Fig. 6, 7). Such effects of
750 35°C can particularly compromise the yields of outdoor algal ponds because they usually
751 do not contain carbon sources but frequently experience moderate high temperatures
752 (Mata *et al.*, 2010; El-Sheekh *et al.*, 2019).
753
754 It is reported that the growth rate of another Chlamydomonas WT strain (CC-125) at 35°C was
755 about 50% of that at 28°C (0.083 vs 0.166) in photoautotrophic medium under constant light and
756 continuous dilution but with 2% CO_2 (Vítová *et al.*, 2011). The 50% growth reduction is
757 comparable to the reduced growth of our data at 35°C without acetate (Fig. 6A). We used air level
758 CO_2, which is 400 ppm or 0.04% CO_2 to mimic the nature condition (1/50th of 2% CO_2 as in (Vítová
759 *et al.*, 2011)). CO_2 provides the inorganic carbon source for algal growth. But the equivalent 50%
760 growth reduction at 35°C as compared to the control temperature with (Vítová *et al.*, 2011) and
761 without (this study) high CO_2 suggests CO_2 (inorganic carbon source) is not as effective as acetate
762 (organic carbon source), to improve thermotolerance in algal cells. Furthermore, different algal
763 strains with changes in cultivation conditions may have varying moderate high temperature
764 ranges. For example, another Chlamydomonas WT strain (CC-137) had optimal growth at 35°C
765 in photoautrophic medium with 2% CO_2 in day/night cycle with semi-dilution (one dilution per day
766 at the end of dark phase) (Lien and Knutsen, 1979). Such semi-dilution may result in a large range
767 of cell densities, which may affect the light perceived by each cell. Additionally. the day/night cycle
768 may also alleviate photooxidative stress as photosynthesis only occurs in light. However, the
769 author mentioned that cytokinesis and sporulation became inhibited at temperature above 36°C
770 (Lien and Knutsen, 1979), indicating 35°C may be close to the moderate high temperature range
771 that would reduce algal growth in this strain under their cultivation condition without acetate.
772

773 The up-regulated carbon metabolism under moderate high temperatures may also occur
774 in land plants, especially in sink tissues (e.g., roots) or mixotrophic tissues (e.g.,
775 developing green seeds) (Koley *et al.*, 2022). Heat-induced glyoxylate cycle,
776 gluconeogenesis, and glycolysis have been reported in plants (Rollins *et al.*, 2013; Zhang
777 *et al.*, 2013; Aprile *et al.*, 2013). Carbon metabolism and sugar availability were shown to
778 be essential for heat tolerance in Arabidopsis (Olas *et al.*, 2021).
779
780 **Heat of 40°C was detrimental to algal cells with and without constant acetate supply**
781 Acute high temperatures at or above 40°C inhibit the algal cell cycle (Fig. 3, 5-7)
782 (Mühlhaus *et al.*, 2011*b*; Hemme *et al.*, 2014; Zachleder *et al.*, 2019; Ivanov *et al.*, 2021),
783 alter thylakoid membranes, reduce photosynthesis, and damage respiration (Zhang *et al.*,
784 2022*a*). These cellular damages took place quickly, within 4 h of heat at 40°C with
785 constant acetate supply (Zhang *et al.*, 2022*a*). However, 40°C-treated cells grew bigger
786 and had more chlorophyll under the constant-acetate condition than the acetate-depleting
787 condition in the short-term (24-h heat) (Fig. 3B, G, D, I, L, N), although the constant
788 acetate supply could not prevent ultimate cell death with 40°C-heat longer than 2-days
789 (Fig. 5). Similarly, without acetate, Chlamydomonas cells also died after 2-day heat at
790 40°C (Fig 6). The death of Chlamydomonas cultures was also reported at 39°C for 33 h
791 in photoautotrophic medium without acetate (Zachleder *et al.*, 2019; Ivanov *et al.*, 2021).
792 Thus, constant heating at 40°C is lethal for Chlamydomonas cells independent of carbon
793 availability.
794
795 Transcripts of many genes involved in carbon metabolism, e.g., acetate
796 uptake/assimilation, glyoxylate cycle and gluconeogenesis pathways, and glycolysis were
797 significantly down-regulated during 40°C (Fig. 2). Most of the reducing power from acetate
798 assimilation is used in mitochondrial respiration to produce ATP (Johnson and Alric, 2012,
799 2013). Our previous results showed that 40°C reduced mitochondrial activities
800 significantly under the 24-h constant-acetate condition (Zhang *et al.*, 2022*a*). When
801 comparing 40°C vs 25°C under the acetate-depleting condition and 40°C vs 35°C
802 regardless the acetate condition, the top enriched function group was related to
803 mitochondrial electron transport (Supplemental Fig. 5B, E), suggesting mitochondria were

804 particularly sensitive to 40ºC. The compromised mitochondrial activities may restrict
805 acetate uptake/assimilation during 40ºC heat treatment. Under the acetate-depleting
806 conditions, the acetate uptake was slightly lower in 40ºC-treated cultures than 25ºC (Fig.
807 1D). The decreased acetate uptake/usage, together with reduced photosynthesis and
808 respiration (Zhang *et al.*, 2022*a*) and cell cycle arrest (Fig. 3, 5-7), may contribute to the
809 significantly reduced algal dry biomass in cultures treated with 8h-heat of 40ºC than 25ºC
810 (Fig. 1C). By the end of 24-h treatment under the acetate-depleting condition, there were
811 comparable amount of dry biomass in cultures treated with 40ºC and 25ºC (Fig. 1C),
812 which could be explained by the arrested cell cycle and almost eliminated energy/biomass
813 consumption for cell division during 40ºC. Such an inefficient system with reduced carbon
814 input and little energy output was not sustainable, eventually killing all the algal cells by
815 the end of 2-day heat of 40ºC, even with constant acetate supply (Fig. 5). Our results
816 suggested that the increased thermotolerance by acetate did not apply to long-term heat
817 at 40ºC.
818
819 At 24-h of the acetate-depleting condition, the transcripts related to large *HSP*s,
820 *HSP60/70/90s*, were down-regulated at 25ºC and 35ºC, but not under 40ºC
821 (Supplemental Fig. 4A-C). The down-regulation of large *HSP*s may be related to the
822 increased cell density and light shading, thus reduced light stress at 24 h of 25ºC and
823 35ºC under the acetate-depleting condition (Fig. 3A). However, the amount of chlorophyll
824 per mL culture was comparable at 24 h of 25ºC, 35ºC, and 40ºC under the acetate-
825 depleting condition, suggesting comparable level of light shading and light stress under
826 all three temperatures (Fig. 3A), although photosynthesis may have more damages at
827 40ºC than 25ºC/35ºC. The up-regulated transcripts related to photoprotection at 24 h of
828 all three temperatures under the acetate-depleting condition may deemphasize the
829 effects of light shading (Supplemental Fig. 4O). Alternatively, the different regulation of
830 large *HSP*s between 25ºC/35ºC and 40ºC at 24 h of the acetate-depleting condition may
831 suggest the energy distribution between growth and heat tolerance. Most large HSPs are
832 ATP-dependent chaperons, especially HSP90s (Al-Whaibi, 2011; Xu *et al.*, 2012; Guihur
833 *et al.*, 2022). Down-regulation of these large HSPs when acetate was depleted may be
834 helpful to reserve energy for cell growth when the temperature stress was none (25ºC) or

835 moderate (35°C). However, under the acute heat of 40°C, thermotolerance has higher
836 priority than growth, thus the expression of these large *HSPs* were maintained while cell
837 cycle was arrested to preserve energy.
838
839 As compared to 40°C, the induction of *HSP*s at 35°C was minimal or none under either
840 acetate condition (Supplemental Fig. 4A-C), suggesting the 35°C-induced
841 thermotolerance by acetate may not be related to the accumulation of HSPs. This may
842 suggest some none-overlapping heat sensing/signaling pathways between 35°C and
843 40°C, as HSPs have important roles in the classical heat shock responses (Guihur *et al.*,
844 2022). Several heat sensors have been proposed (Vu *et al.*, 2019), including membrane
845 fluidity (Martinière *et al.*, 2011), Ca^{2+} channels in the plasma membrane (Gao *et al.*, 2012;
846 Finka *et al.*, 2012), unfolded proteins (Rütgers *et al.*, 2017; Li *et al.*, 2020), and
847 phytochromes (Jung *et al.*, 2016; Legris *et al.*, 2016), and some circadian clock
848 components (e.g. EARLY FLOWERING 3, ELF3) (Jung *et al.*, 2020). Among these, the
849 heat effects on phytochromes and ELF3 have been reported around the temperature
850 ranges of 30-35°C (Jung *et al.*, 2016, 2020; Legris *et al.*, 2016), providing potential heat
851 sensor candidates for moderate high temperatures. Future research to investigate the
852 shared and unique heat sensors for moderate and acuate high temperatures may provide
853 more information about how plants sense and adapt to different high temperatures.
854
855 Most previous heat treatments in Chlamydomonas used cultures grown with acetate-
856 containing medium in flasks without turbidostatic controls (Hemme *et al.*, 2014; Rütgers
857 *et al.*, 2017). Our results showed that such heat treatment could not last more than 8 h at
858 35°C or 24 h of 40°C due to acetate-depletion (Fig. 1D). In fact, many previous heat
859 experiments were conducted for a short-term, e.g., 1 h (Légeret *et al.*, 2016; Rütgers *et*
860 *al.*, 2017). Using our highly controlled PBR systems, we could not only conduct heat
861 experiments under the 24-h acetate-depleting condition but also during 4-day heating with
862 and without acetate under the turbidostatic control with constant nutrient supply to
863 uniquely reveal the effects of carbon availability on thermotolerance.
864

865 In summary, by using highly controlled cultivation systems in PBRs and the model green
866 alga Chlamydomonas, we revealed how the availability of an organic carbon source,
867 acetate, interacted with different intensities and duration of high temperatures in
868 photosynthetic cells. Our research revealed the overlooked effects of moderate high
869 temperature of 35°C, which can be beneficial with constant carbon supply or detrimental
870 with insufficient or no carbon supply. We also showed that the damaging effects of acute
871 high temperature of 40°C is dominant and independent of carbon availability. Our
872 research not only helps us understand heat responses in photosynthetic cells but also
873 provides insights for high temperature effects on the production of algal biofuels and
874 bioproducts.
875
876 **Supplementary data**
877 **Supplemental Table 1**: Gene IDs and primers for RT-qPCR analysis in Fig. 2 and
878 Supplemental Fig. 2 and 3.
879
880 **Supplemental Dataset 1**. RNA-seq data and plots of each transcript detected, including
881 mean normalized read count plots, mean normalized read count heat map, log_2(fold
882 change) of mean normalized read counts relative to the pre-heat time point under the
883 same condition, and statistical analysis using False Discovery Rate (FDR).
884
885 **Supplemental Dataset 2**. Log_2(fold change, FC) of mean normalized read counts of
886 groups of transcripts based on MapMan function annotation (MapMan folder) or manual
887 curation (Manual_curation folder). Manual curation was based on the gene lists from this
888 paper (Zhang *et al.*, 2022*a*). Each line in the plots represent one unique transcript in that
889 function category under one of six conditions. RNA-seq data with normalized read counts
890 were used for this analysis. Log_2FC is relative to the pre-heat time point under the same
891 condition. Black vertical lines indicated the start of heat treatments under 35°C or 40°C
892 or the equivalent time point at 25°C. ANOVA test was applied to the time course (five time
893 points) of one transcript for each condition. If a transcript differed significantly during the
894 time course (or underwent a global significant change) of one condition, it is colored
895 purple (ANOVA significant); blue lines had no significant changes during the time course.

896 Different intensities of purple and blue colors were used to distinguish different transcripts.
897 Each file opens as a web page. Please use the interactive feature of the figures to see
898 the gene IDs for each panel.
899
900 **Supplemental Dataset 3**. MapMan ontology enrichment. Ontology enrichment was
901 performed for transcripts with significantly differential expression in the indicated
902 comparisons using the extended MapMan ontology. The p values were calculated using
903 a hypergeometric test and corrected for multiple testing using the Benjamini-Hochberg
904 method.
905
906 **Supplemental Dataset 4**. Normalized RNA-seq read counts.
907
908 **Supplemental Dataset 5**. RNA-seq data summary, including gene IDs, MapMan function
909 groups, annotation, adjusted False Discovery Rate (FDR) values for comparisons of
910 different conditions, mean and standard deviation (sd) of normalized read counts.
911
912 **Supplemental figures -6** (see figure file)
913
914 **Acknowledgements**
915 We would like to thank Dr. Michael Schroda for discussing the initial experimental idea
916 under the acetate-depleting conditions and Dr. Trent Northen for recommending the
917 acetate quantification assay. We also want to thank the team of the Department of Energy
918 (DOE) Joint Genome Institute (JGI) Community Science Program (Anna Lipzen, Christa
919 Pennacchio, Kerrie Barry, Dr. Jeremy Schmutz, and others) for managing and
920 sequencing our RNA samples.
921
922 **Author contributions**
923 RZ designed the experiments. CB and MX operated and maintained the algal growth in
924 photobioreactors. NZ, CB, and MX harvested algal samples at different time points and
925 quantified biomass. NZ and MX performed acetate quantification assay. NZ performed
926 RT-qPCR analysis and extracted RNA for RNA-seq. CB and NZ performed light

927 microscope imaging. CB and MX quantified cell density, cell size, and chlorophyll
928 contents, and recorded OD_{608}/OD_{720} readings. CB and MX performed 4-day heating
929 experiments and quantified growth rates as well as cell parameters. CB analyzed PSII
930 data. BV, TM, RZ did RNA-seq analysis. EMM did initial analysis of the acetate pathways.
931 NZ, BV, CB, RZ, MX, and EMM prepared the figures. BV wrote the RNA-seq method and
932 RZ wrote the rest of the manuscript. RZ, EMM, BV, and CB revised the manuscript.
933

934 **Conflict of interest**

935 No conflict of interest declared.
936

937 **Funding statement**

938 This work was supported by the start-up funding from the Donald Danforth Plant Science
939 Center (DDPSC) and the DOE Biological & Environmental Research (BER) grant (DE-
940 SC0020400) to RZ. EMM was supported by the William H. Danforth Fellowship in Plant
941 Sciences and the DDPSC start-up funding (to RZ). BV and TM were supported by the
942 Germany funding TRR 175 (Project No: 270050988). The RNA-seq service support was
943 from the Department of Energy (DOE) Joint Genome Institute (JGI) Community Science
944 Program (CSP, 503414) to RZ. The NovaSeq for RNA-seq (proposal:
945 10.46936/10.25585/60001126) was conducted by the U.S. Department of Energy Joint
946 Genome Institute (https://ror.org/04xm1d337), a DOE Office of Science User Facility, is
947 supported by the Office of Science of the U.S. Department of Energy operated under
948 Contract No. DE-AC02-05CH11231.
949

950 **Data availability**

951 All data supporting the findings of this study are available within the paper and within its
952 supplementary materials published online.
953

References

Altschuler M, Mascarenhas JP. 1982. Heat shock proteins and effects of heat shock in plants. Plant molecular biology **1**, 103–115.

Al-Whaibi MH. 2011. Plant heat-shock proteins: A mini review. Journal of King Saud University - Science **23**, 139–150.

Anderson CM, Mattoon EM, Zhang N, *et al.* 2021. High light and temperature reduce photosynthetic efficiency through different mechanisms in the C4 model Setaria viridis. Communications Biology **4**, 1092.

Aprile A, Havlickova L, Panna R, *et al.* 2013. Different stress responsive strategies to drought and heat in two durum wheat cultivars with contrasting water use efficiency. BMC genomics **14**, 821.

Bajhaiya AK, Dean AP, Zeef LAH, Webster RE, Pittman JK. 2016. PSR1 Is a Global Transcriptional Regulator of Phosphorus Deficiency Responses and Carbon Storage Metabolism in Chlamydomonas reinhardtii. Plant physiology **170**, 1216–1234.

Baker NR, Harbinson J, Kramer DM. 2007. Determining the limitations and regulation of photosynthetic energy transduction in leaves. Plant, cell & environment **30**, 1107–1125.

Balfagón D, Sengupta S, Gómez-Cadenas A, Fritschi FB, Azad RK, Mittler R, Zandalinas SI. 2019. Jasmonic acid Is required for plant acclimation to a combination of high light and heat stress. Plant physiology **181**, 1668–1682.

Baud S, Wuillème S, Dubreucq B, de Almeida A, Vuagnat C, Lepiniec L, Miquel M, Rochat C. 2007. Function of plastidial pyruvate kinases in seeds of Arabidopsis thaliana. The Plant journal: for cell and molecular biology **52**, 405–419.

BBDuk. 2022. BBMap short read aligner, and other bioinformatic tools.

Benjamini Y, Hochberg Y. 1995. Controlling the false discovery rate: a practical and powerful approach to multiple testing. Journal of the Royal Statistical Society. Series B, Statistical methodology **57**, 289–300.

Bigeard J, Hirt H. 2018. Nuclear Signaling of Plant MAPKs. Frontiers in plant science **9**, 469.

Bourgine B, Guihur A. 2021. Heat Shock Signaling in Land Plants: From Plasma Membrane Sensing to the Transcription of Small Heat Shock Proteins. Frontiers in plant science **12**, 710801.

Boyle NR, Page MD, Liu B, *et al.* 2012. Three acyltransferases and nitrogen-responsive regulator are implicated in nitrogen starvation-induced triacylglycerol accumulation in Chlamydomonas. The Journal of biological chemistry **287**, 15811–15825.

de Carpentier F, Maes A, Marchand CH, Chung C, Durand C, Crozet P, Lemaire SD, Danon A. 2022. How abiotic stress-induced socialization leads to the formation of massive aggregates in Chlamydomonas. Plant physiology **190**, 1927–1940.

Chapman S, Paget C, Johnson G, Schwartz J-M. 2015. Flux balance analysis reveals acetate metabolism modulates cyclic electron flow and alternative glycolytic pathways in Chlamydomonas reinhardtii. Frontiers in plant science **6**.

Chew SY, Chee WJY, Than LTL. 2019. The glyoxylate cycle and alternative carbon metabolism as metabolic adaptation strategies of Candida glabrata: perspectives from Candida albicans and Saccharomyces cerevisiae. Journal of Biomedical Science **26**.

Chioccioli M, Hankamer B, Ross IL. 2014. Flow Cytometry Pulse Width Data Enables Rapid and Sensitive Estimation of Biomass Dry Weight in the Microalgae Chlamydomonas reinhardtii and Chlorella vulgaris. PLoS ONE **9**, e97269.

Crozet P, Navarro FJ, Willmund F, *et al.* 2018. Birth of a photosynthetic chassis: A MoClo toolkit enabling synthetic biology in the microalga *Chlamydomonas reinhardtii*. ACS synthetic biology **7**, 2074–2086.

Delorge I, Janiak M, Carpentier S, Van Dijck P. 2014. Fine tuning of trehalose biosynthesis and hydrolysis as novel tools for the generation of abiotic stress tolerant plants. Frontiers in plant science **5**.

Dhokane D, Bhadra B, Dasgupta S. 2020. CRISPR based targeted genome editing of *Chlamydomonas reinhardtii* using programmed Cas9-gRNA ribonucleoprotein. Molecular biology reports **47**, 8747–8755.

van Dongen JT, Gupta KJ, Ramírez-Aguilar SJ, Araújo WL, Nunes-Nesi A, Fernie AR. 2011. Regulation of respiration in plants: a role for alternative metabolic pathways. Journal of plant physiology **168**, 1434–1443.

El-Sheekh MM, Gheda SF, El-Sayed AE-KB, Abo Shady AM, El-Sheikh ME, Schagerl M. 2019. Outdoor cultivation of the green microalga Chlorella vulgaris under stress conditions as a feedstock for biofuel. Environmental science and pollution research international **26**, 18520–18532.

Emrich-Mills TZ, Yates G, Barrett J, *et al.* 2021. A recombineering pipeline to clone large and complex genes in Chlamydomonas. The Plant Cell **33**, 1161–1181.

Fei X, Yu J, Li Y, Deng X. 2017. CrMAPK3 regulates the expression of iron-deficiency-responsive genes in Chlamydomonas reinhardtii. BMC biochemistry **18**, 6.

Finka A, Cuendet AFH, Maathuis FJM, Saidi Y, Goloubinoff P. 2012. Plasma membrane cyclic nucleotide gated calcium channels control land plant thermal sensing and acquired thermotolerance. The Plant cell **24**, 3333–3348.

Gao F, Han X, Wu J, Zheng S, Shang Z, Sun D, Zhou R, Li B. 2012. A heat-activated calcium-permeable channel - Arabidopsis cyclic nucleotide-gated ion channel 6 - is involved in heat shock responses. The Plant Journal **70**, 1056–1069.

González-Ballester D, Casero D, Cokus S, Pellegrini M, Merchant SS, Grossman AR. 2010. RNA-seq analysis of sulfur-deprived Chlamydomonas cells reveals aspects of acclimation critical for cell survival. The Plant cell **22**, 2058–2084.

Greiner A, Kelterborn S, Evers H, Kreimer G, Sizova I, Hegemann P. 2017. Targeting of photoreceptor genes in *Chlamydomonas reinhardtii* via zinc-finger nucleases and CRISPR/Cas9. The Plant cell **29**, 2498–2518.

Guihur A, Rebeaud ME, Goloubinoff P. 2022. How do plants feel the heat and survive? Trends in biochemical sciences **47**, 824–838.

Haq S, Khan A, Ali M, Khattak AM, Gai W-X, Zhang H-X, Wei A-M, Gong Z-H. 2019. Heat Shock Proteins: Dynamic Biomolecules to Counter Plant Biotic and Abiotic Stresses. International journal of molecular sciences **20**, 5321.

Harris EH. 2009. *The Chlamydomonas Sourcebook: Introduction to Chlamydomonas and Its Laboratory Use: Volume 1*. Academic Press.

Hellemans J, Mortier G, De Paepe A, Speleman F, Vandesompele J. 2007. QBase relative quantification framework and software for management and automated analysis of real-time quantitative PCR data. Genome biology **8**, R19.

Hemme D, Veyel D, Mühlhaus T, *et al.* 2014. Systems-wide analysis of acclimation responses to long-term heat stress and recovery in the photosynthetic model organism *Chlamydomonas reinhardtii*. The Plant cell **26**, 4270–4297.

Hennacy JH, Jonikas MC. 2020. Prospects for engineering biophysical CO2 concentrating mechanisms into land Plants to enhance yields. Annual review of plant biology **71**, 461–485.

Ivanov IN, Zachleder V, Vítová M, Barbosa MJ, Bišová K. 2021. Starch production in *Chlamydomonas reinhardtii* through supraoptimal temperature in a pilot-scale photobioreactor. Cells **10**, 1084.

Jagodzik P, Tajdel-Zielinska M, Ciesla A, Marczak M, Ludwikow A. 2018. Mitogen-Activated Protein Kinase Cascades in Plant Hormone Signaling. Frontiers in plant science **9**, 1387.

Janni M, Gullì M, Maestri E, Marmiroli M, Valliyodan B, Nguyen HT, Marmiroli N. 2020. Molecular and genetic bases of heat stress responses in crop plants and breeding for increased resilience and productivity. Journal of experimental botany **71**, 3780–3802.

Jee H. 2016. Size dependent classification of heat shock proteins: a mini-review. Journal of exercise rehabilitation **12**, 255–259.

Ji S, Siegel A, Shan S-O, Grimm B, Wang P. 2021. Chloroplast SRP43 autonomously protects chlorophyll biosynthesis proteins against heat shock. Nature plants **7**, 1420–1432.

Johnson GN. 2011. Physiology of PSI cyclic electron transport in higher plants. Biochimica et Biophysica Acta (BBA) - Bioenergetics **1807**, 384–389.

Johnson X, Alric J. 2012. Interaction between starch breakdown, acetate assimilation, and photosynthetic cyclic electron flow in *Chlamydomonas reinhardtii*. The Journal of biological chemistry **287**, 26445–26452.

Johnson X, Alric J. 2013. Central carbon metabolism and electron transport in *Chlamydomonas reinhardtii*: metabolic constraints for carbon partitioning between oil and starch. Eukaryotic cell **12**, 776–793.

Jung J-H, Barbosa AD, Hutin S, *et al.* 2020. A prion-like domain in ELF3 functions as a thermosensor in Arabidopsis. Nature **585**, 256–260.

Jung J-H, Domijan M, Klose C, *et al.* 2016. Phytochromes function as thermosensors in Arabidopsis. Science **354**, 886–889.

Karpowicz SJ, Prochnik SE, Grossman AR, Merchant SS. 2011. The GreenCut2 resource, a phylogenomically derived inventory of proteins specific to the plant lineage. The Journal of biological chemistry **286**, 21427–21439.

Kim S-C, Guo L, Wang X. 2020. Nuclear moonlighting of cytosolic glyceraldehyde-3-phosphate dehydrogenase regulates Arabidopsis response to heat stress. Nature communications **11**, 3439.

Kim D, Langmead B, Salzberg SL. 2015. HISAT: a fast spliced aligner with low memory requirements. Nature methods **12**, 357–360.

Koley S, Chu KL, Mukherjee T, Morley SA, Klebanovych A, Czymmek KJ, Allen DK. 2022. Metabolic synergy in Camelina reproductive tissues for seed development. Science advances **8**, eabo7683.

Kropat J, Hong-Hermesdorf A, Casero D, Ent P, Castruita M, Pellegrini M, Merchant SS, Malasarn D. 2011. A revised mineral nutrient supplement increases biomass and growth rate in Chlamydomonas reinhardtii. The Plant journal: for cell and molecular biology **66**, 770–780.

Légeret B, Schulz-Raffelt M, Nguyen HM, Auroy P, Beisson F, Peltier G, Blanc G, Li-Beisson Y. 2016. Lipidomic and transcriptomic analyses of *Chlamydomonas reinhardtii* under heat stress unveil a direct route for the conversion of membrane lipids into storage lipids. Plant, cell & environment **39**, 834–847.

Legris M, Klose C, Burgie ES, Rojas CCR, Neme M, Hiltbrunner A, Wigge PA, Schäfer E, Vierstra RD, Casal JJ. 2016. Phytochrome B integrates light and temperature signals in Arabidopsis. Science **354**, 897–900.

Li X, Fauser F, Jinkerson RE, *et al.* 2019. A genome-wide algal mutant library and functional screen identifies genes required for eukaryotic photosynthesis. Nature genetics **51**, 627–635.

Li Z, Tang J, Srivastava R, Bassham DC, Howell SH. 2020. The transcription factor bZIP60 links the unfolded protein response to the heat stress response in maize. The Plant cell **32**, 3559–3575.

Li X, Zhang R, Patena W, *et al.* 2016. An indexed, mapped mutant library enables reverse genetics studies of biological processes in *Chlamydomonas reinhardtii*. The Plant cell **28**, 367–387.

Liao Y, Smyth GK, Shi W. 2014. featureCounts: an efficient general purpose program for assigning sequence reads to genomic features. Bioinformatics **30**, 923–930.

Lien T, Knutsen G. 1979. Synchronous growth of *Chlamydomonas reinhardtii*(chlorophyceae): a review of optimal conditions. Journal of phycology **15**, 191–200.

Livak KJ, Schmittgen TD. 2001. Analysis of relative gene expression data using real-time quantitative PCR and the 2(-Delta Delta C(T)) Method. Methods **25**, 402–408.

Love MI, Huber W, Anders S. 2014. Moderated estimation of fold change and dispersion for RNA-seq data with DESeq2. Genome biology **15**, 550.

Lucker B, Kramer DM. 2013. Regulation of cyclic electron flow in *Chlamydomonas reinhardtii* under fluctuating carbon availability. Photosynthesis research **117**, 449–459.

Martinière A, Shvedunova M, Thomson AJW, Evans NH, Penfield S, Runions J, McWatters HG. 2011. Homeostasis of plasma membrane viscosity in fluctuating temperatures. The New phytologist **192**, 328–337.

Mata TM, Martins AA, Caetano NS. 2010. Microalgae for biodiesel production and other applications: A review. Renewable and Sustainable Energy Reviews **14**, 217–232.

Mathimani T, Pugazhendhi A. 2019. Utilization of algae for biofuel, bio-products and bio-remediation. Biocatalysis and agricultural biotechnology **17**, 326–330.

Mattoon EM, McHargue W, Bailey CE, *et al.* 2022. High-throughput Identification of Novel Heat Tolerance Genes via Genome-wide Pooled Mutant Screens in the Model Green Alga Chlamydomonas reinhardtii. bioRxiv, 2022.07.13.499508.

Merchant SS, Prochnik SE, Vallon O, *et al.* 2007. The *Chlamydomonas* genome reveals the evolution of key animal and plant functions. Science **318**, 245–250.

Meyer MT, Whittaker C, Griffiths H. 2017. The algal pyrenoid: key unanswered questions. Journal of experimental botany **68**, 3739–3749.

Minagawa J, Tokutsu R. 2015. Dynamic regulation of photosynthesis in *Chlamydomonas reinhardtii*. The Plant journal: for cell and molecular biology **82**, 413–428.

Mittler R, Finka A, Goloubinoff P. 2012. How do plants feel the heat? Trends in biochemical sciences **37**, 118–125.

Mühlhaus T, Weiss J, Hemme D, Sommer F, Schroda M. 2011*a*. Quantitative Shotgun Proteomics Using a Uniform 15N-Labeled Standard to Monitor Proteome Dynamics in Time Course Experiments Reveals New Insights into the Heat Stress Response of Chlamydomonas reinhardtii. Molecular & Cellular Proteomics **10**, M110.004739.

Mühlhaus T, Weiss J, Hemme D, Sommer F, Schroda M. 2011*b*. Quantitative shotgun proteomics using a uniform ^{15}N-labeled standard to monitor proteome dynamics in time course experiments reveals new insights into the heat stress response of *Chlamydomonas reinhardtii*. Molecular & cellular proteomics: MCP **10**, M110.004739.

Munekage Y, Hashimoto M, Miyake C, Tomizawa K-I, Endo T, Tasaka M, Shikanai T. 2004. Cyclic electron flow around photosystem I is essential for photosynthesis. Nature **429**, 579–582.

Murata N, Nishiyama Y. 2018. ATP is a driving force in the repair of photosystem II during photoinhibition. Plant, cell & environment **41**, 285–299.

Niemeyer J, Scheuring D, Oestreicher J, Morgan B, Schroda M. 2021. Real-time monitoring of subcellular H2O2 distribution in *Chlamydomonas reinhardtii*. The Plant cell.

Olas JJ, Apelt F, Annunziata MG, John S, Richard SI, Gupta S, Kragler F, Balazadeh S, Mueller-Roeber B. 2021. Primary carbohydrate metabolism genes participate in heat-stress memory at the shoot apical meristem of Arabidopsis thaliana. Molecular plant **14**, 1508–1524.

Ortiz-Bobea A, Wang H, Carrillo CM, Ault TR. 2019. Unpacking the climatic drivers of US agricultural yields. Environmental research letters: ERL [Web site] **14**, 064003.

Porra RJ, Thompson WA, Kriedemann PE. 1989. Determination of accurate extinction coefficients and simultaneous equations for assaying chlorophylls a and b extracted with four different solvents: verification of the concentration of chlorophyll standards by atomic absorption spectroscopy. Biochimica et Biophysica Acta (BBA) - Bioenergetics **975**, 384–394.

Pospíšil P. 2016. Production of reactive oxygen species by photosystem II as a response to light and temperature stress. Frontiers in plant science **7**, 1950.

Pröschold T, Harris EH, Coleman AW. 2005. Portrait of a species: *Chlamydomonas reinhardtii*. Genetics **170**, 1601–1610.

Remans T, Keunen E, Bex GJ, Smeets K, Vangronsveld J, Cuypers A. 2014. Reliable gene expression analysis by reverse transcription-quantitative PCR: reporting and minimizing the uncertainty in data accuracy. The Plant cell **26**, 3829–3837.

Roach T, Sedoud A, Krieger-Liszkay A. 2013. Acetate in mixotrophic growth medium affects photosystem II in Chlamydomonas reinhardtii and protects against photoinhibition. Biochimica et Biophysica Acta (BBA) - Bioenergetics **1827**, 1183–1190.

Rollins JA, Habte E, Templer SE, Colby T, Schmidt J, von Korff M. 2013. Leaf proteome alterations in the context of physiological and morphological responses to drought and heat stress in barley (Hordeum vulgare L.). Journal of experimental botany **64**, 3201–3212.

Rütgers M, Muranaka LS, Schulz-Raffelt M, Thoms S, Schurig J, Willmund F, Schroda M. 2017. Not changes in membrane fluidity but proteotoxic stress triggers heat shock protein expression in *Chlamydomonas reinhardtii*. Plant, cell & environment **40**, 2987–3001.

Sager R. 1955-7. Inheritance in the green alga *Chlamydomonas reinhardtii*. Genetics **40**, 476–489.

Sasso S, Stibor H, Mittag M, Grossman AR. 2018. From molecular manipulation of domesticated Chlamydomonas reinhardtii to survival in nature. eLife **7**, e39233.

Schloss JA. 1990. A *Chlamydomonas* gene encodes a G protein β subunit-like polypeptide. Molecular & general genetics: MGG **221**, 443–452.

Schmollinger S, Mühlhaus T, Boyle NR, *et al.* 2014. Nitrogen-sparing mechanisms in *Chlamydomonas* affect the transcriptome, the proteome, and photosynthetic metabolism. The Plant cell **26**, 1410–1435.

Schneider K, Venn B, Mühlhaus T. 2022. Plotly.net: A fully featured charting library for .NET programming languages. F1000Research **11**, 1094.

Schroda M, Hemme D, Mühlhaus T. 2015. The *Chlamydomonas* heat stress response. The Plant journal: for cell and molecular biology **82**, 466–480.

Schulz-Raffelt M, Lodha M, Schroda M. 2007. Heat shock factor 1 is a key regulator of the stress response in *Chlamydomonas*. The Plant journal: for cell and molecular biology **52**, 286–295.

Scranton MA, Ostrand JT, Fields FJ, Mayfield SP. 2015. *Chlamydomonas* as a model for biofuels and bio-products production. The Plant journal: for cell and molecular biology **82**, 523–531.

Shimogawara K, Fujiwara S, Grossman A, Usuda H. 1998. High-efficiency transformation of *Chlamydomonas reinhardtii* by electroporation. Genetics **148**, 1821–1828.

Sommer F, Kropat J, Malasarn D, Grossoehme NE, Chen X, Giedroc DP, Merchant SS. 2010. The CRR1 nutritional copper sensor in Chlamydomonas contains two distinct metal-responsive domains. The Plant cell **22**, 4098–4113.

Song Z-T, Zhang L-L, Han J-J, Zhou M, Liu J-X. 2021. Histone H3K4 methyltransferases SDG25 and ATX1 maintain heat-stress gene expression during recovery in Arabidopsis. The Plant journal: for cell and molecular biology **105**, 1326–1338.

Strenkert D, Schmollinger S, Gallaher SD, *et al.* 2019. Multiomics resolution of molecular events during a day in the life of *Chlamydomonas*. Proceedings of the National Academy of Sciences of the United States of America **116**, 2374–2383.

Takano W, Hisabori T, Wakabayashi K-I. 2021. Rapid estimation of cytosolic ATP concentration from the ciliary beating frequency in the green alga Chlamydomonas reinhardtii. The Journal of biological chemistry **296**, 100156.

Usadel B, Poree F, Nagel A, Lohse M, Czedik-Eysenberg A, Stitt M. 2009. A guide to using MapMan to visualize and compare Omics data in plants: a case study in the crop species, Maize. Plant, cell & environment **32**, 1211–1229.

Venn B, Mühlhaus T. 2022. CSBiology/OntologyEnrichment: Release 0.0.1 (0.0.1). Zenodo. https://doi.org/10.5281/zenodo.6340412.

Venn B, Weil L, Schneider K, Zimmer D, Mühlhaus T. 2022. fslaborg/FSharp.Stats. Zenodo. https://doi.org/10.5281/zenodo.6337056.

Vítová M, Bišová K, Hlavová M, Kawano S, Zachleder V, Cížková M. 2011. *Chlamydomonas reinhardtii*: duration of its cell cycle and phases at growth rates affected by temperature. Planta **234**, 599–608.

Voß B, Meinecke L, Kurz T, Al-Babili S, Beck CF, Hess WR. 2010. Hemin and Magnesium-Protoporphyrin IX Induce Global Changes in Gene Expression in Chlamydomonas reinhardtii. Plant physiology **155**, 892–905.

Vu LD, Gevaert K, De Smet I. 2019. Feeling the Heat: Searching for Plant Thermosensors. Trends in plant science **24**, 210–219.

Walker RP, Chen Z-H, Famiani F. 2021. Gluconeogenesis in Plants: A Key Interface between Organic Acid/Amino Acid/Lipid and Sugar Metabolism. Molecules **26**.

Wang L, Yang L, Wen X, Chen Z, Liang Q, Li J, Wang W. 2019. Rapid and high efficiency transformation of *Chlamydomonas reinhardtii* by square-wave electroporation. Bioscience reports **39**, BSR20181210.

Wulfert S, Schilasky S, Krueger S. 2020. Transcriptional and Biochemical Characterization of Cytosolic Pyruvate Kinases in Arabidopsis thaliana. Plants **9**.

Xiao L, Young EB, Grothjan JJ, Lyon S, Zhang H, He Z. 2015. Wastewater treatment and microbial communities in an integrated photo-bioelectrochemical system affected by different wastewater algal inocula. Algal Research **12**, 446–454.

Xie B, Bishop S, Stessman D, Wright D, Spalding MH, Halverson LJ. 2013. *Chlamydomonas reinhardtii* thermal tolerance enhancement mediated by a mutualistic interaction with vitamin B12-producing bacteria. The ISME journal **7**, 1544–1555.

Xu Z-S, Li Z-Y, Chen Y, Chen M, Li L-C, Ma Y-Z. 2012. Heat shock protein 90 in plants: molecular mechanisms and roles in stress responses. International journal of molecular sciences **13**, 15706–15723.

Yamori W, Shikanai T. 2016. Physiological functions of cyclic electron transport around Photosystem I in sustaining photosynthesis and plant growth. Annual review of plant biology **67**, 81–106.

Young EB, Reed L, Berges JA. 2022. Growth parameters and responses of green algae across a gradient of phototrophic, mixotrophic and heterotrophic conditions. PeerJ **10**, e13776.

Zachleder V, Ivanov I, Vítová M, Bišová K. 2019. Cell cycle arrest by supraoptimal temperature in the alga *Chlamydomonas reinhardtii*. Cells **8**, 1237.

Zhang N, Mattoon EM, McHargue W, *et al.* 2022*a*. Systems-wide analysis revealed shared and unique responses to moderate and acute high temperatures in the green alga Chlamydomonas reinhardtii. Communications biology **5**, 460.

Zhang N, Pazouki L, Nguyen H, *et al.* 2022*b*. Comparative phenotyping of two commonly used Chlamydomonas reinhardtii background strains: CC-1690 (21gr) and CC-5325 (The CLiP mutant library background). Plants **11**, 585.

Zhang X, Rerksiri W, Liu A, Zhou X, Xiong H, Xiang J, Chen X, Xiong X. 2013. Transcriptome profile reveals heat response mechanism at molecular and metabolic levels in rice flag leaf. Gene **530**, 185–192.

Zhang M, Zhang S. 2022. Mitogen-activated protein kinase cascades in plant signaling. Journal of integrative plant biology **64**, 301–341.

Zones JM, Blaby IK, Merchant SS, Umen JG. 2015. High-resolution profiling of a synchronized diurnal transcriptome from *Chlamydomonas reinhardtii* reveals continuous cell and metabolic differentiation. The Plant cell **27**, 2743–2769.

Figures

Fig. 1.

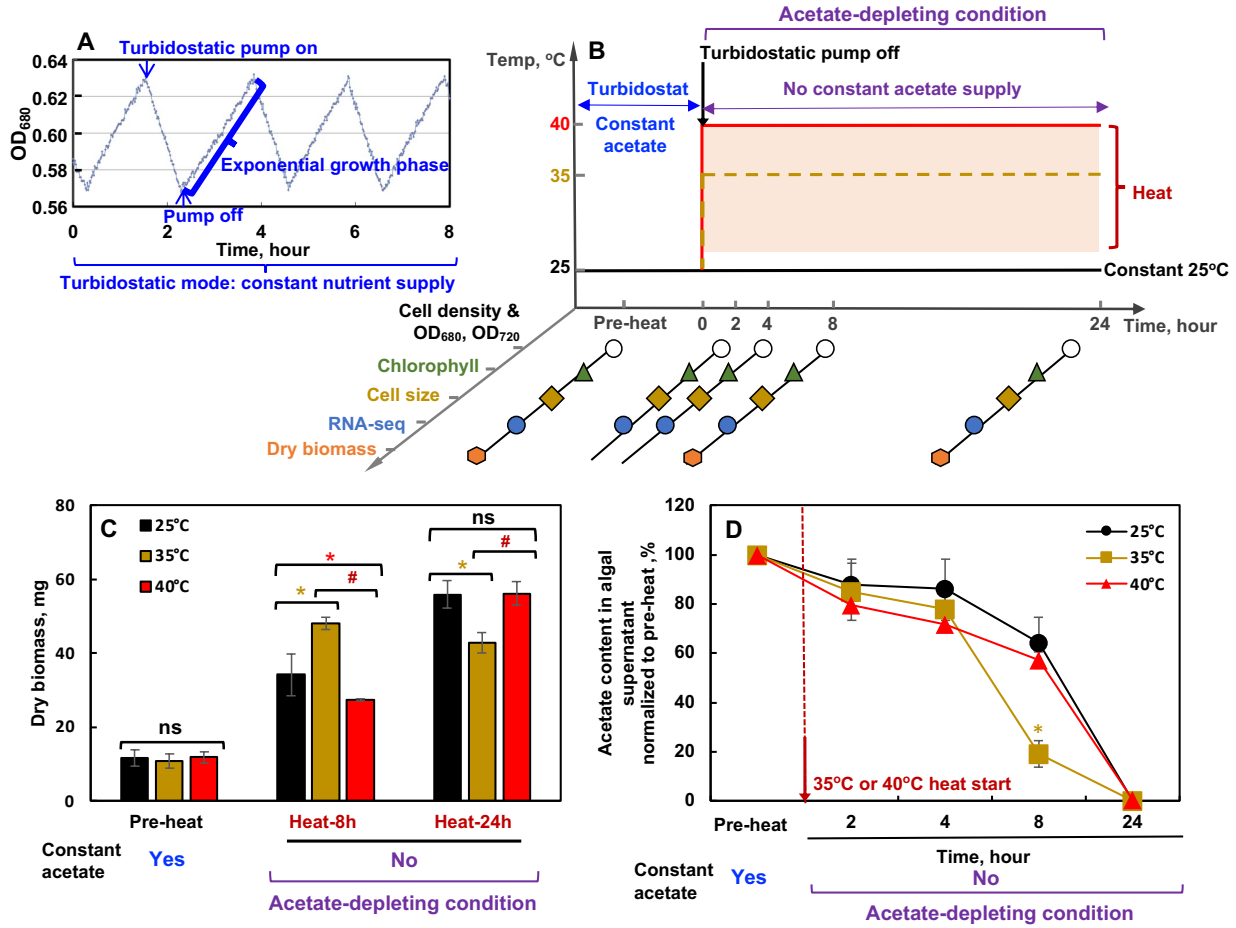

Fig. 1. Under the acetate-depleting condition, moderate high temperature of 35°C transiently increased but then decreased Chlamydomonas biomass accumulation. **(A)** Before heat treatments, Chlamydomonas cells (CC-1690, also called *21gr*, wild-type) were grown in photobioreactors (PBRs) in Tris-acetate-phosphate (TAP) medium (acetate as an organic carbon source) with a light intensity of 100 μmol photons m^{-2} s^{-1} and constantly bubbling of air. Algal cultures were maintained turbidostatically within a small range of OD_{680}, which monitors chlorophyll content (μg chlorophyll mL^{-1} cultures). When PBR cultures grew to the set maximum OD_{680}, pumps were turned on to add fresh medium and dilute the cultures to the set minimal OD_{680}, then pumps were turned off to allow for exponential growth to the maximum set OD_{680}. Figure cited and modified from a supplemental figure of this paper (Zhang *et al.*, 2022*a*). **(B)** Experimental outline for the acetate-depleting condition. The PBR cultures were first maintained at 25°C with constant

nutrient supply using the turbidostatic mode as mentioned above. After the cultures reached steady growth (pre-heat time point), the turbidostatic pumps were turned off and the cultures were grown under the indicated temperature for 24 hours (h) without fresh medium supply (thus no constant acetate supply, defined as the acetate-depleting condition). Algal cultures were harvested at different time points for the indicated parameters. Each temperature treatment was conducted in an individual PBR with at least 3 replicates. **(C)** Under the acetate-depleting condition, algal dry biomass increased with 8-h heat but decreased with 24-h heat of 35°C as compared to the constant 25°C. Mean ± SE, *n*=3-8 biological replicates. **(D)** Heat at 35°C accelerated acetate consumption. Algal cultures were harvested at different time points during the acetate-depleting condition and acetate content in algal supernatant was quantified using the Acetate Colorimetric Assay Kit. The red dashed line marks the start of heating at 35°C or 40°C or equivalent time point at the control 25°C. **(C, D)** Statistical analyses were performed using two-tailed t-test assuming unequal variance; *, $p<0.05$, the colors of the asterisks match the heated condition as compared to 25°C at the same time points; #, $p<0.05$, for the comparisons between 35°C and 40°C at the same time points. ns, not significant.

Fig. 2.

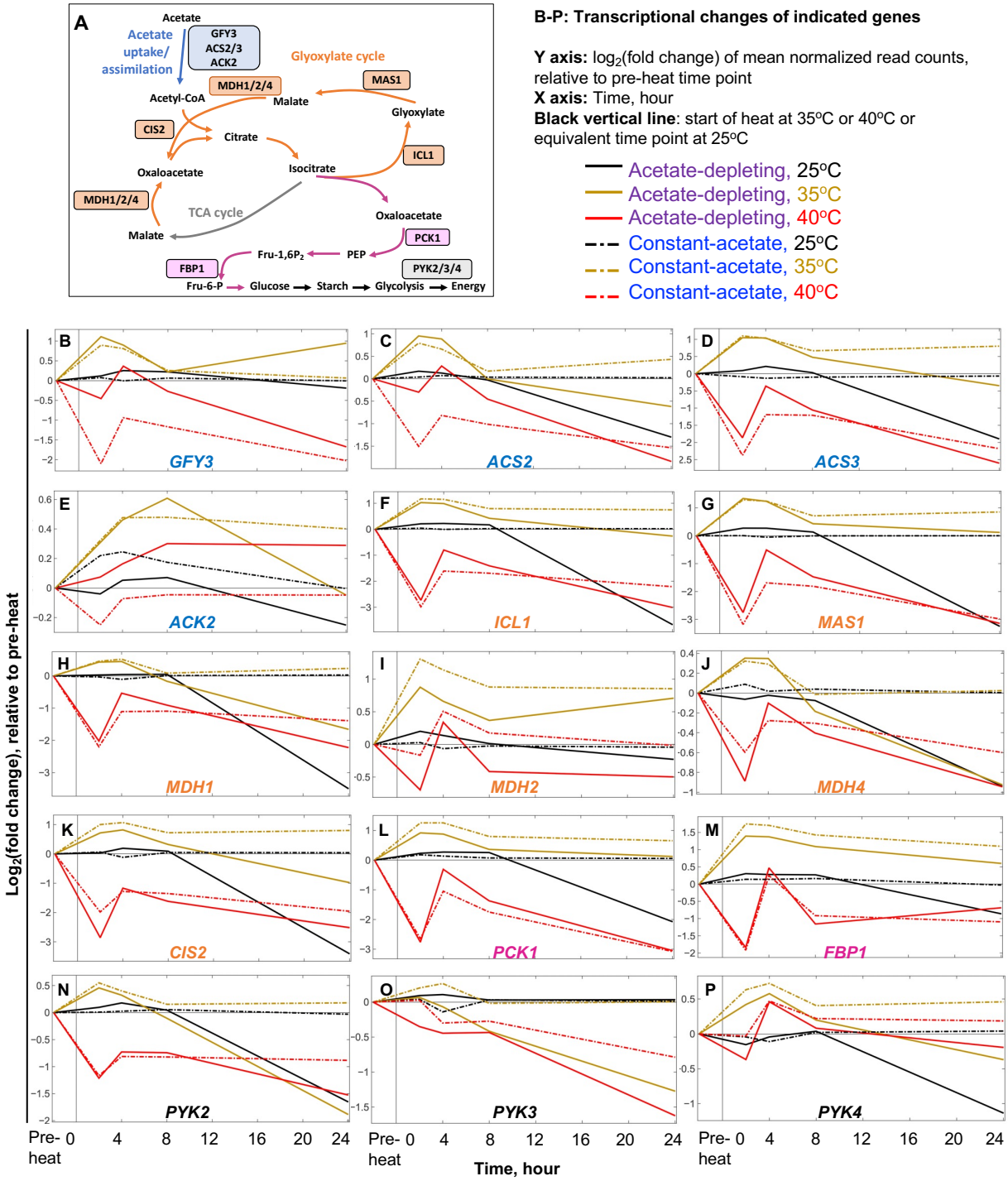

Fig. 2. Moderate high temperature of 35ºC up-regulated transcripts related to acetate uptake/assimilation, glyoxylate cycle, gluconeogenesis, and glycolysis pathways. (A) Simplified pathways of acetate uptake/assimilation, glyoxylate cycle,

gluconeogenesis, and glycolysis based on these papers (Johnson and Alric 2013; Durante et al. 2019). Key enzymes are in boxes and were analyzed via RNA-seq in panels B-P. Acetate uptake/assimilation enzymes: GFY3, putative acetate transporter; ACS2/3, acetyl-CoA synthases; ACK2, acetate kinase. Glyoxylate cycle key enzymes: ICL1, isocitrate lyase; MAS1, malate synthase; CIS2, Citrate synthase; MDH1/2/4, NAD-dependent malate dehydrogenases. Gluconeogenesis key enzymes: PCK1, phosphoenolpyruvate carboxykinase; FBP1, fructose-1,6-bisphosphatase. Glycolysis key enzymes: PYK2/3/4, pyruvate kinase 2/3/4. See all gene IDs and annotations in Supplementary Table 1. PEP, phosphoenolpyruvate. Fru-6-P, fructose-6-phosphate. Fru-1,6-P_2, fructose-1,6-bisphosphate. **(B-P)** Transcriptional change of the indicated genes under six different conditions, presented as $\log_2$(fold change) of mean normalized read counts relative to the pre-heat time point. In each panel, each line represents the transcriptional time course of the indicated gene under one condition as indicated by the legend. Solid lines for the acetate-depleting condition and dashed lines for the constant-acetate condition. Black, brown, red lines for 25°C, 35°C, and 40°C temperature treatments, respectively. See Supplemental Dataset 1 for bigger pictures and more information.

Fig. 3.

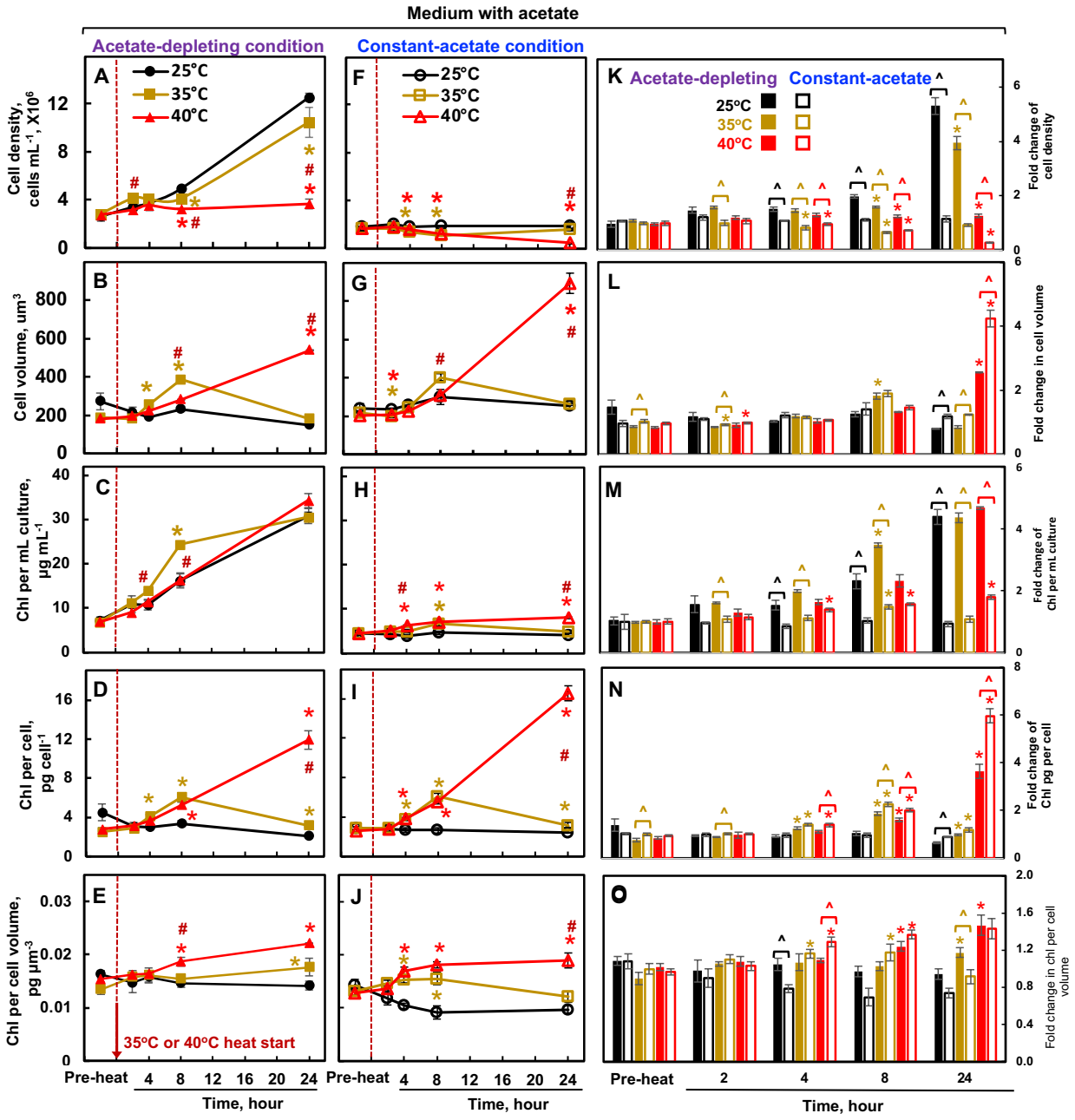

Fig. 3. Algal cell physiologies with different temperature treatments under the acetate-depleting condition were compared with those under the constant-acetate condition. (A-E) Cell parameters from algal cultures under the acetate-depleting condition. The algal cultivation and heat treatments were the same as in Fig. 1B. **(F-J)** Cell parameters from algal cultures under the constant-acetate condition, with constant acetate supply via turbidostatic mode, data plotted based on the results from this paper

(Zhang *et al.*, 2022*a*). (**A-J**) Two panels on the same row share the same y axis. The red dashed line marks the start of heat. **(K-O)** Fold change of the indicated cell parameters from algal cultures under the acetate-depleting condition (filled bars) and under the constant-acetate condition (empty bars). (**A-O**) Mean ± SE, n = 3-7 biological replicates. Statistical analyses were performed with two-tailed t-test assuming unequal variance; *, $p<0.05$, for the comparisons between 35°C or 40°C with 25°C at the same time point under the same acetate condition, the colors of the asterisks match the heat condition; #, $p<0.05$, for the comparisons between 35°C and 40°C at the same time point under the same acetate condition; ^, $p<0.05$, for the comparisons between the acetate-depleting and constant-acetate conditions at the same time point and under the same temperature. **(D, E, I, J)** Cell parameters at different time points during constant 25°C had little change, not significantly different from the pre-heat time points ($p>0.05$).

Fig. 4.

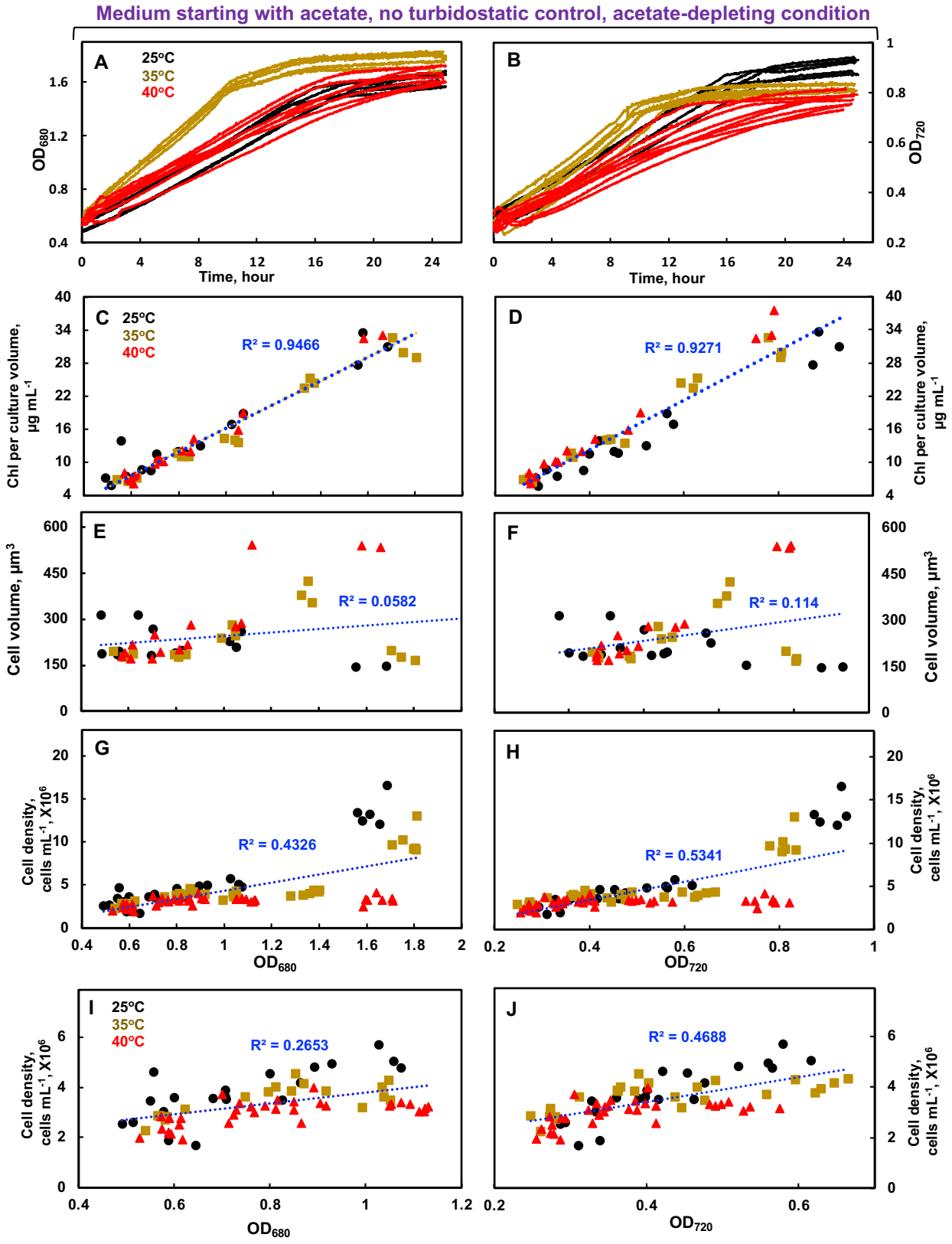
Medium starting with acetate, no turbidostatic control, acetate-depleting condition
A
25°C
35°C
40°C
OD680
Time, hour
B
OD720
Time, hour
C
R² = 0.9466
Chl per culture volume, µg mL-1
D
R² = 0.9271
E
R² = 0.0582
Cell volume, µm3
F
R² = 0.114
G
R² = 0.4326
Cell density, cells mL-1, X10^6
OD680
H
R² = 0.5341
OD720
I
R² = 0.2653
J
R² = 0.4688

Fig. 4. Both OD_{680} and OD_{720} were linearly proportional to chlorophyll contents under different temperatures and can be used to estimate algal growth rates. Black, brown, red lines/symbols represent 25°C, 35°C, and 40°C treatments, respectively. **(A, B)** OD_{680} and OD_{720} automatically monitored algal growth every one min in algal cultures grown in photobioreactors with different temperatures under the acetate-depleting conditions (medium starting with acetate but no turbidostatic control when heat started). The algal cultivation and heat treatments were the same as in Fig. 1B. Multiple lines with the same colors represent biological replicates (n= 4-8) under the same condition. **(C-J)** OD_{680} and OD_{720} were linearly proportional to Chlorophyll (Chl) contents per mL cultures but not cell volume or cell density. Chl contents (**C, D**), cell volume (**E, F**), and cell densities (**G-J**) were plotted against OD_{680} or OD_{720} readings in algal cultures with different treatments mentioned above. Dashed blue lines are linear trendlines of best fit and R-squared values are displayed. **(I, J)** The same data as in panel G-H but with smaller ranges for X values.

Fig. 5.

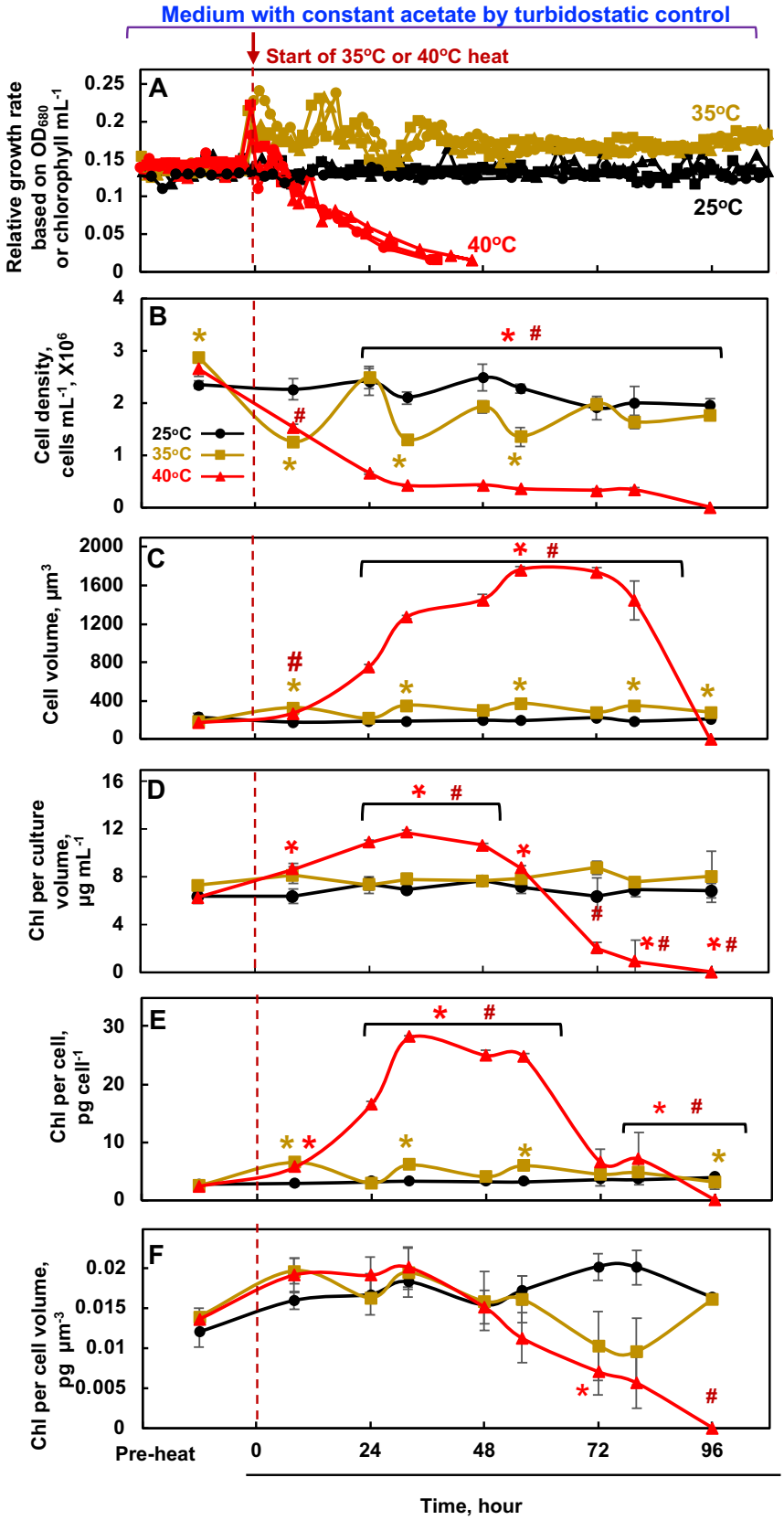
Medium with constant acetate by turbidostatic control
Start of 35°C or 40°C heat
A
Relative growth rate based on OD680 or chlorophyll mL-1
35°C
25°C
40°C
B
Cell density, cells mL-1, X10^6
25°C
35°C
40°C
C
Cell volume, µm3
D
Chl per culture volume, µg mL-1
E
Chl per cell, pg cell-1
F
Chl per cell volume, pg µm-3
Pre-heat
0
24
48
72
96
Time, hour

Fig. 5. Under the constant-acetate condition with turbidostatic control, moderate (35ºC) and acute high temperatures (40ºC) increased and reduced algal growth during 4-day heating, respectively. Black, brown, red lines/symbols represent 25ºC, 35ºC, and 40ºC treatments, respectively. The red dashed lines mark the start of heat at 35ºC or 40ºC. **(A)** Chlamydomonas cultures were grown in photobioreactors (PBRs) under turbidostatic conditions at different temperatures in acetate-containing medium. Algal cultures were first acclimated at 25ºC for 4 days before the temperature was switched to 35ºC or 40ºC or stayed at 25ºC for 4 days. Relative growth rates were calculated based on the cycling of OD_{680} caused by the turbidostatic control (see Fig. 1A and method for details). Each temperature treatment had 3 biological replicates in separate PBRs. **(B-F)** Cell parameters were quantified from algal cultures harvested at different time points with different treatments. Statistical analyses were performed with two-tailed t-test assuming unequal variance by comparing 35ºC or 40ºC with 25ºC at the same time point. *, $p<0.05$, the colors of the asterisks match the heat condition; #, $p<0.05$, for the comparisons between 35ºC and 40ºC at the same time point. Chl, Chlorophyll.

Fig. 6.

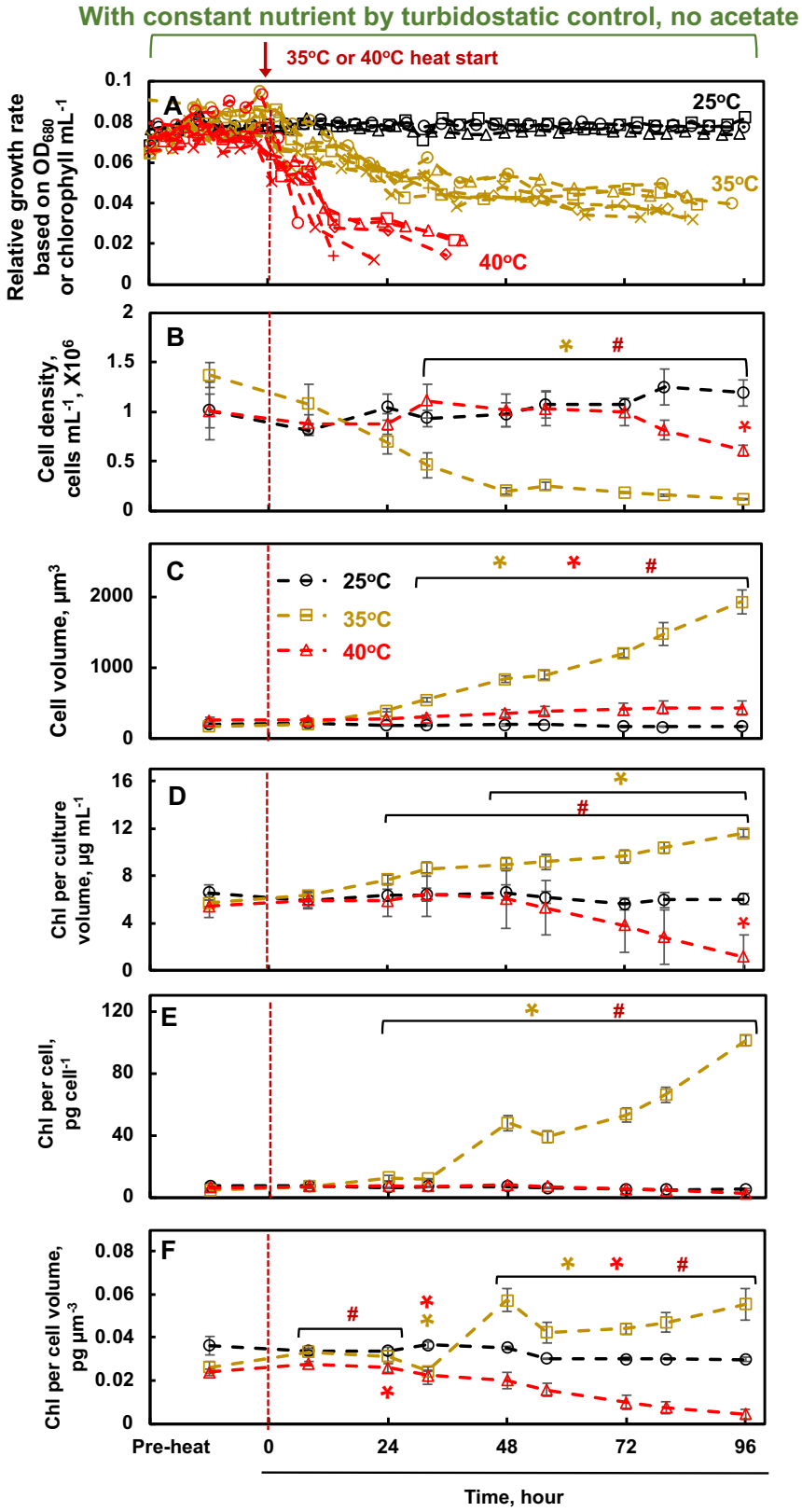
With constant nutrient by turbidostatic control, no acetate
35°C or 40°C heat start
A
25°C
35°C
40°C
Relative growth rate based on OD680 or chlorophyll mL-1
B
Cell density, cells mL-1, X10^6
C
Cell volume, µm3
D
Chl per culture volume, µg mL-1
E
Chl per cell, pg cell-1
F
Chl per cell volume, pg µm-3
Pre-heat
0
24
48
72
96
Time, hour

Fig. 6. Under the no-acetate condition (photoautotrophic medium) with turbidostatic control, both moderate (35°C) and acute high temperatures (40°C) reduced algal growth during 4-day heating. Black, brown, red lines/symbols represent 25°C, 35°C, and 40°C treatments, respectively. The red dashed lines mark the start of heat at 35°C or 40°C. **(A)** Chlamydomonas cultures were grown in photobioreactors (PBRs) under turbidostatic conditions at different temperatures in photoautotrophic medium without acetate. Algal cultures were first acclimated at 25°C for 4 days before the temperature was switched to 35°C or 40°C or stayed at 25°C for 4 days. Relative growth rates were calculated based on the cycling of OD_{680} caused by the turbidostatic control (see Fig. 1A and method for details). Each temperature treatment had at least 3 biological replicates in separate PBRs. **(B-F)** Cell parameters were quantified from algal cultures harvested at different time points with different treatments. Statistical analyses were performed with two-tailed t-test assuming unequal variance by comparing 35°C or 40°C with 25°C at the same time point. *, $p<0.05$, the colors of the asterisks match the heat condition; #, $p<0.05$, for the comparisons between 35°C and 40°C at the same time point. Chl, Chlorophyll.

Fig. 7

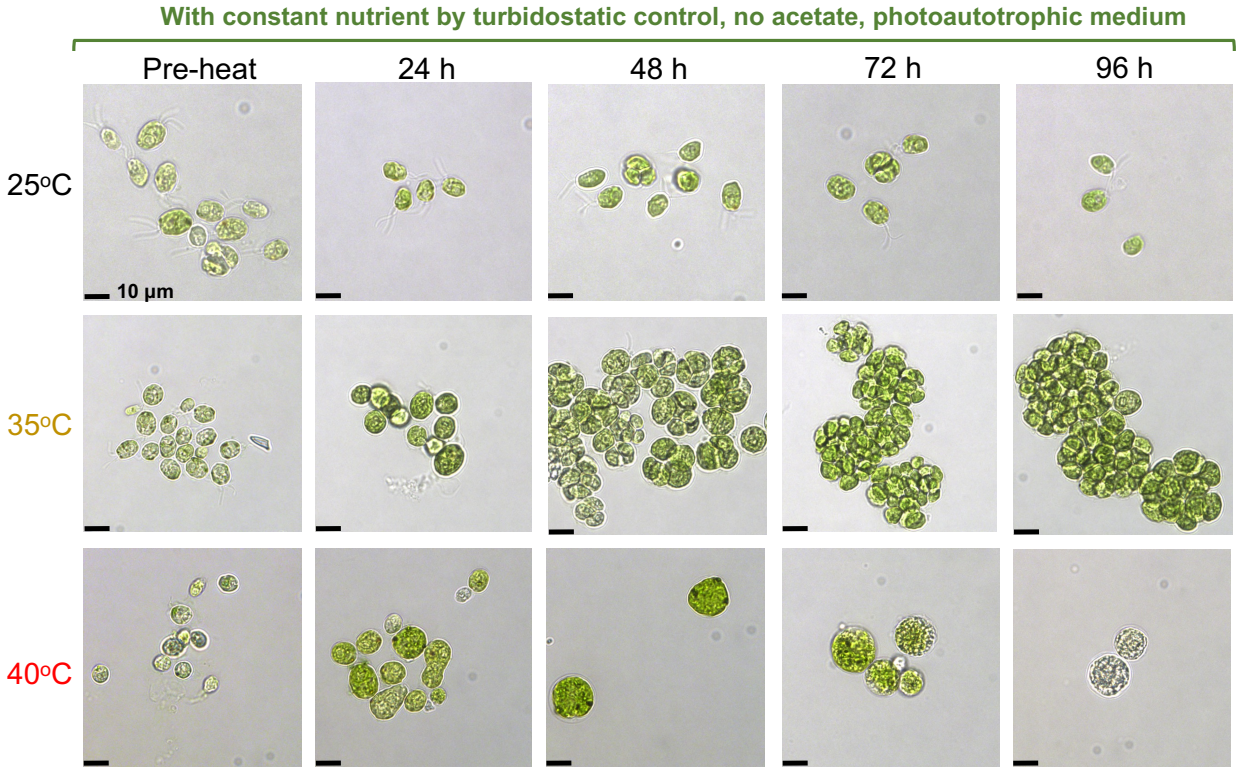

Fig. 7. Under the no-acetate condition (photoautotrophic medium) with turbidostatic control, 35°C-treated cells formed palmelloids and 40°C-treated cells were bleached after 4-day heat treatments. Light microscopic images of Chlamydomonas cells under different conditions. The algal cultivation and heat treatments were the same as in Fig. 6. Images shown are representative results from three biological replicates. Black scale bar on each panel represents 10 µm.

Fig. 8

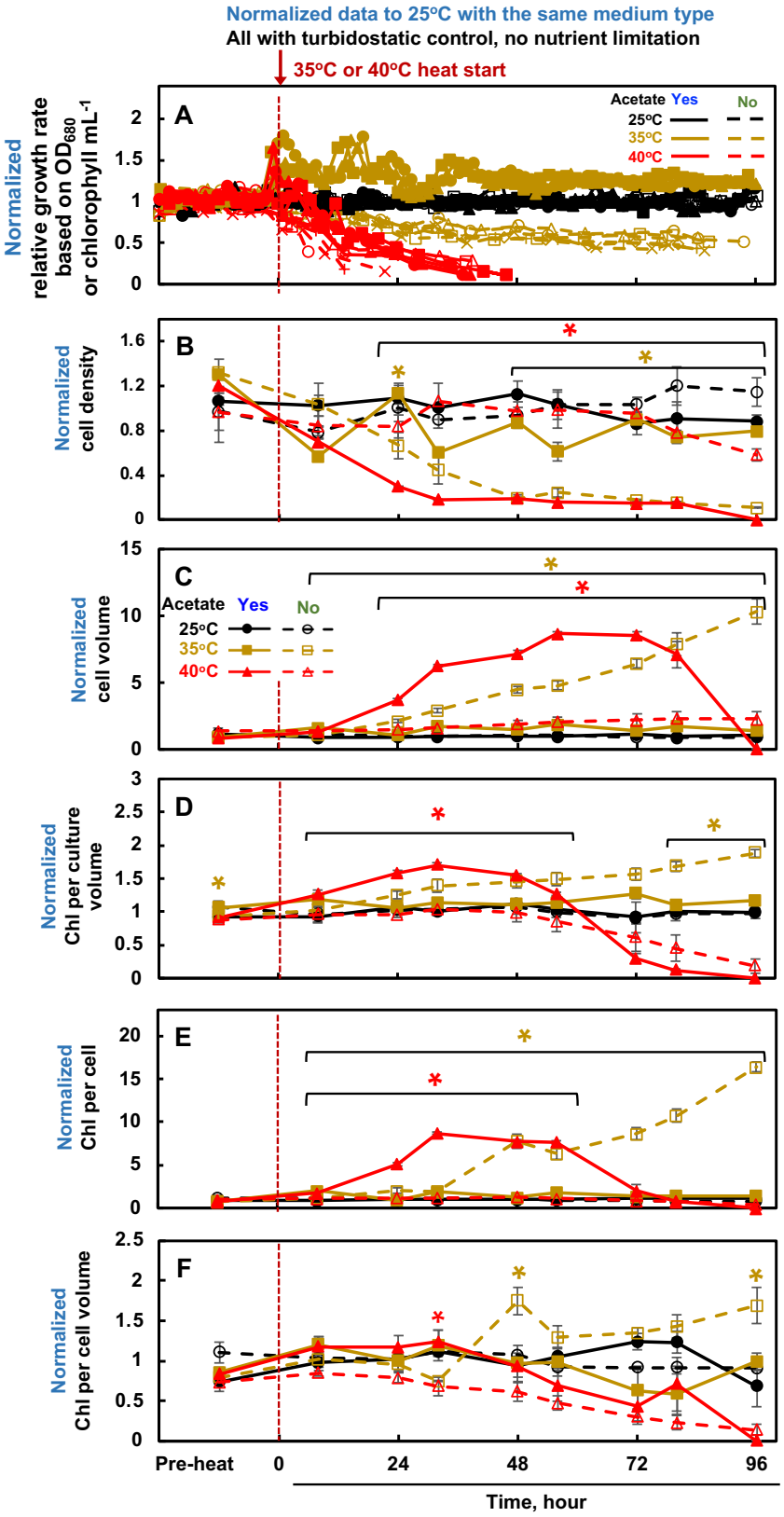
Normalized data to 25°C with the same medium type
All with turbidostatic control, no nutrient limitation
35°C or 40°C heat start
A
Normalized relative growth rate based on OD680 or chlorophyll mL-1
Acetate Yes No
25°C
35°C
40°C
B
Normalized cell density
C
Normalized cell volume
D
Normalized Chl per culture volume
E
Normalized Chl per cell
F
Normalized Chl per cell volume
Pre-heat
0
24
48
72
96
Time, hour

Fig. 8. Under the turbidostatic control without nutrient limitation, moderate high temperatures (35°C) increased algal growth rates with constant acetate but reduced algal growth rates without acetate. Plotted data were from Fig. 5 and 6 but were normalized to the corresponding controls at the 25°C with the same medium type to compare the relative effects of high temperatures with (filled symbols and solid lines) and without (open symbols and dashed lines) acetate. Black, brown, red lines/symbols represent 25°C, 35°C, and 40°C treatments, respectively. The red dashed lines mark the start of heat at 35°C or 40°C. **(A)** Chlamydomonas cultures were grown in photobioreactors (PBRs) under turbidostatic conditions at different temperatures with and without acetate. Algal cultures were first acclimated at 25°C for 4 days before the temperature was switched to 35°C or 40°C or stayed at 25°C for 4 days. Relative growth rates were calculated based on the cycling of OD_{680} caused by the turbidostatic control (see Fig. 1A and method for details), normalized to the corresponding controls at the 25°C with the same medium type. Each temperature treatment had at least 3 biological replicates in separate PBRs. **(B-F)** Cell parameters were quantified from algal cultures harvested at different time points with different treatments, normalized to the corresponding controls at the 25°C with the same medium type. Statistical analyses were performed with two-tailed t-test assuming unequal variance by comparing the data with and without acetate under the same high temperature treatment. *, $p<0.05$, the colors of the asterisks match the heat condition, brown asterisks for 35°C and red asterisks for 40°C comparisons. Chl, Chlorophyl.

Fig. 9

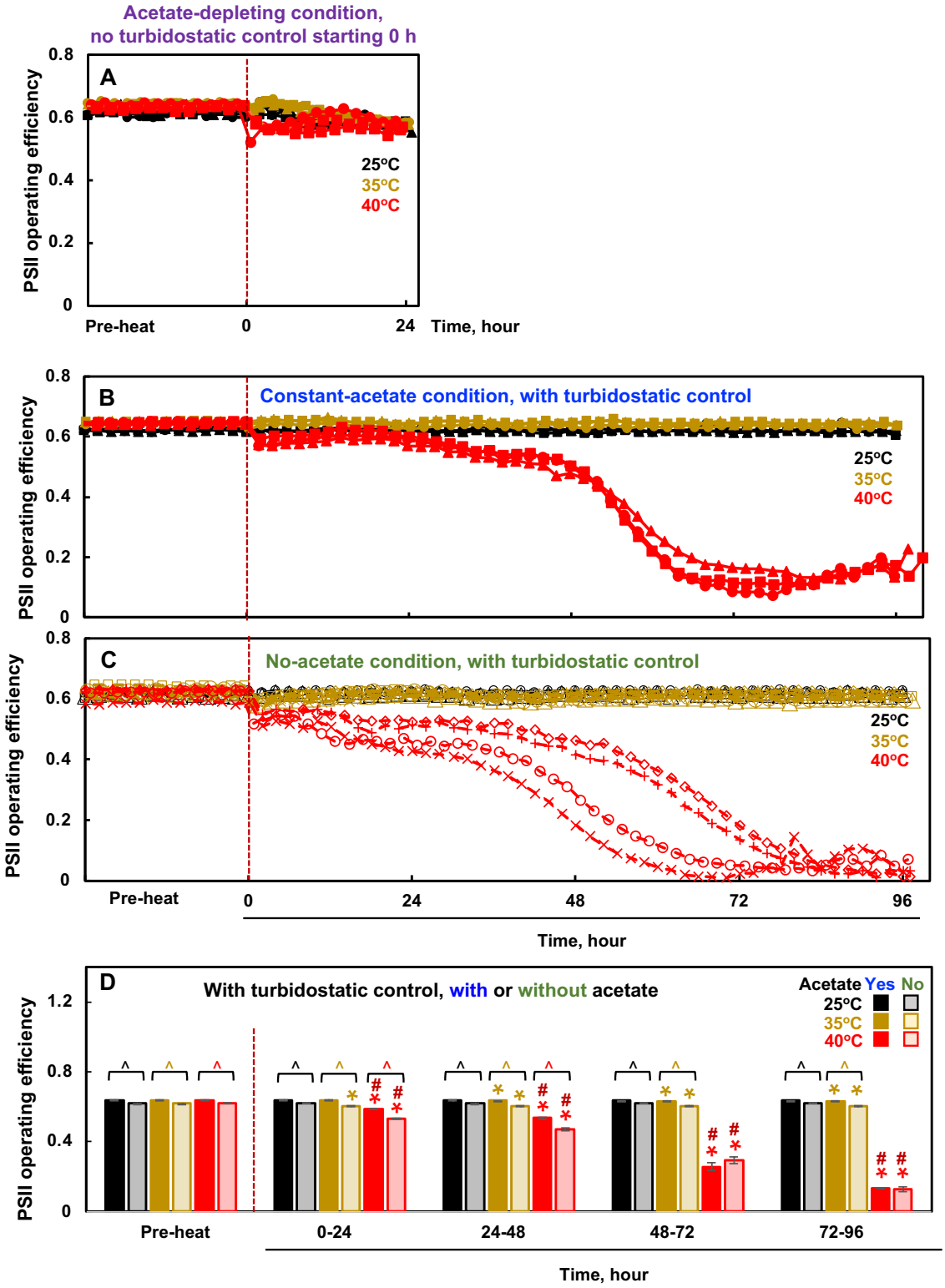
Acetate-depleting condition,
no turbidostatic control starting 0 h
A
PSII operating efficiency
0.8
0.6
0.4
0.2
0
25°C
35°C
40°C
Pre-heat
0
24
Time, hour
B
Constant-acetate condition, with turbidostatic control
C
No-acetate condition, with turbidostatic control
48
72
96
Time, hour
D
With turbidostatic control, with or without acetate
Acetate Yes No
1.2
Pre-heat
0-24
24-48
48-72
72-96
Time, hour

Fig. 9. Under the turbidostatic control and no nutrient limitation, algal cultures had higher photosystem II (PSII) operating efficiency with acetate than without acetate during treatment of 25°C, 35°C, or 40°C, although the acetate effects diminished after 2-day heat of 40°C due to cell death. PSII operating efficiency was measured automatically in photobioreactors under different conditions. Black, brown, red lines/symbols represent 25°C, 35°C, and 40°C treatments, respectively. The red dashed lines mark the start of heat at 35°C or 40°C. **(A)** Acetate-depleting condition at 25°C, 35°C, or 40°C for 24 h, in medium started with acetate but no turbidostatic control, thus no constant acetate supply. **(B)** Constant-acetate condition at 25°C, 35°C, or 40°C for 4 days, in medium with acetate and turbidostatic control, thus no nutrient limitation. **(C)** No-acetate condition at 25°C, 35°C, or 40°C for 4 days, in photoautotrophic medium without acetate but with turbidostatic control, thus no nutrient limitation. **(D)** The comparison of PSII operating efficiency in the constant-acetate (data from panel B, darker color bars) and no-acetate (data from panel C, light color bars) conditions during the indicated periods at 25°C, 35°C, or 40°C for 4 days. Statistical analyses were performed with two-tailed t-test assuming unequal variance by comparing the indicated groups. *, $p<0.05$, comparing 35°C or 40°C with 25°C with the same medium type at the same time; #, $p<0.05$, for the comparisons between 35°C and 40°C with the same medium type at the same time; ^, $p<0.05$, for the comparisons between the same temperature treatment at the same time but with and without acetate. The colors of the significant marks match the heat condition, brown for 35°C and bright red color for 40°C related comparisons, and dark red for 35°C/40°C comparisons.

Fig. 10.

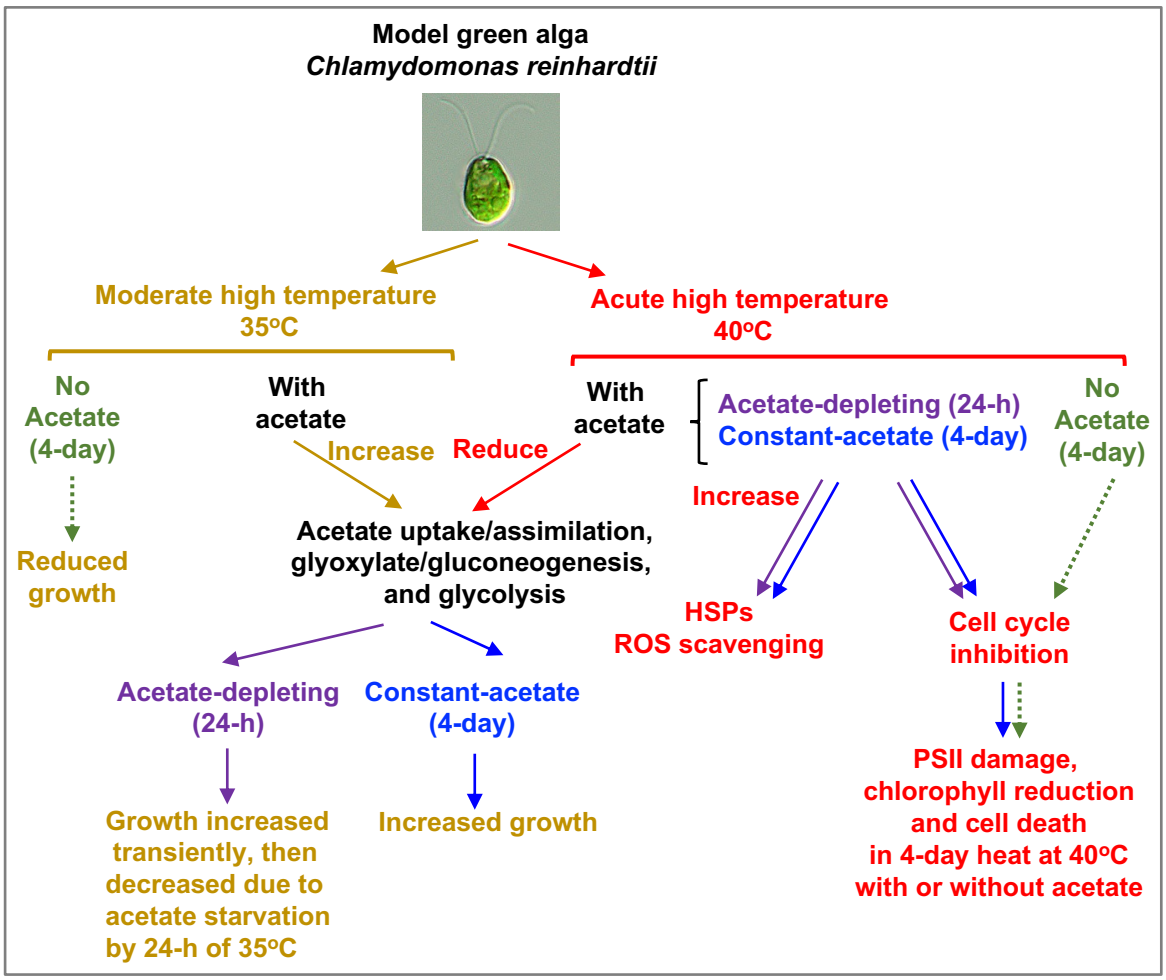

Fig. 10. Carbon (acetate) availability affected Chlamydomonas heat tolerance under the moderate high temperature (35°C), but acetate had much less effects under the acute high temperature (40°C). In medium containing the organic carbon source, acetate, heat of 35°C accelerated carbon metabolisms by upregulating transcripts related to acetate uptake/assimilation, glyoxylate cycle, gluconeogenesis, and glycolysis pathways. With constant acetate supply, 35°C increased algal growth. Under the acetate-depleting condition, 35°C increased algal growth transiently followed by decreased growth and biomass accumulation due to acetate starvation. Without acetate supply in photoautotrophic medium, 35°C reduced algal growth rates. Under either constant-acetate or depleting-acetate condition, heat of 40°C down-regulated transcripts related to acetate uptake, glyoxylate cycle, gluconeogenesis, and glycolysis pathways, but up-regulated transcripts related to heat shock proteins (HSPs) and reactive oxygen species

(ROS) scavenging. In medium with or without acetate, 40°C decreased algal growth rates, inhibited cell division, damaged PSII efficiency, reduced chlorophyll contents, and eventually led to cell death. Thus, Chlamydomonas cells could not survive continuous heat of 40°C for longer than 2-days, independent of acetate supply. Brown and red labels/lines represent the effects of 35°C and 40°C, respectively. Purple, blue, and green labels/lines represent the acetate-depleting, constant-acetate, and no-acetate conditions, respectively.

See supplemental figures below.

Supplemental Fig. 1.

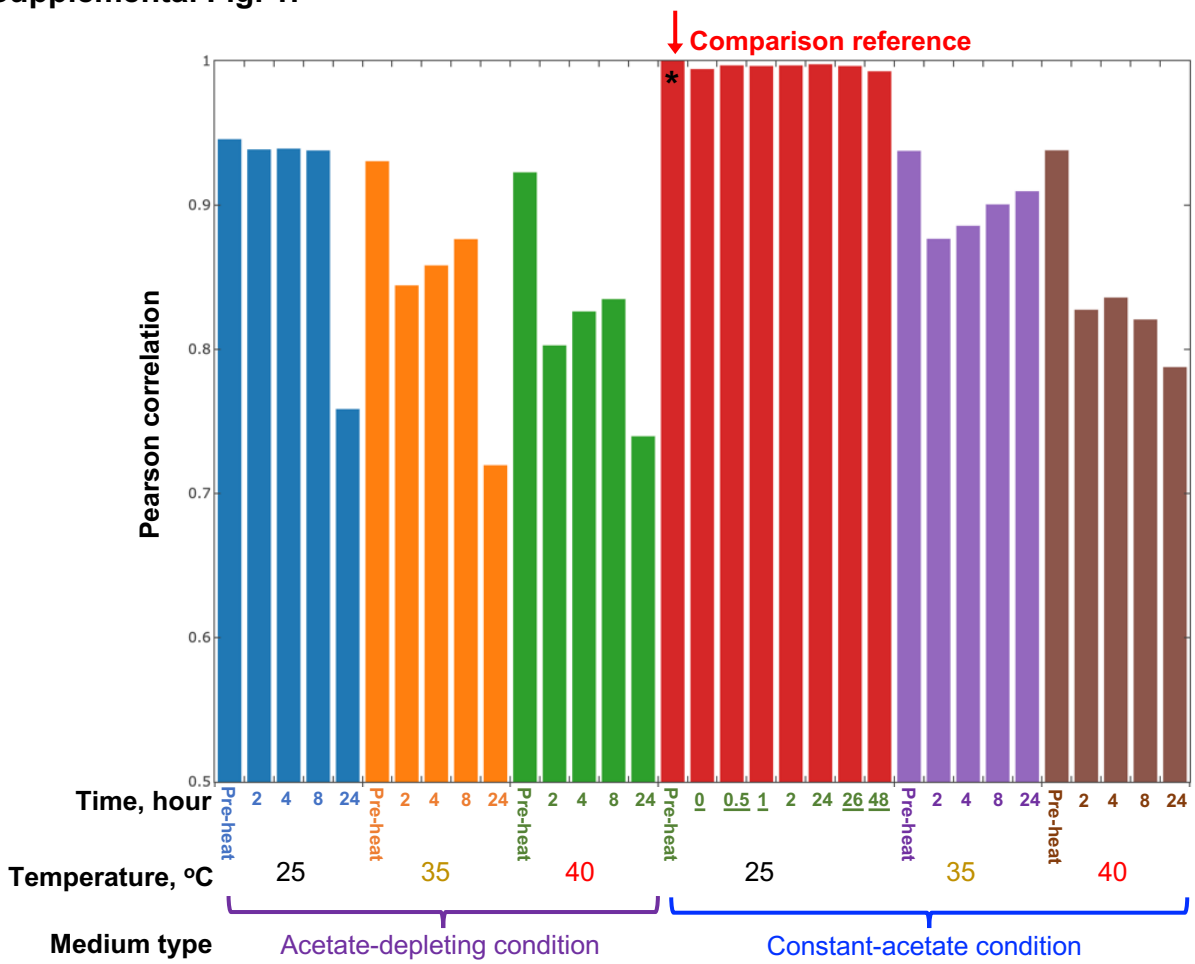

Supplemental Fig. 1. RNA-seq data from algal samples harvested from photobioreactors (PBRs) under the constant-acetate-25°C with turbidostatic control were highly correlated with each other. The Pearson correlations were generated by comparing all RNA-seq samples to the first sample (marked by *) of the constant-acetate-25°C condition. Under constant acetate, 25°C, and light (constant-acetate-25°C) with turbidostatic control in PBRs, the algal growth rates and cell physiologies stay constant (Fig. 5). We had RNA-seq data for 8 time points under the constant-acetate-25°C condition, and these samples were highly correlated with each other (with Pearson correlation ≥ 0.993). The 0 h of the constant-acetate-25°C condition corresponds to the time when PBRs reach expected high temperatures during heat treatments, which takes about 30 min from 25°C to 35°C or 40°C. All pre-heat samples were harvested from PBRs under the same constant-acetate-25°C condition with turbidostatic control and these RNA-seq samples had Pearson correlation > 0.95.

Because the cell status and transcriptome stay steady under the constant-acetate-25°C, we used the five extra time points under the constant-acetate-25°C condition (with underlines) to impute the 2 h and 4 h time points under the constant-acetate-25°C condition. See method for details.

Supplemental Fig. 2.

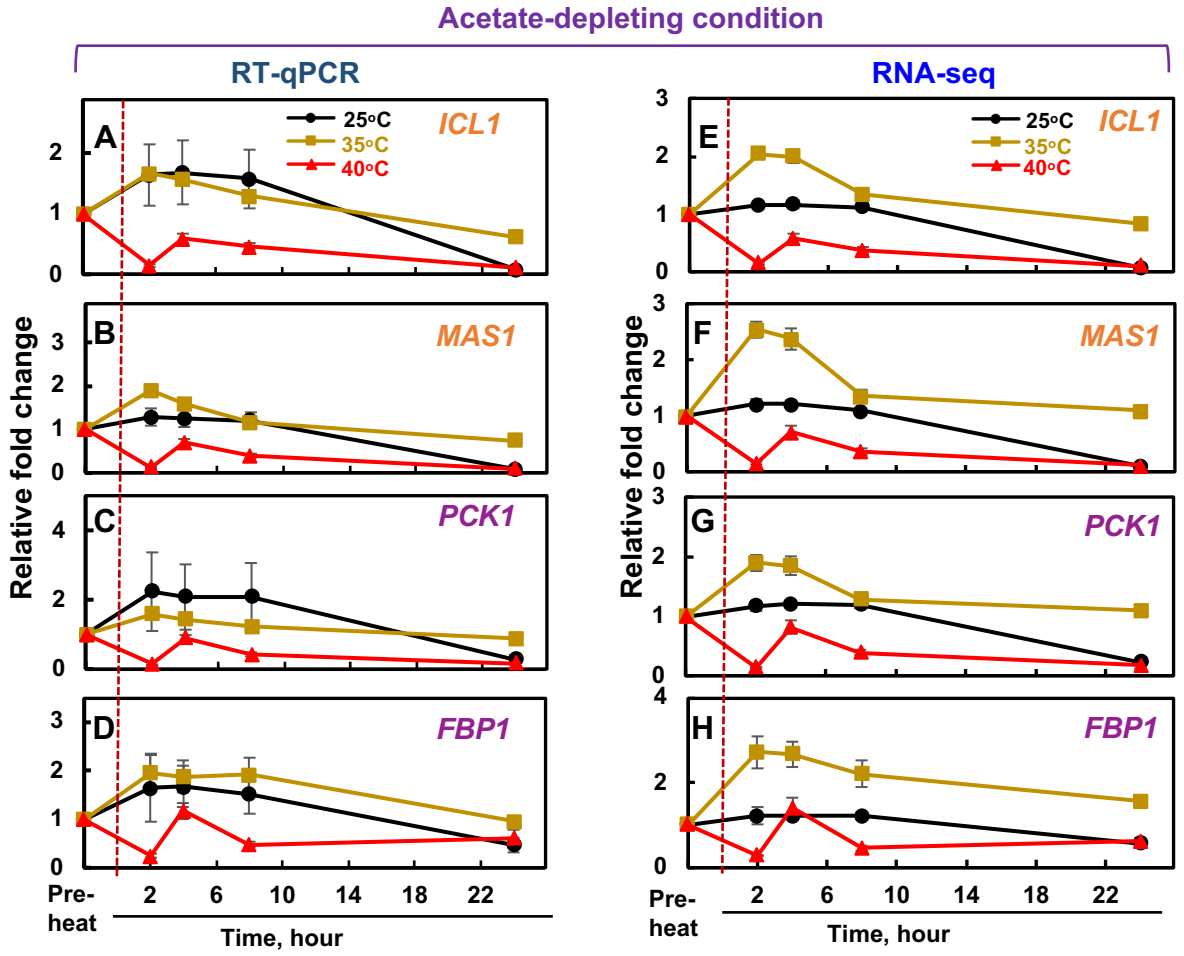

Supplemental Fig. 2. RT-qPCR analysis was consistent with RNA-seq results. Transcript fold-changes of four selected transcripts involved in the glyoxylate cycle (ICL1 and MAS1) and gluconeogenesis cycle (PCK1 and FBP1) as in Fig. 2A were calculated based on RT-qPCR (**A-D**) or RNA-seq (**E-H**) results. Red dashed lines represent the start of heat treatments. For RT-qPCR results, the relative fold changes were calculated by normalizing the transcript expression to the reference genes *CBLP*, *EIF1A* and the pre-heat level. For RNA-seq results, the relative fold changes were calculated based on normalized RNA-seq read counts relative to the pre-heat level. Values are mean ± SE, n = 3 biological replicates. Glyoxylate cycle key enzymes: ICL1, isocitrate lyase; MAS1, malate synthase. Gluconeogenesis key enzymes: PCK1, phosphoenolpyruvate carboxykinase; FBP1, fructose-1,6-bisphosphatase (See all gene IDs and RT-qPCR primers in Supplemental Table 1).

Supplemental Fig. 3

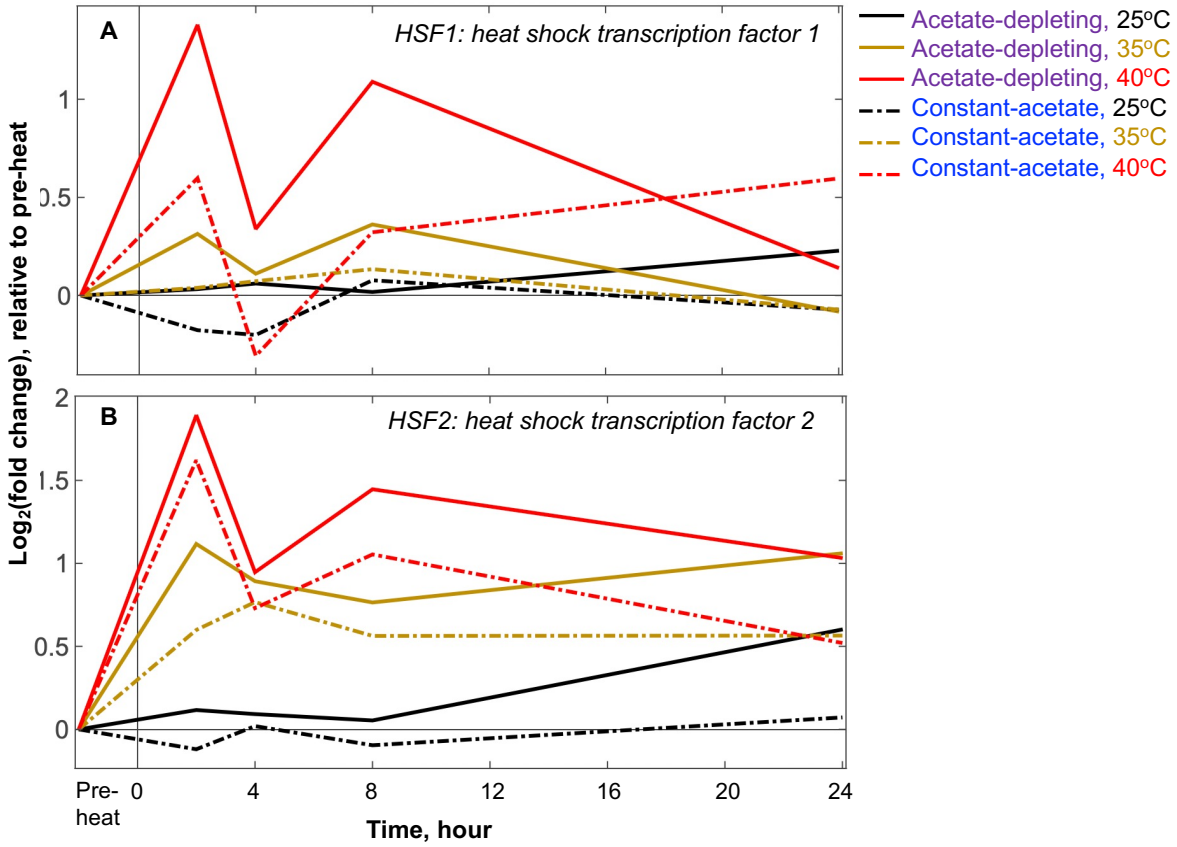

Supplemental Fig. 3 continued

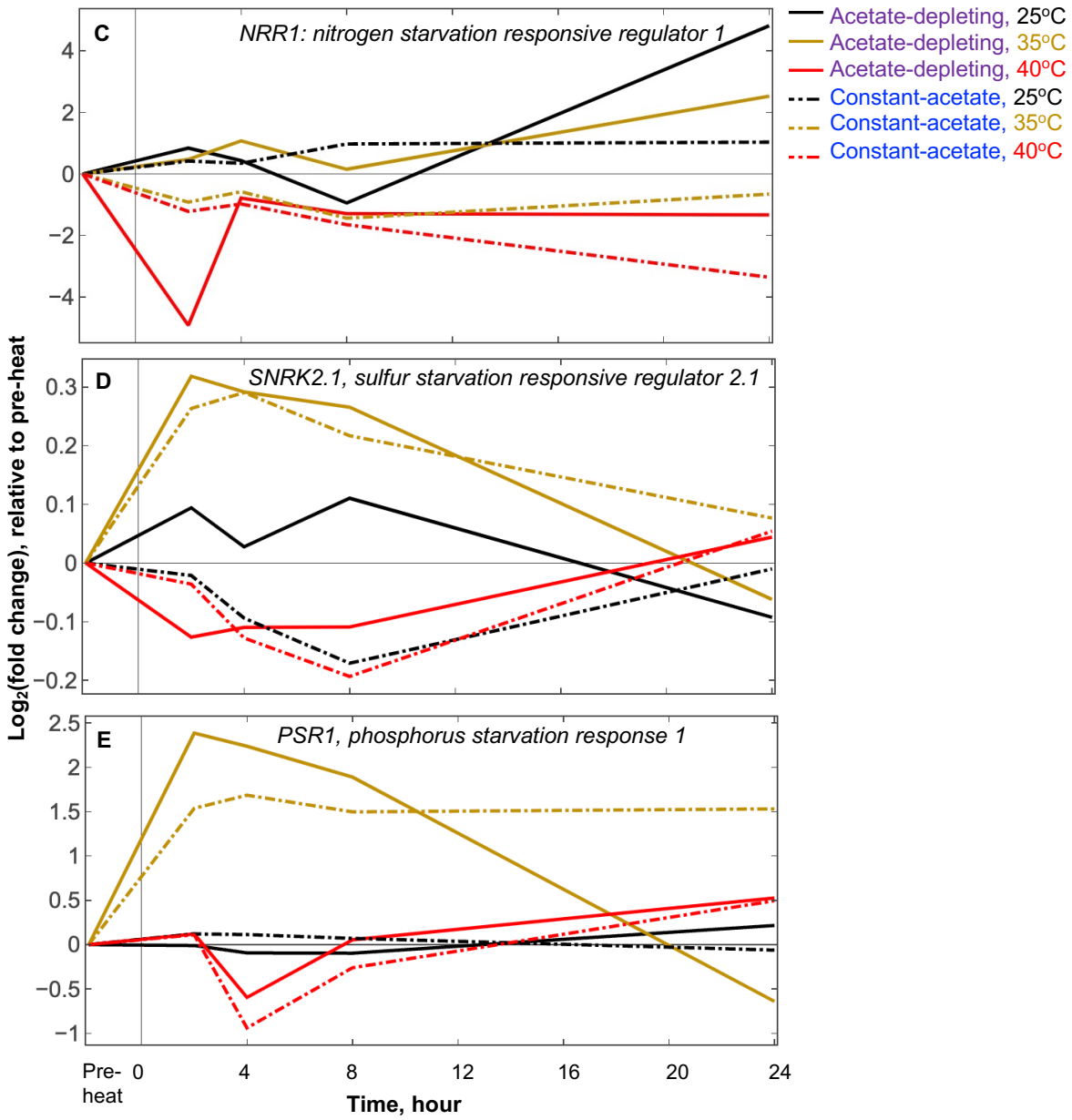

Supplemental Fig. 3 continued

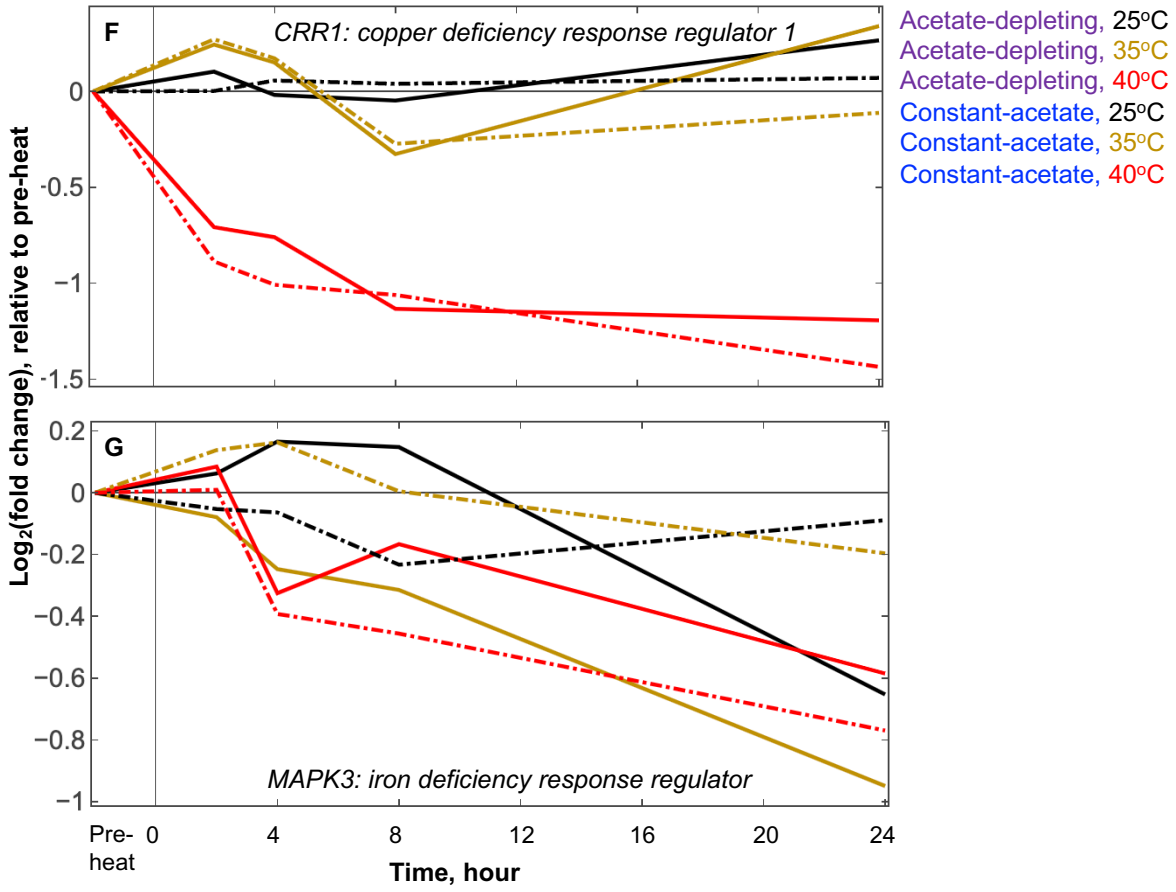

Supplemental Fig. 3. Log_2(fold change) of the indicated transcript relative to pre-heat under different conditions. Log_2(fold change) were determined on the mean normalized transcript abundance, relative to the pre-heat time point. Each line represents one condition as indicated by the legend. Solid lines for the acetate-depleting condition and dashed lines for the constant-acetate condition. Black, brown, red lines for 25°C, 35°C, and 40°C temperature treatments, respectively. See all gene IDs in Supplemental Table 1 and Supplemental Dataset 1 for bigger pictures and more information.

Supplemental Fig. 4.

A. Transcripts related to HSP60s (HSP, heat shock protein)

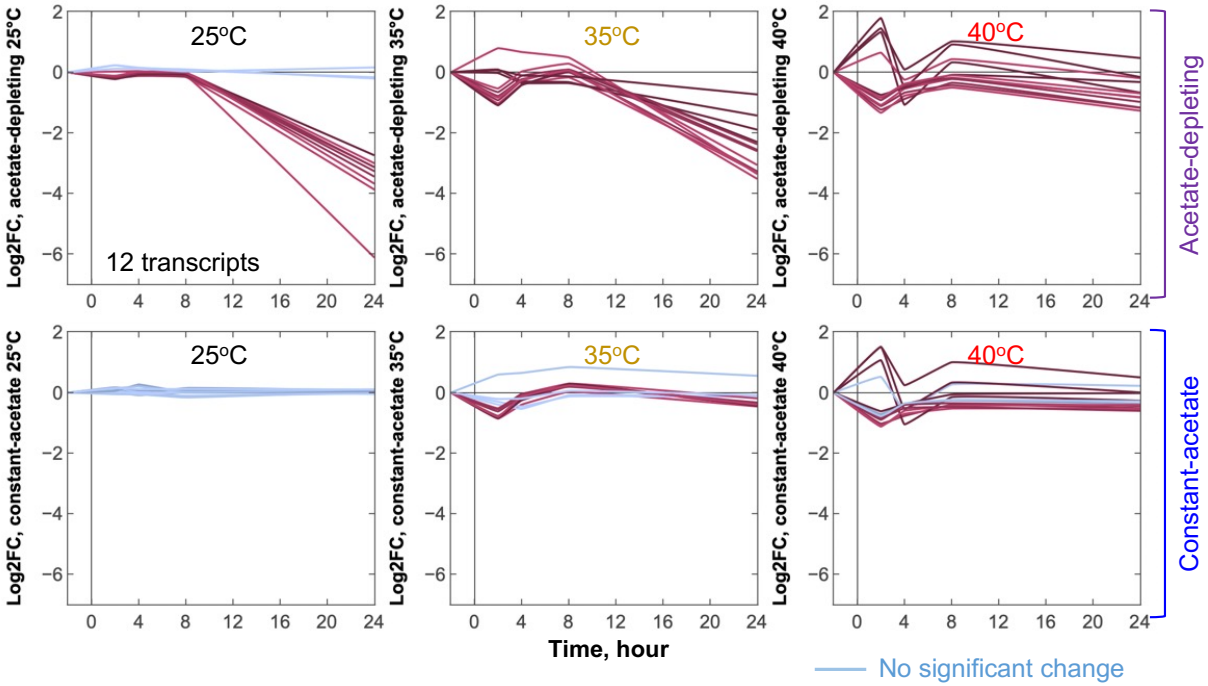

No significant change
Global significant change

B. Transcripts related to HSP70s

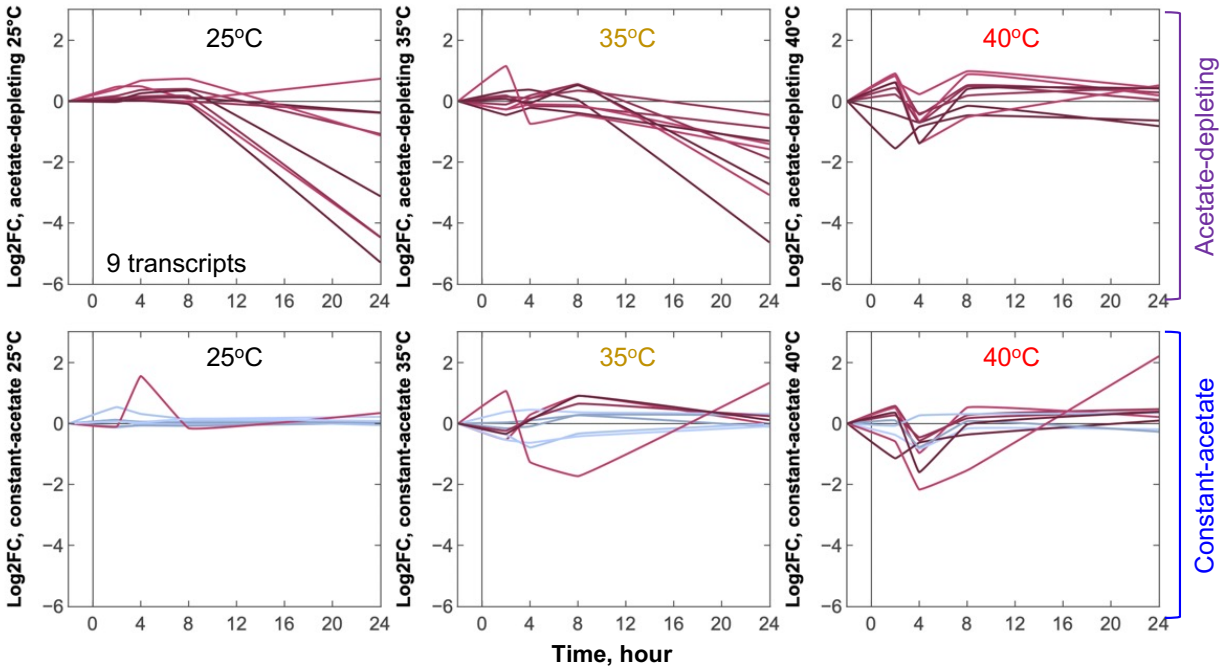

Supplemental Fig. 4. Log_2(fold change, FC) of mean normalized read counts of groups of transcripts based on MapMan function annotation or manual curation. Plots are Log_2FC of transcripts related to the indicated function groups under six different treatments, as compared to the pre-heat time points. RNA-seq data with normalized read counts were used for this analysis. Black vertical lines indicate the start of heat treatments under 35°C or 40°C or the equivalent time point at 25°C. Each line represents one unique transcript in the indicated function group. ANOVA test was applied to the time course (five time points) of one transcript for each condition. If a transcript differed significantly during the time course (or underwent a global significant change) of one condition, it is colored purple (ANOVA significant); blue lines had no significant changes during the time course. Different intensities of purple and blue colors were used to distinguish different transcripts. The total number of transcripts plotted in each function group is marked on the top left panel for each sub-figure. See the interactive figures with gene IDs and annotations in Supplemental Dataset 2.

See more panels of Supplemental Fig. 4 below.

Supplemental Fig. 4. continued

C. Transcripts related to HSP90s

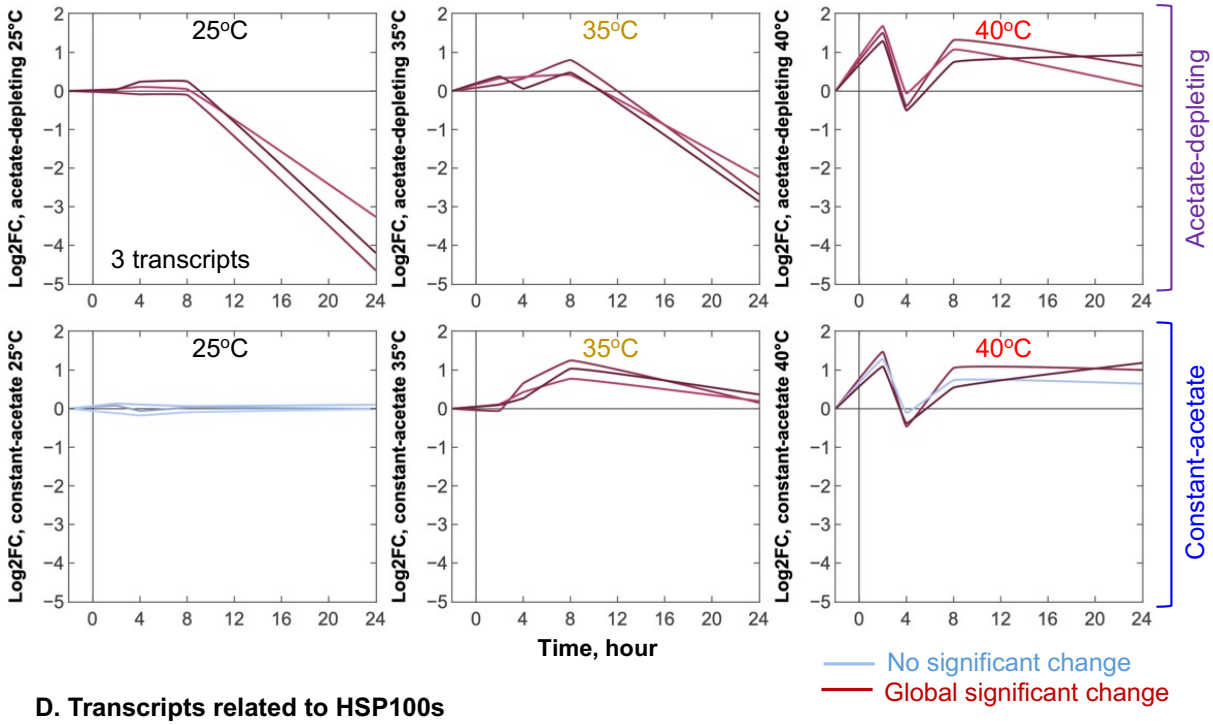

D. Transcripts related to HSP100s

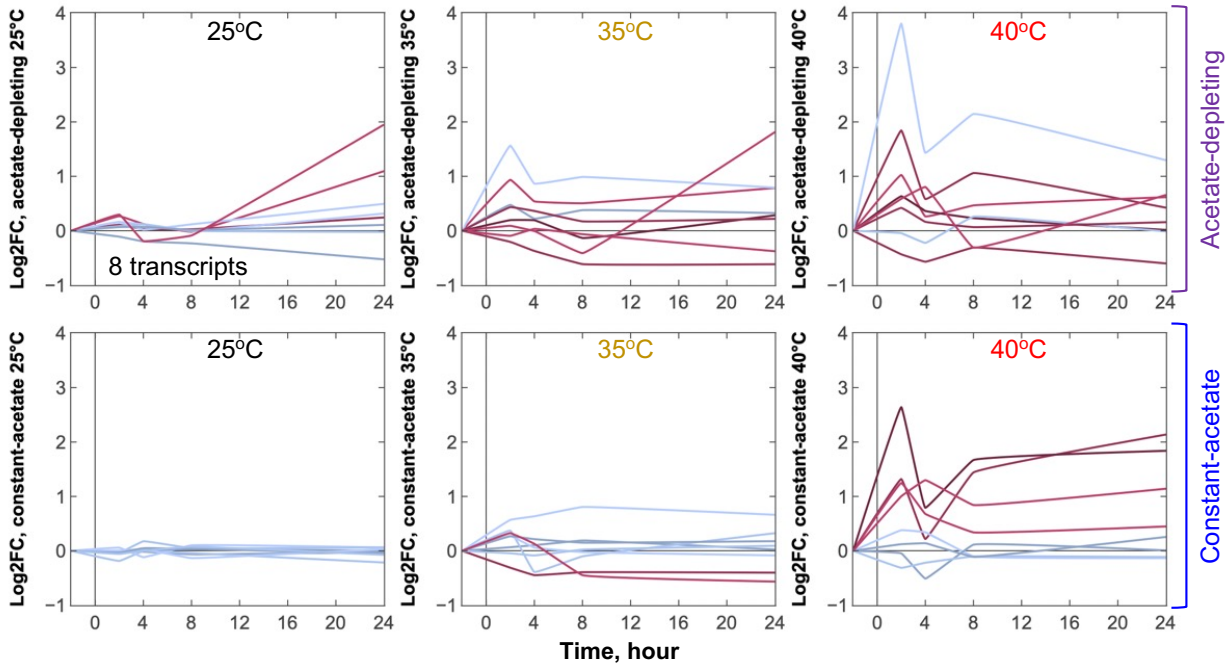

Supplemental Fig. 4. continued

E. Transcripts related to small HSPs

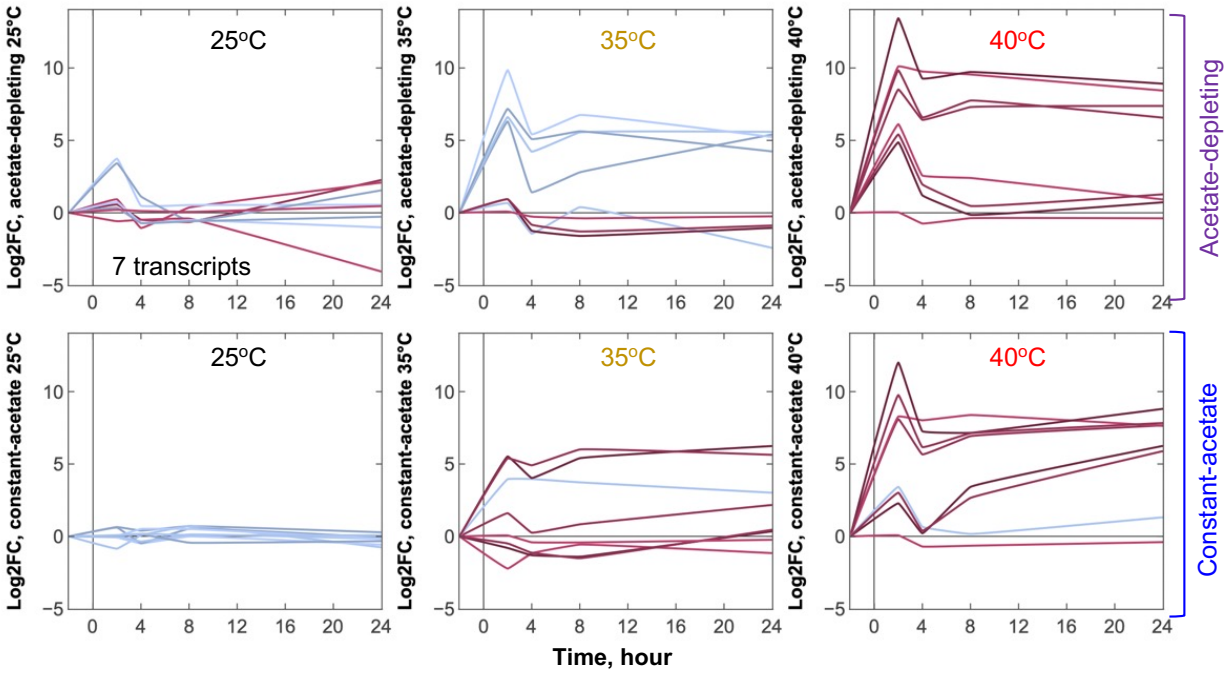

F. Transcripts related to LHCII

No significant change
Global significant change

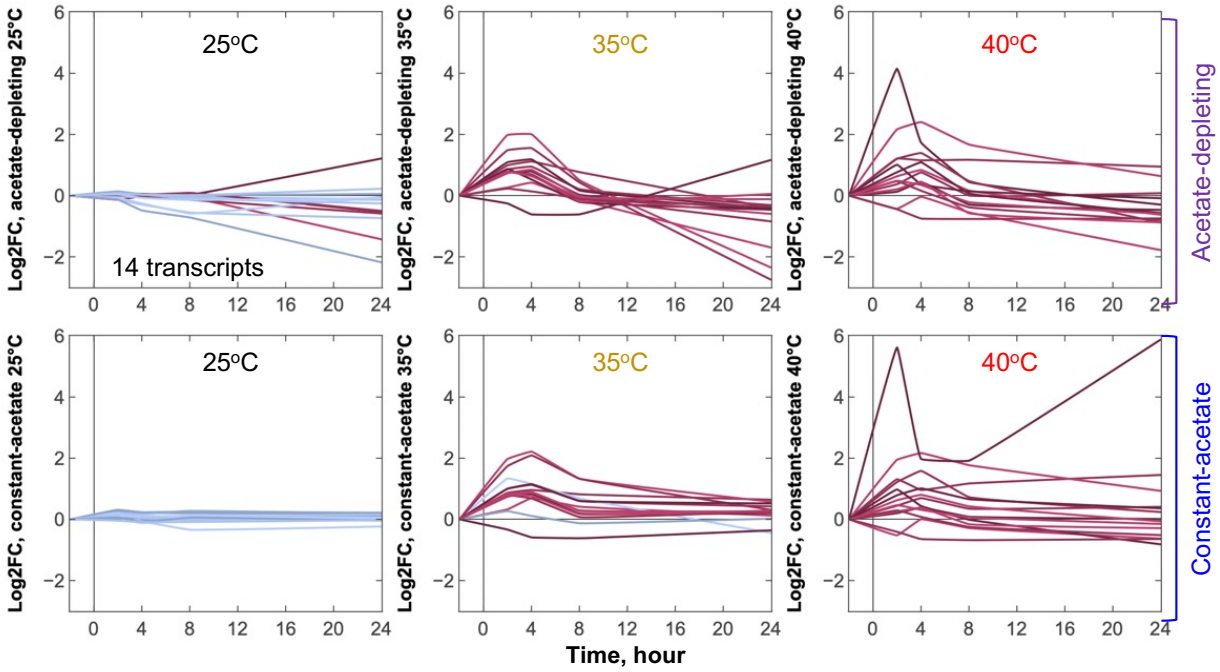

Supplemental Fig. 4. continued

G. Transcripts related to PSII biogenesis

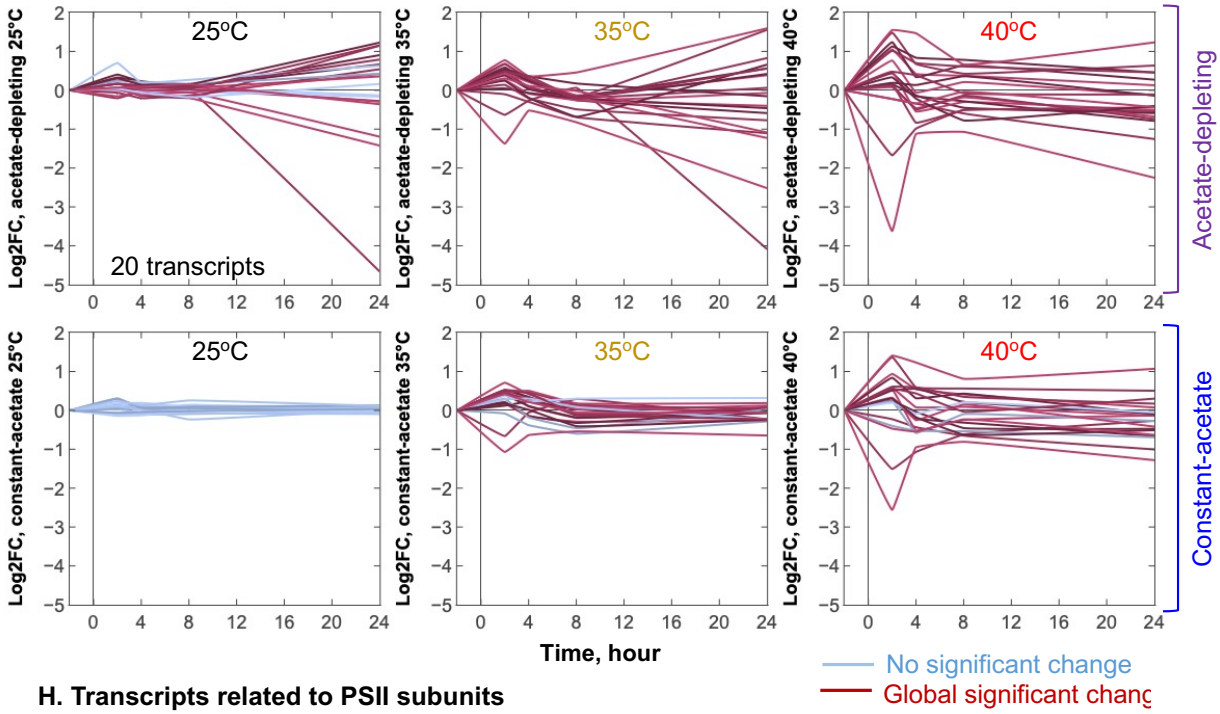

H. Transcripts related to PSII subunits

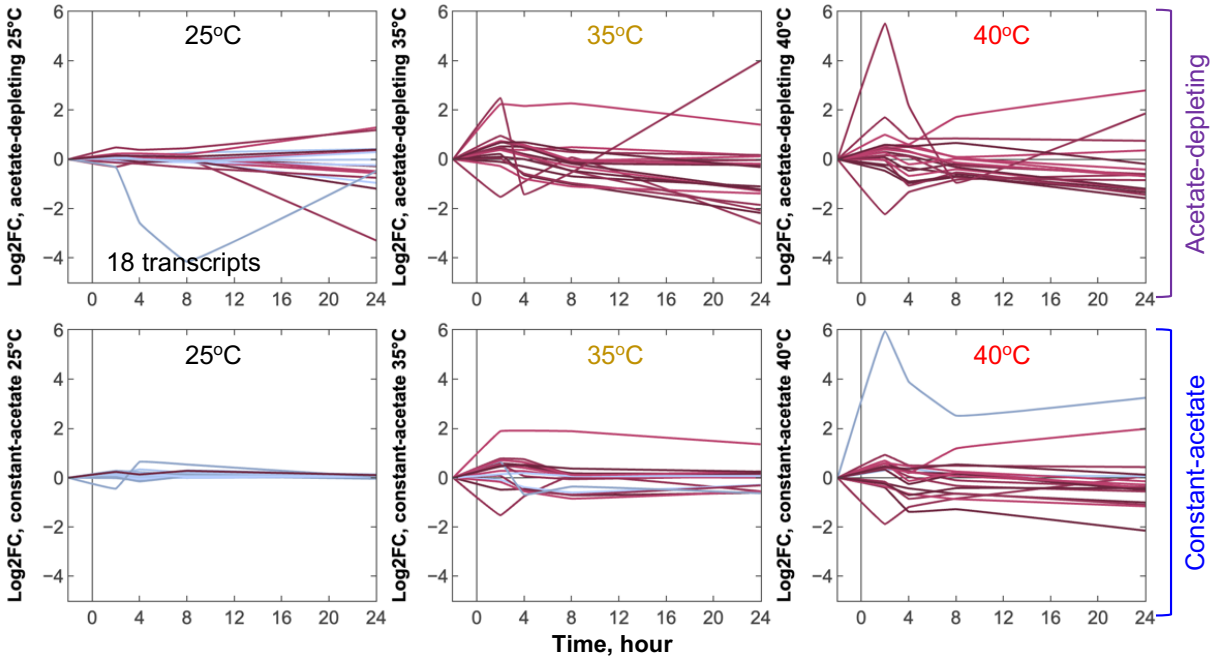

Supplemental Fig. 4. continued

I. Transcripts related to LHCI

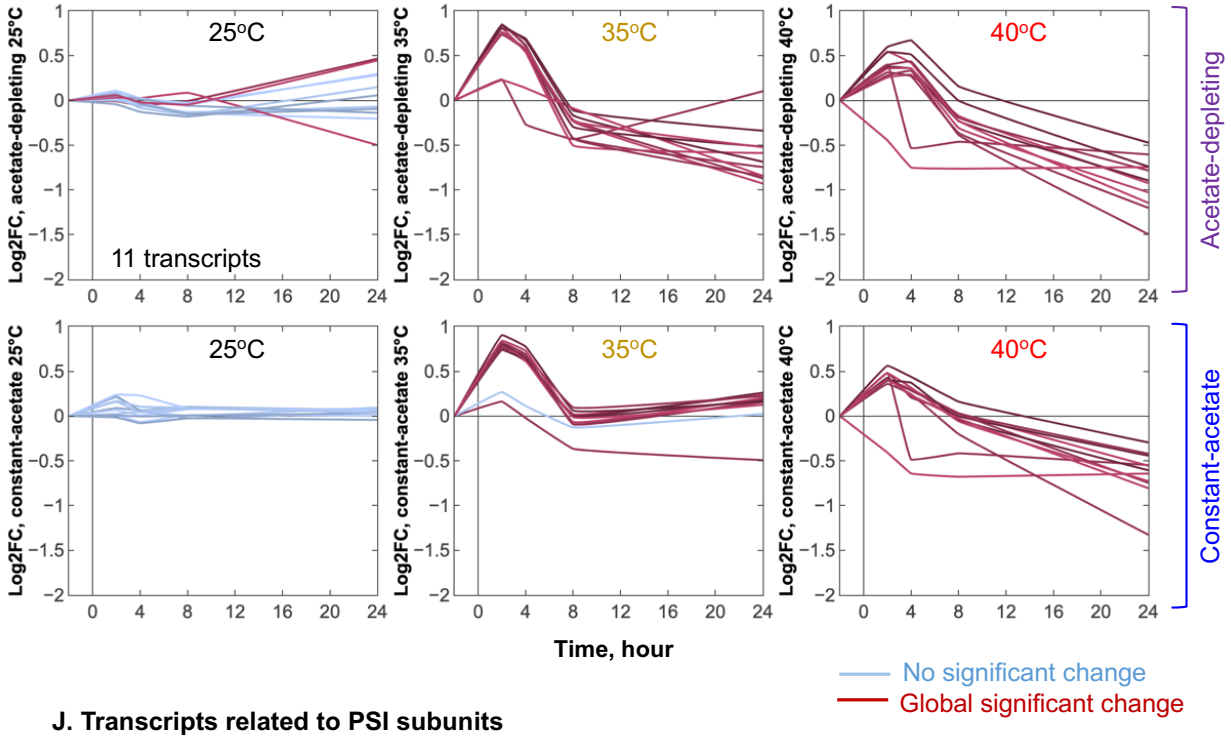

J. Transcripts related to PSI subunits

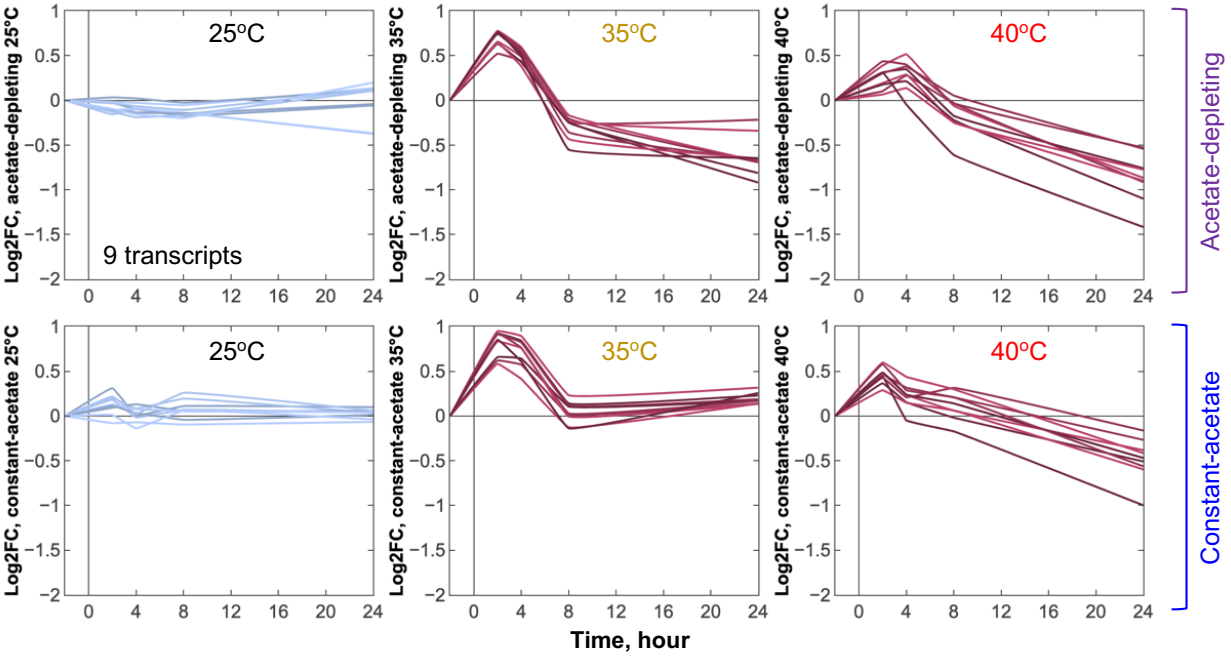

Supplemental Fig. 4. continued

K. Transcripts related to Cytochrome b_6f subunits

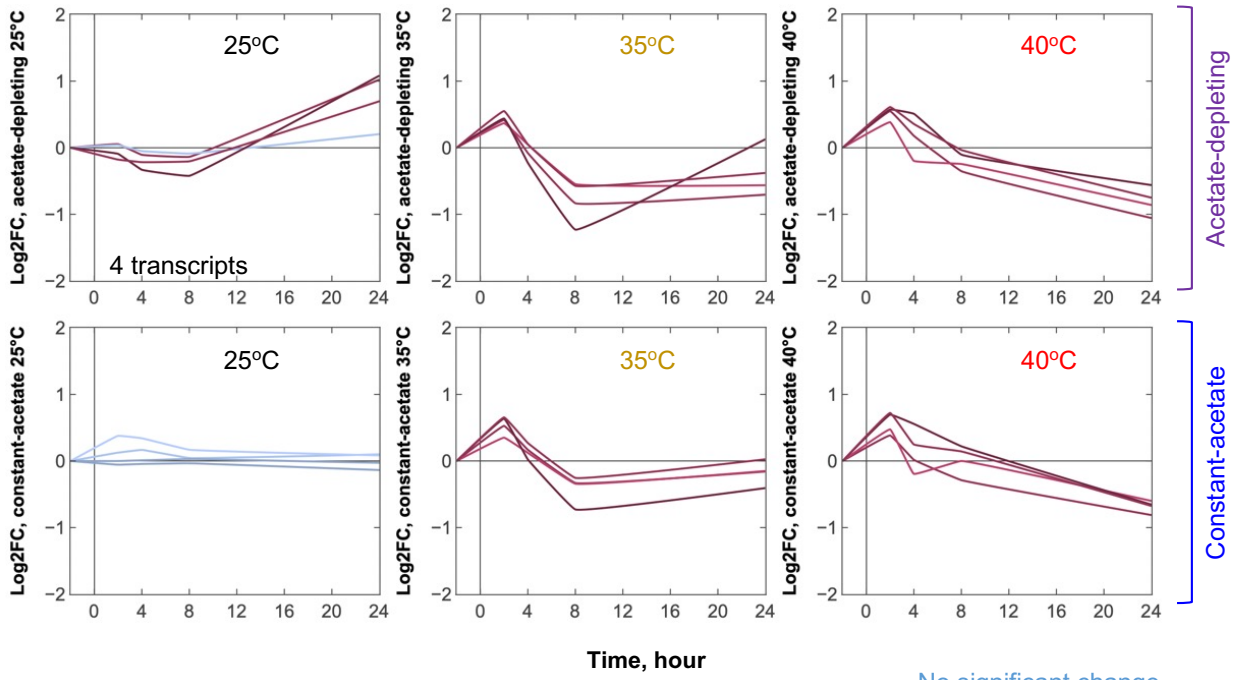

L. Transcripts related to ATP synthase subunits

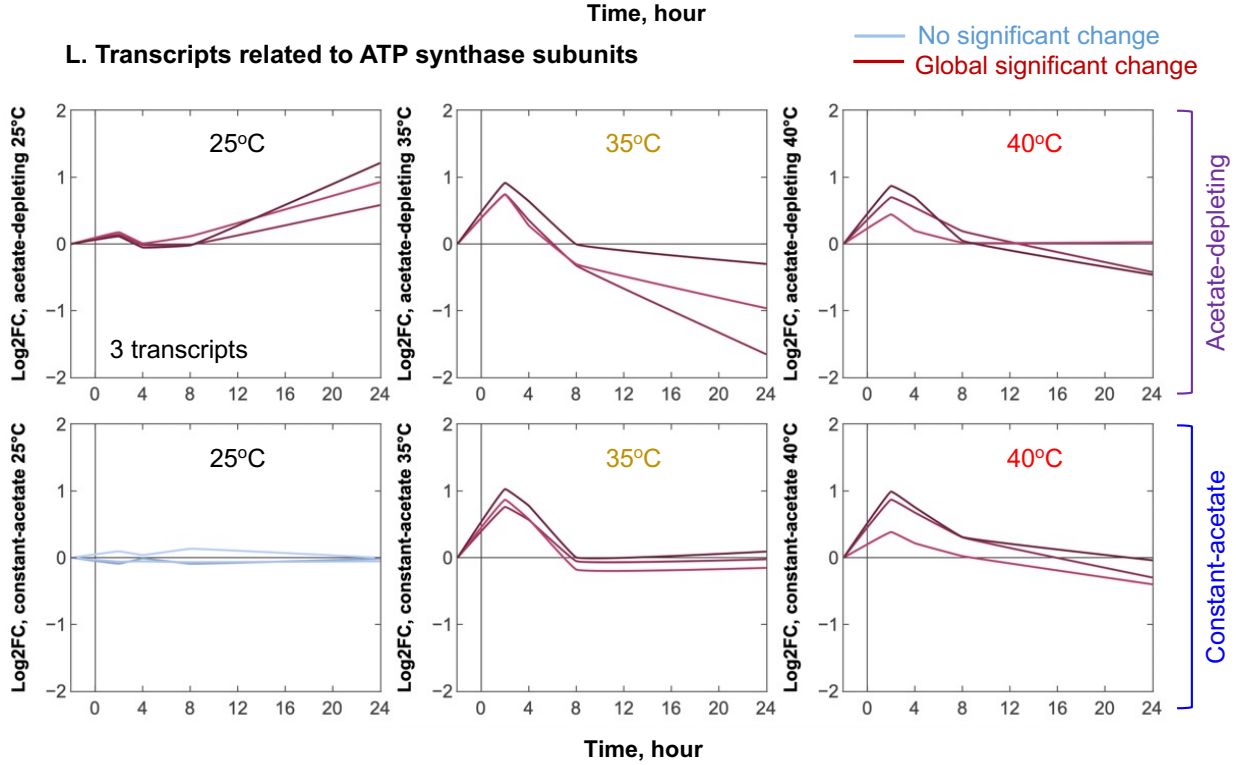

Supplemental Fig. 4. continued

M. Transcripts related to Calvin-Benson cycle

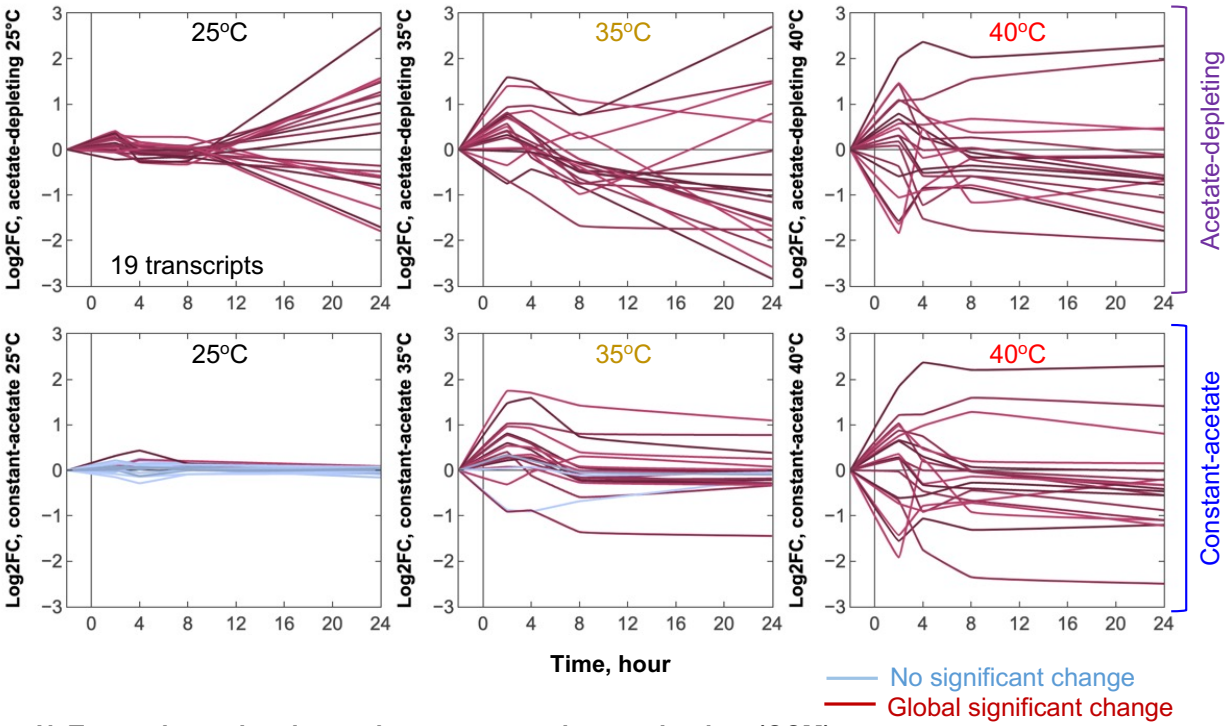

N. Transcripts related to carbon concentrating mechanism (CCM)

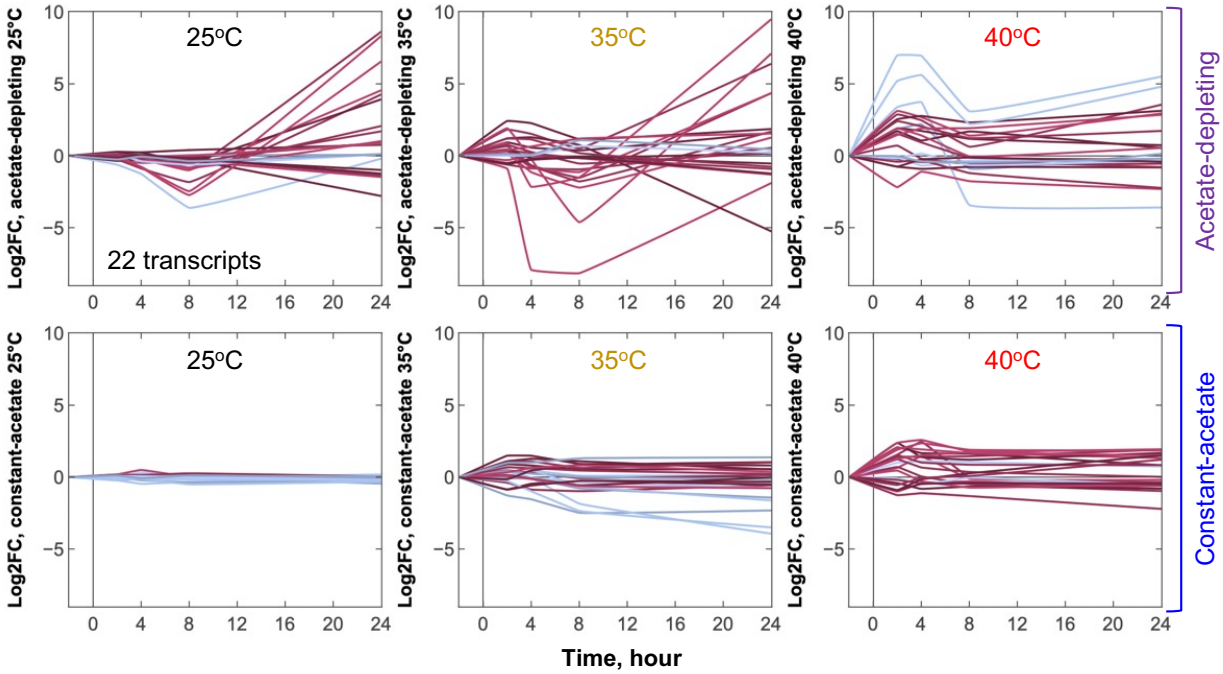

Supplemental Fig. 4. continued

O. Transcripts related to photoprotection

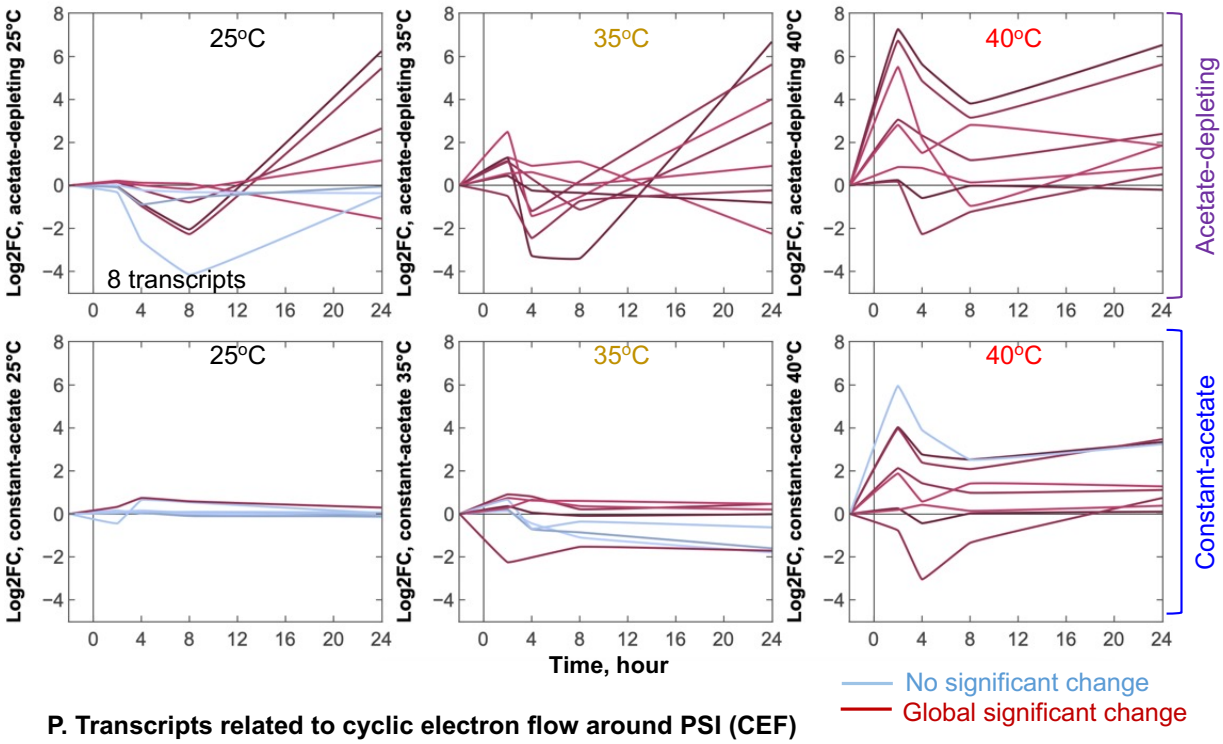

P. Transcripts related to cyclic electron flow around PSI (CEF)

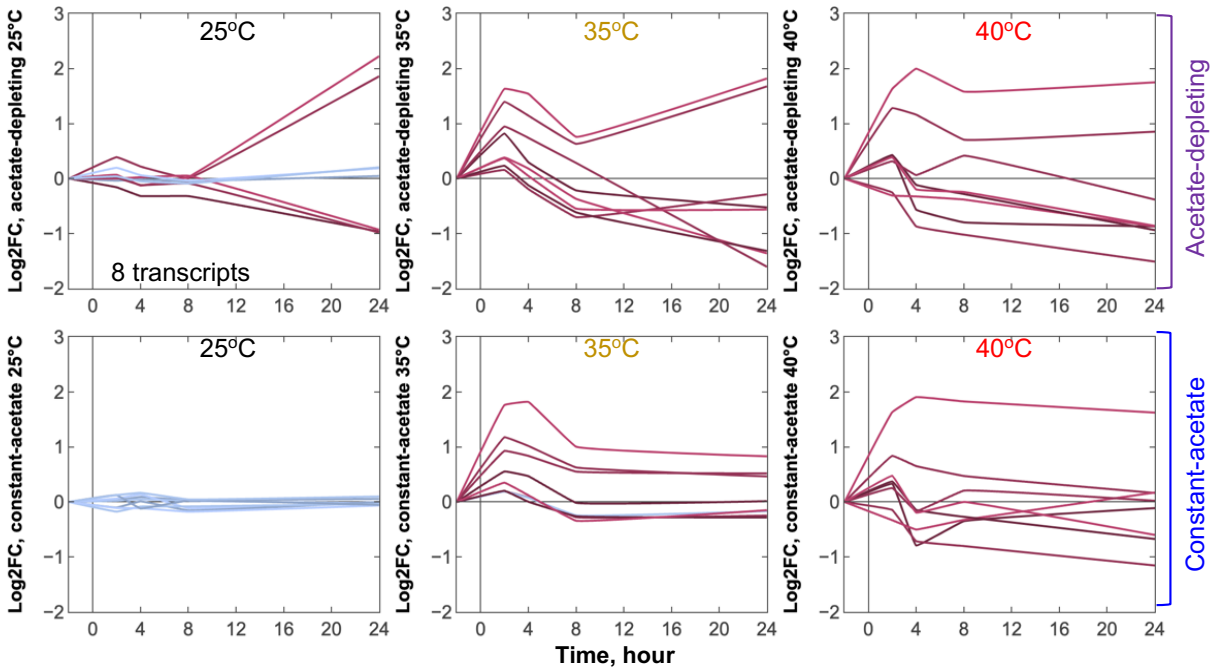

Supplemental Fig. 4. continued

Q. Transcripts related to chlorophyll biosynthesis

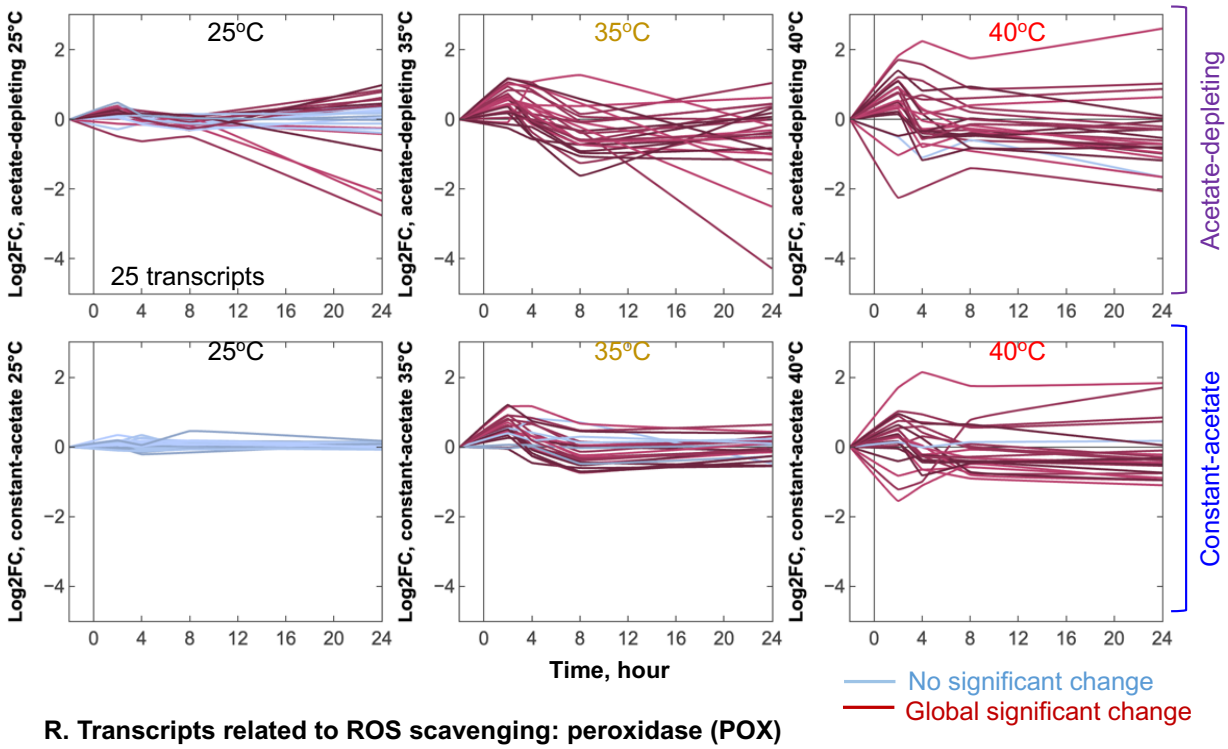

R. Transcripts related to ROS scavenging: peroxidase (POX)

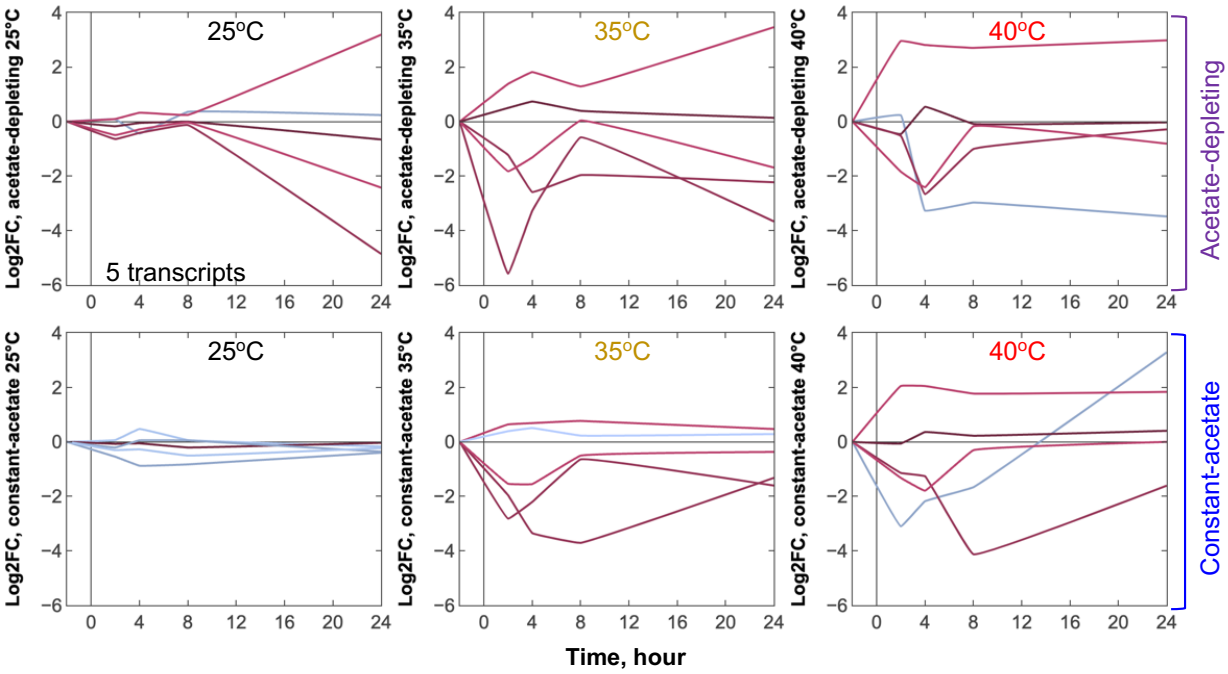

Supplemental Fig. 4. continued

S. Transcripts related to ROS scavenging: ascorbate peroxidase (APX)

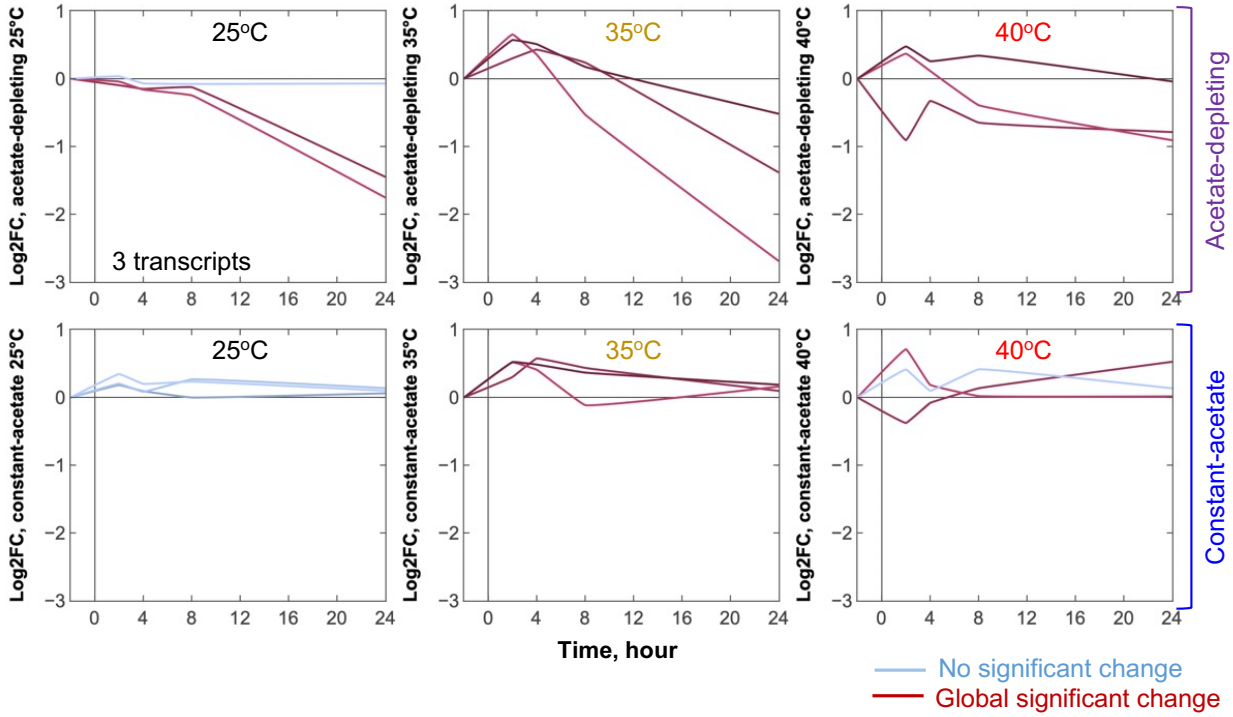

T. Transcripts related to ROS scavenging: catalase (CAT)

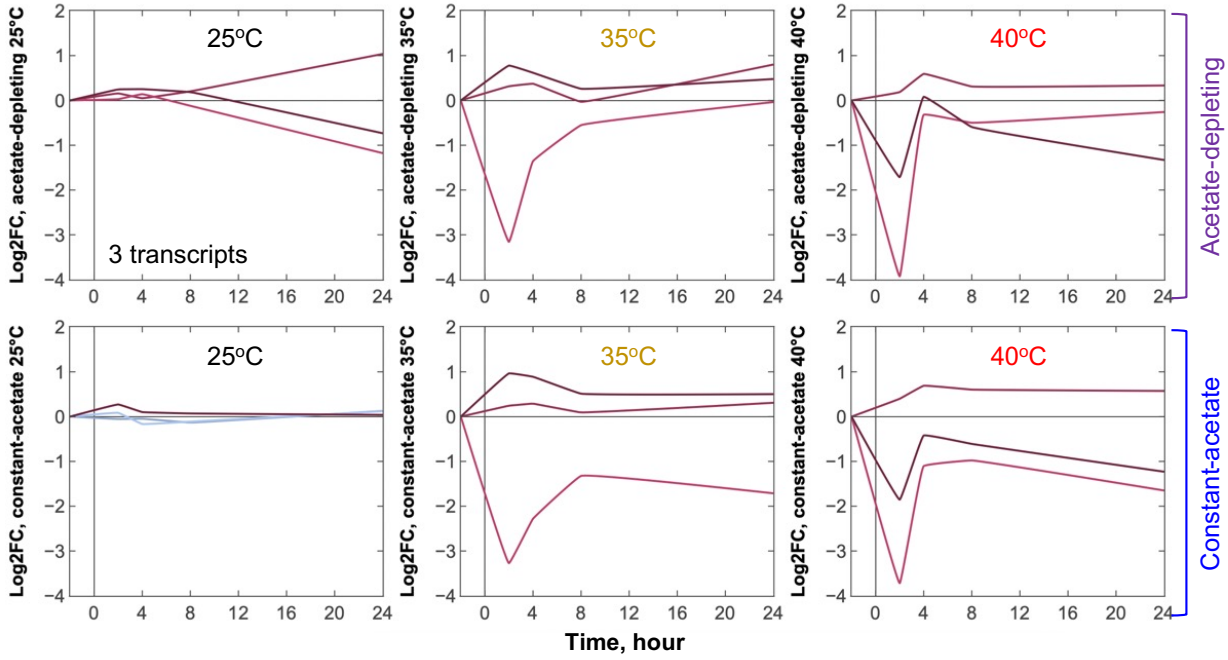

Supplemental Fig. 4. continued

U. Transcripts related to ROS scavenging: glutathione reductase (GR)

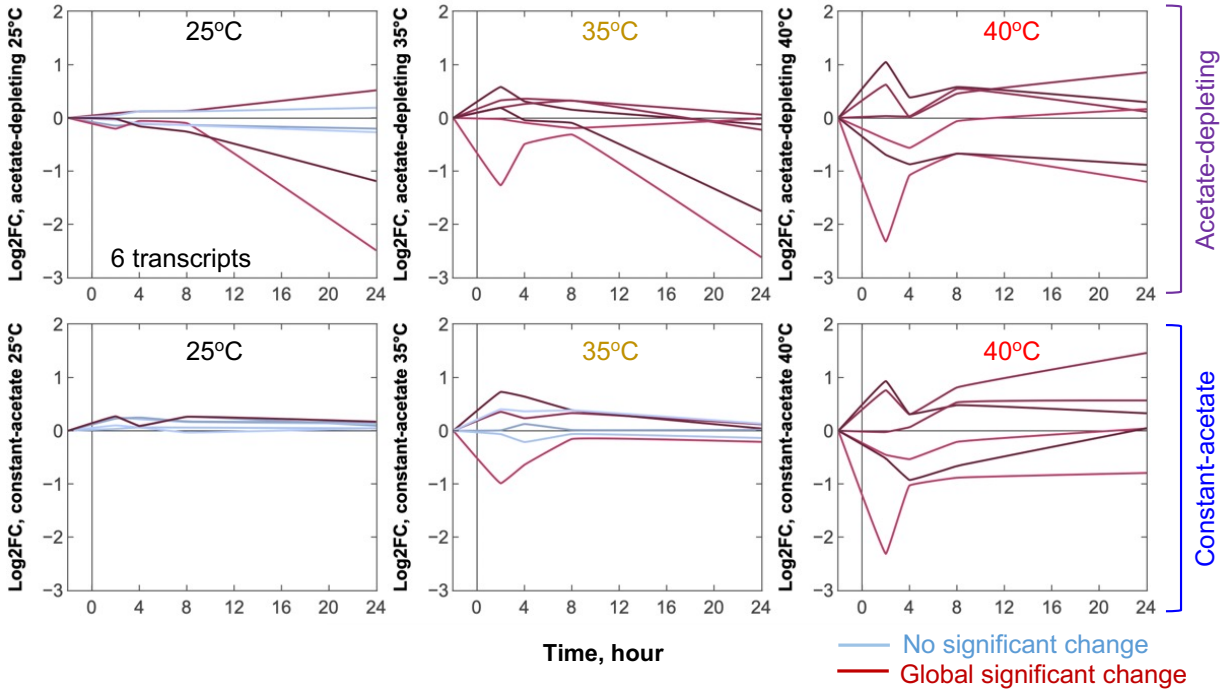

V. Transcripts related to ROS scavenging: glutathione S-transferase (GST)

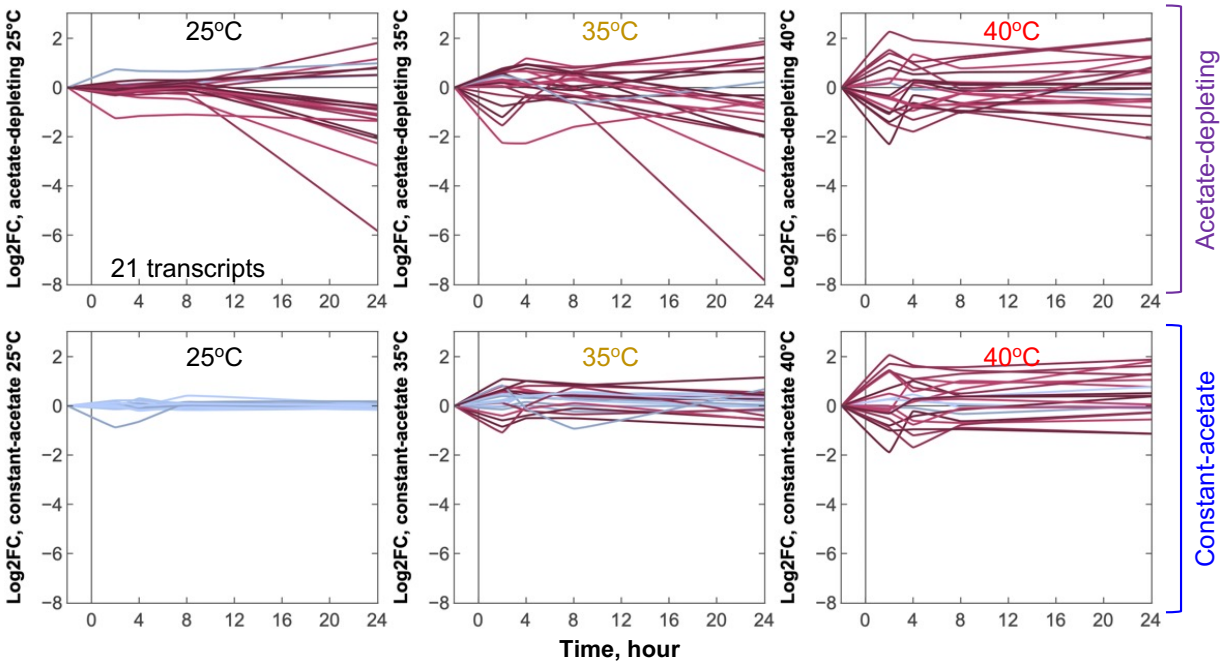

Supplemental Fig. 4. Continued

W. Transcripts related to cell cycle

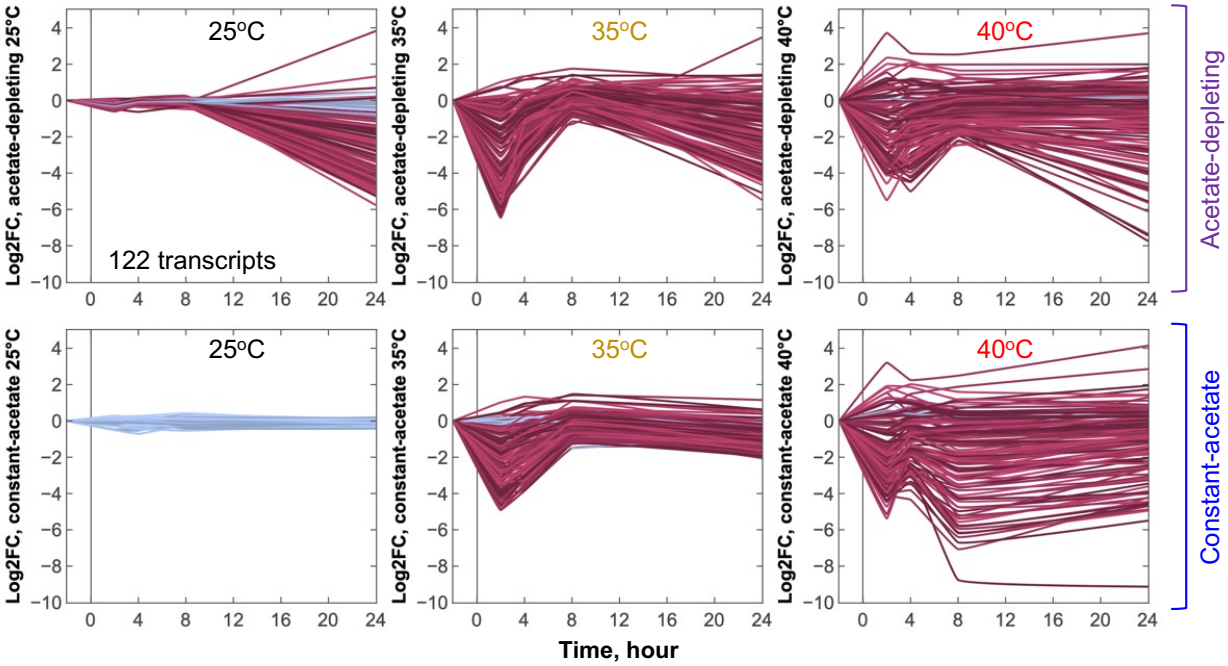

X. Transcripts related to cell wall

No significant change
Global significant change

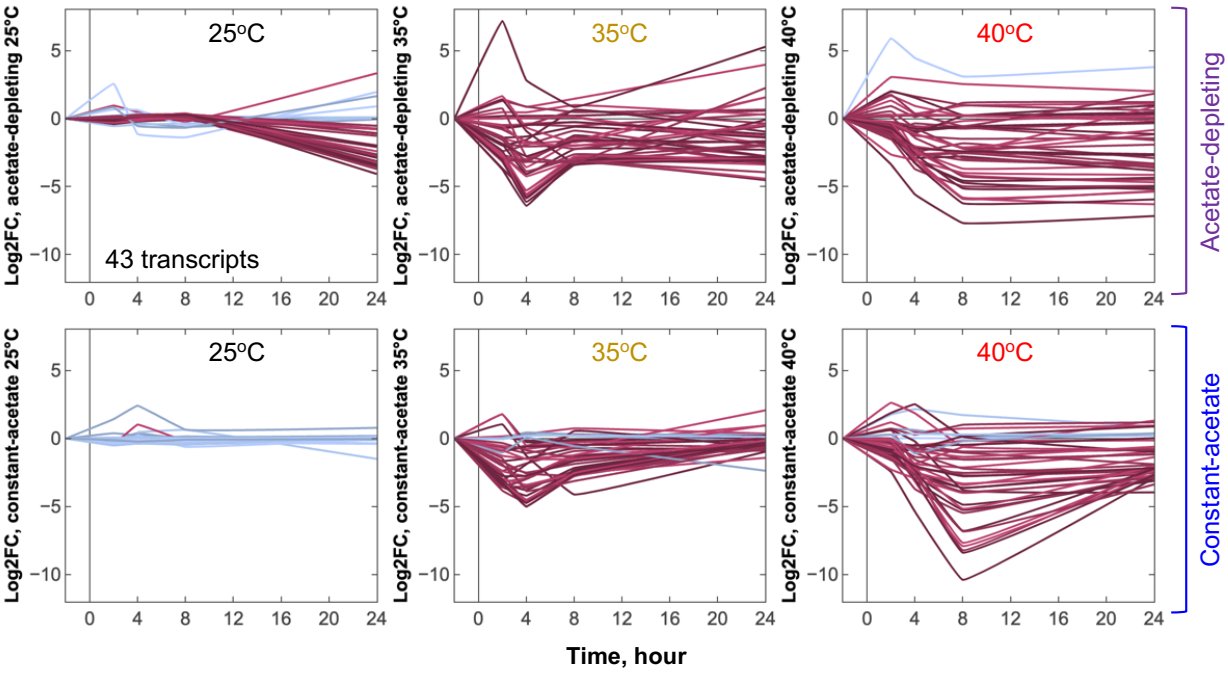

Supplemental Fig. 4. Continued

Y. Transcripts related to protein synthesis, ribosomal protein, prokaryotic

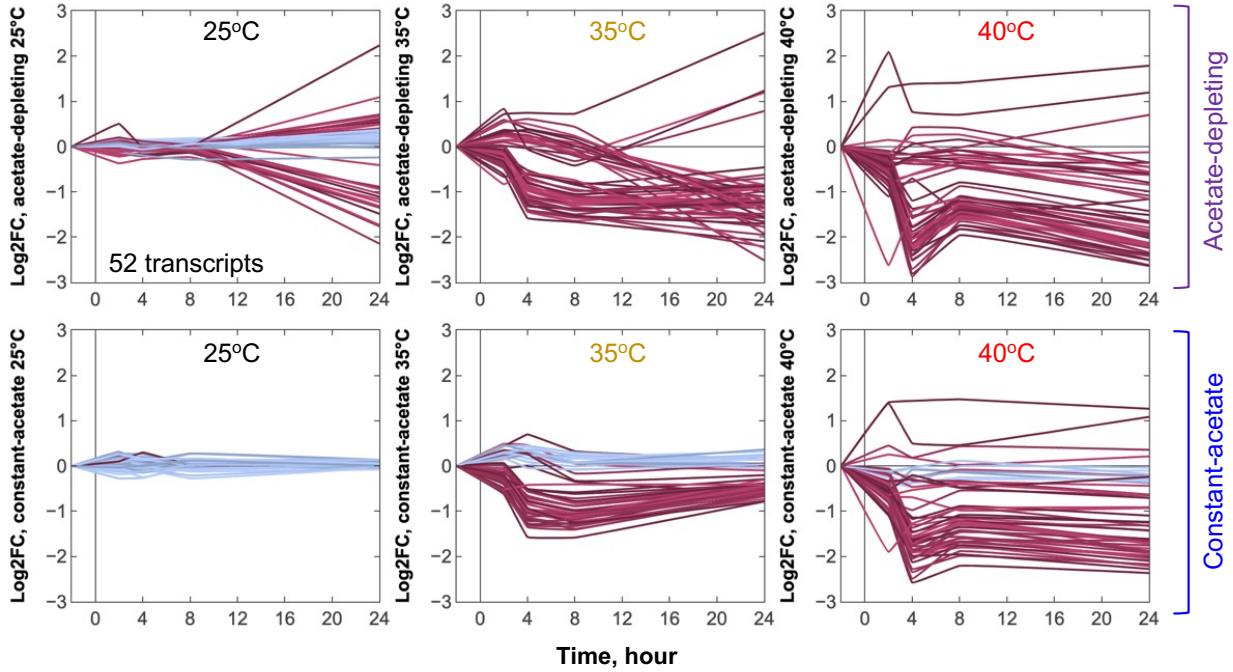

Z. Transcripts related to protein synthesis, ribosomal protein, chloroplast

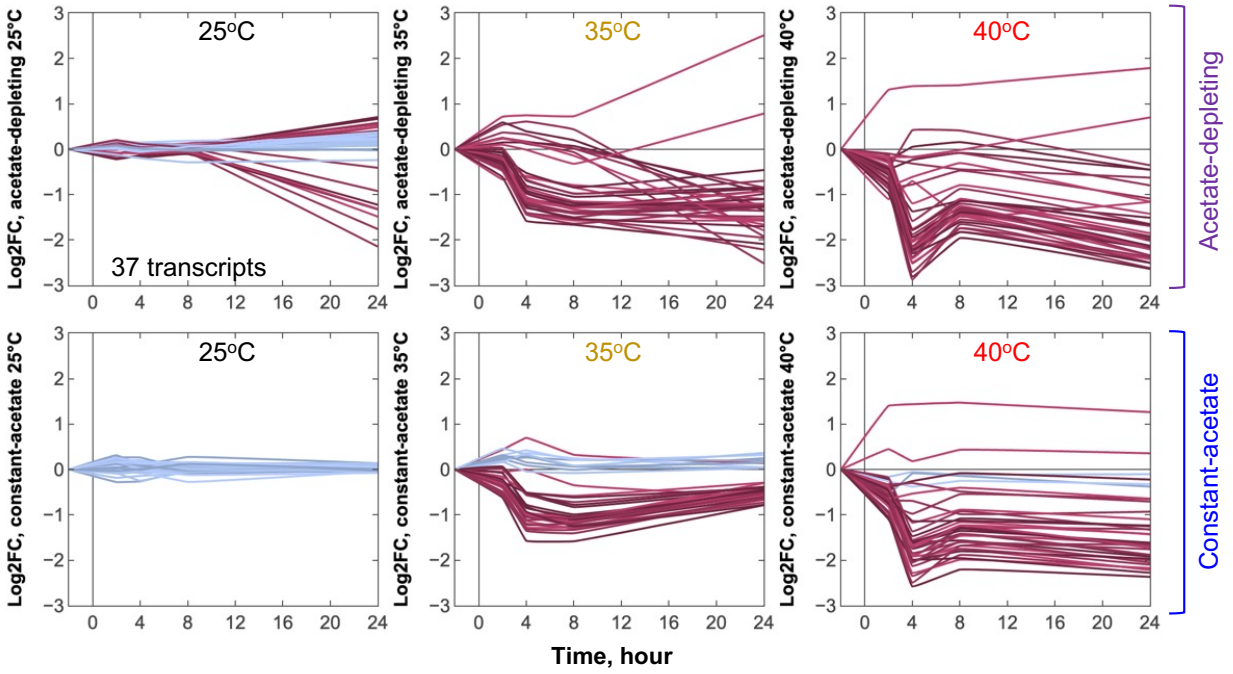

Supplemental Fig. 4. Continued

AA. Transcripts related to mitochondrial electron transport / ATP synthesis (NADH-DH type 1)

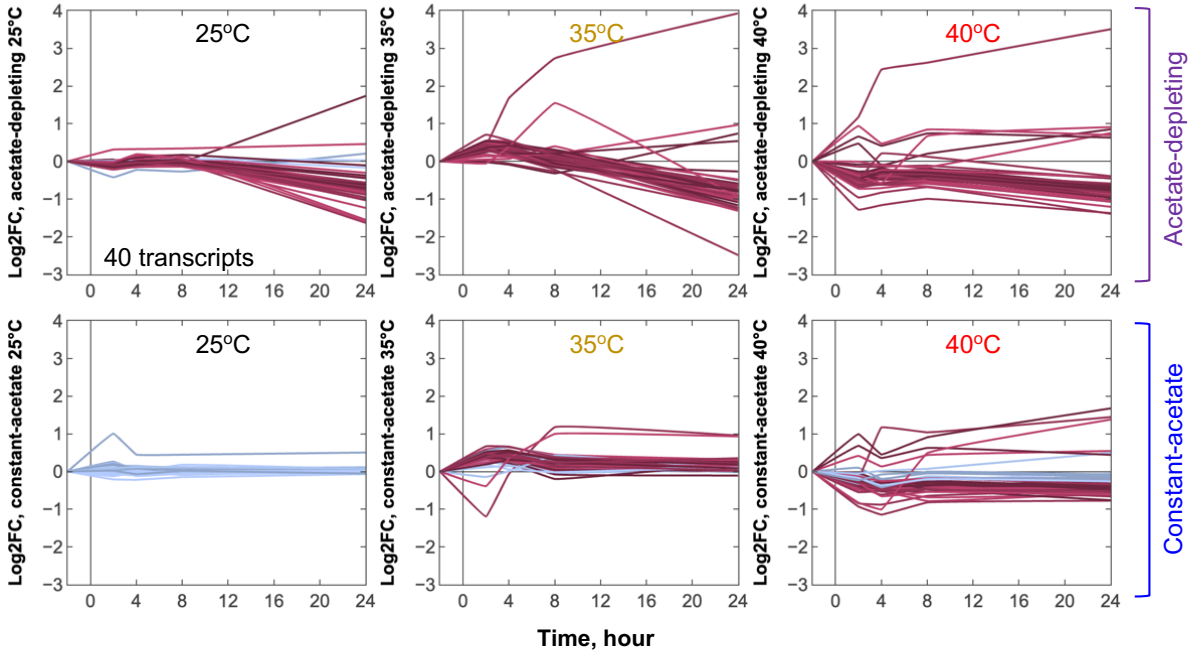

AB. Transcripts related to mitochondrial electron transport / ATP synthesis

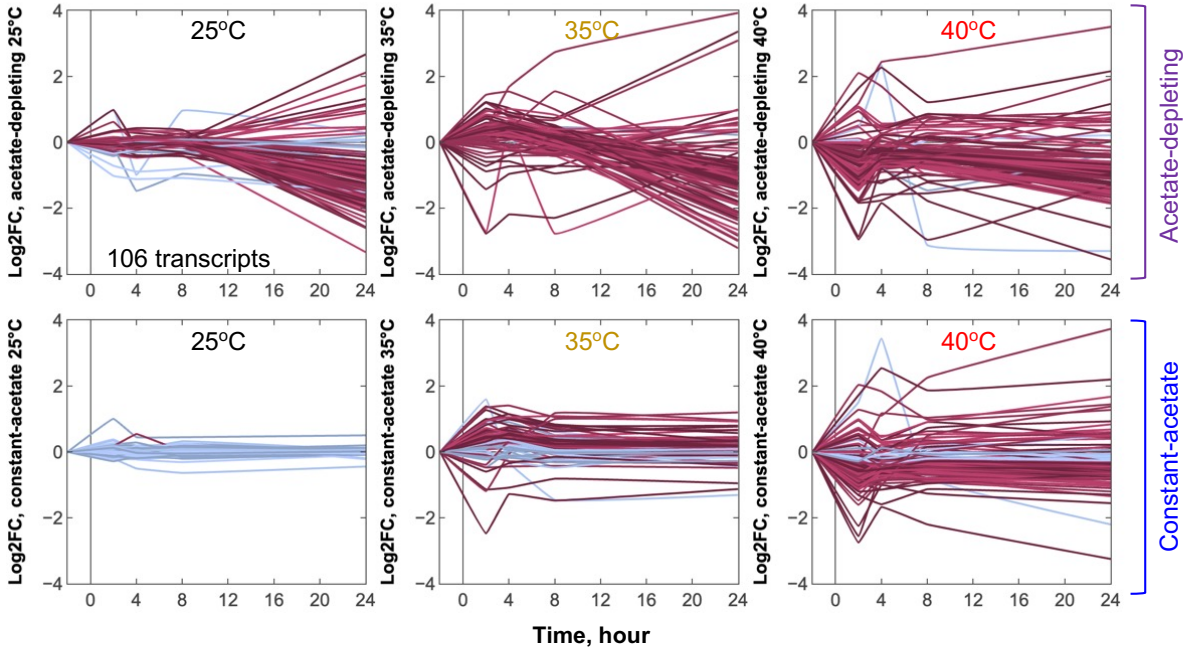

Supplemental Fig. 4. Continued

AC. Transcripts related to RNA

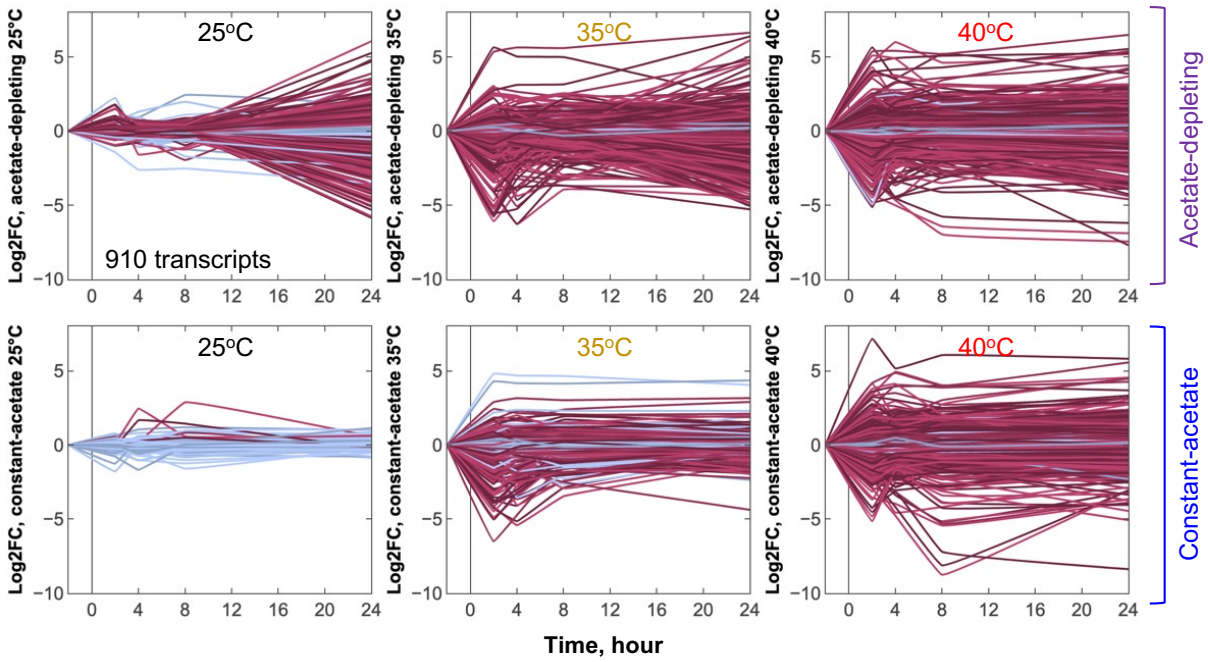

AD. Transcripts related to RNA processing

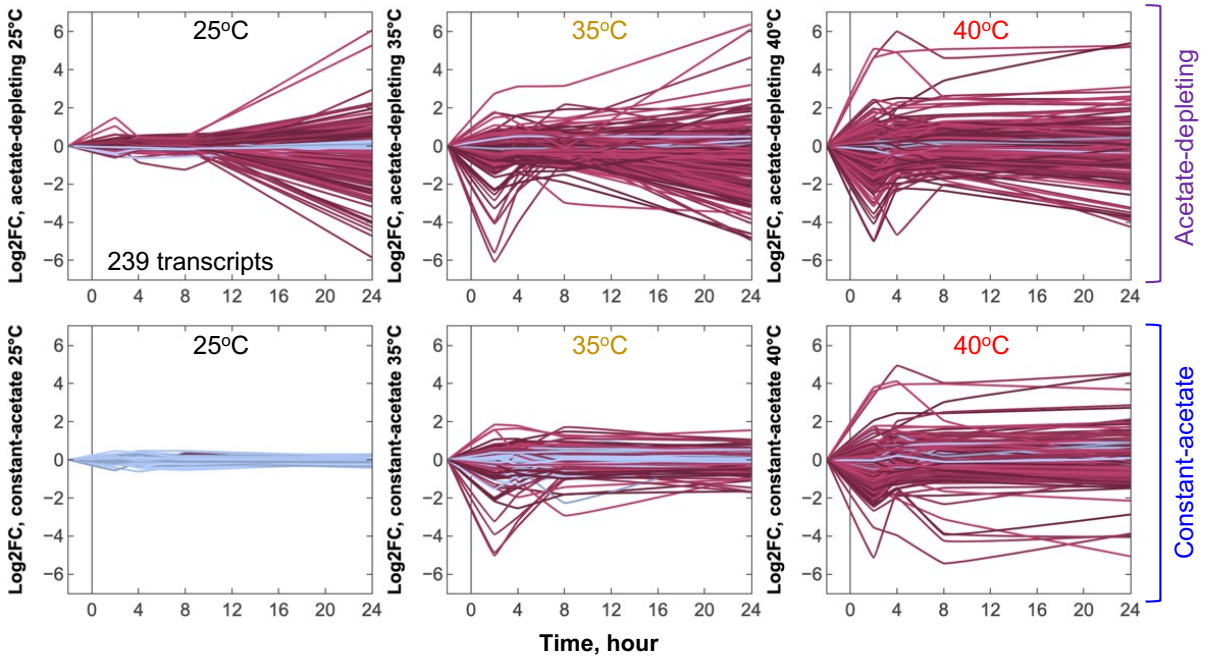

Supplemental Fig. 4. Continued

AE. Transcripts related to transport. phosphate

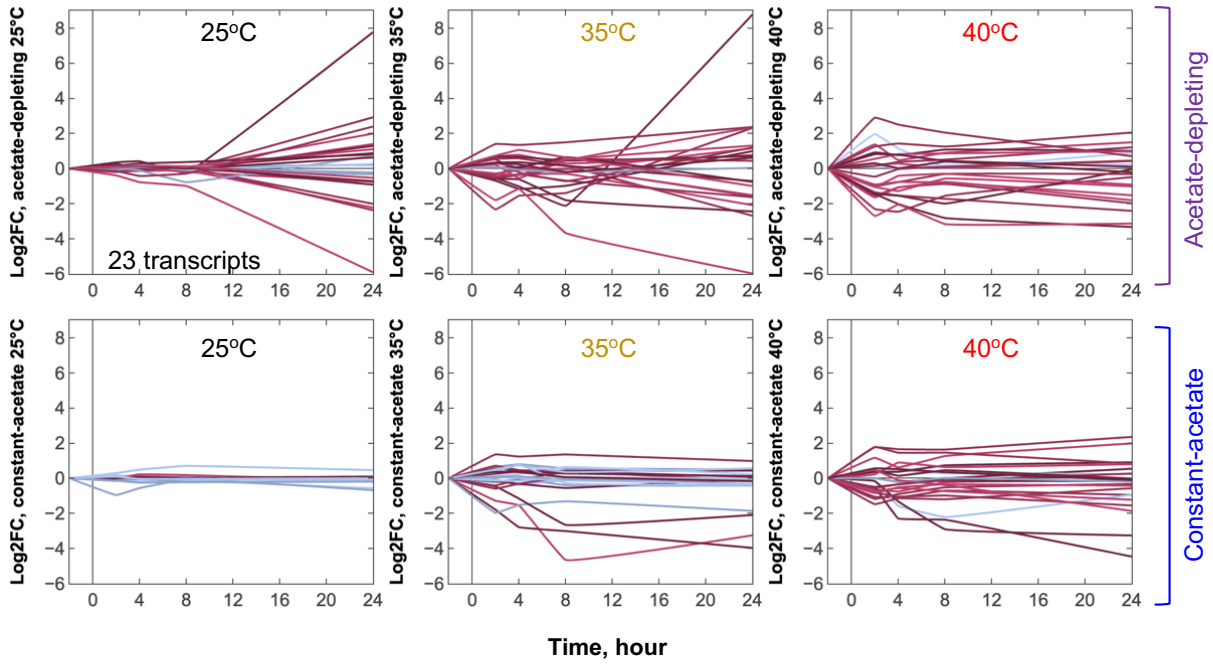

AF. Transcripts related to signaling. mitogen-activated protein kinase (MAP kinase)

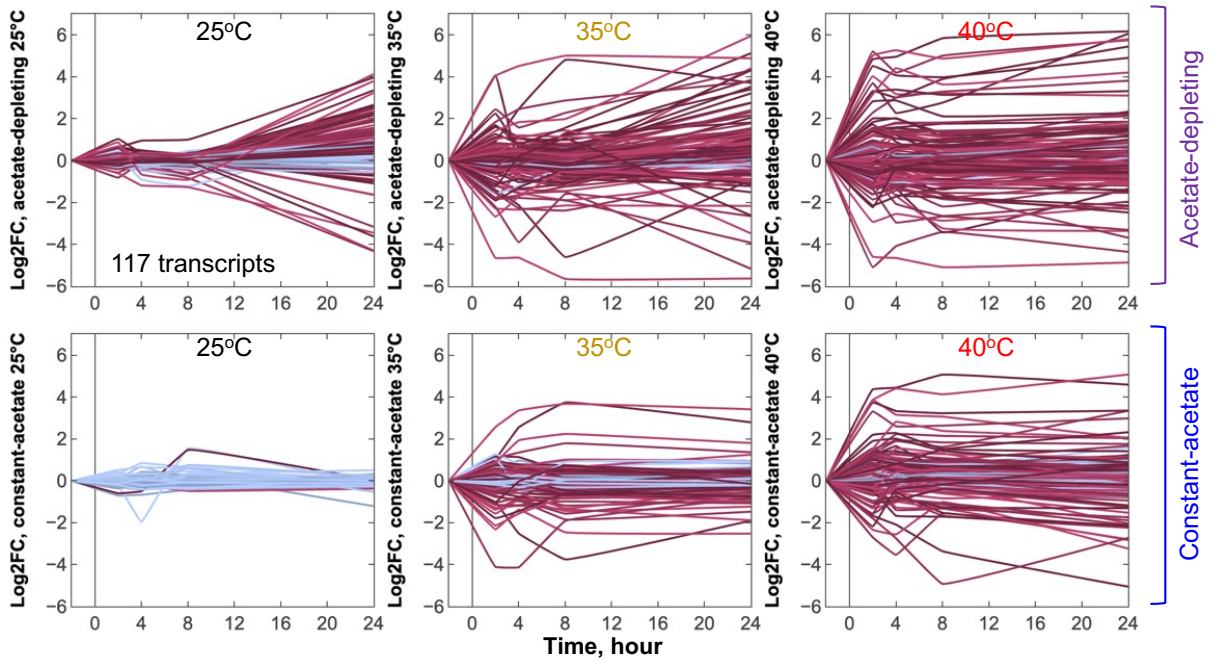

Supplemental Fig. 4. Continued

AG. Transcripts related to cell motility. eukaryotes. axonemal dyneins

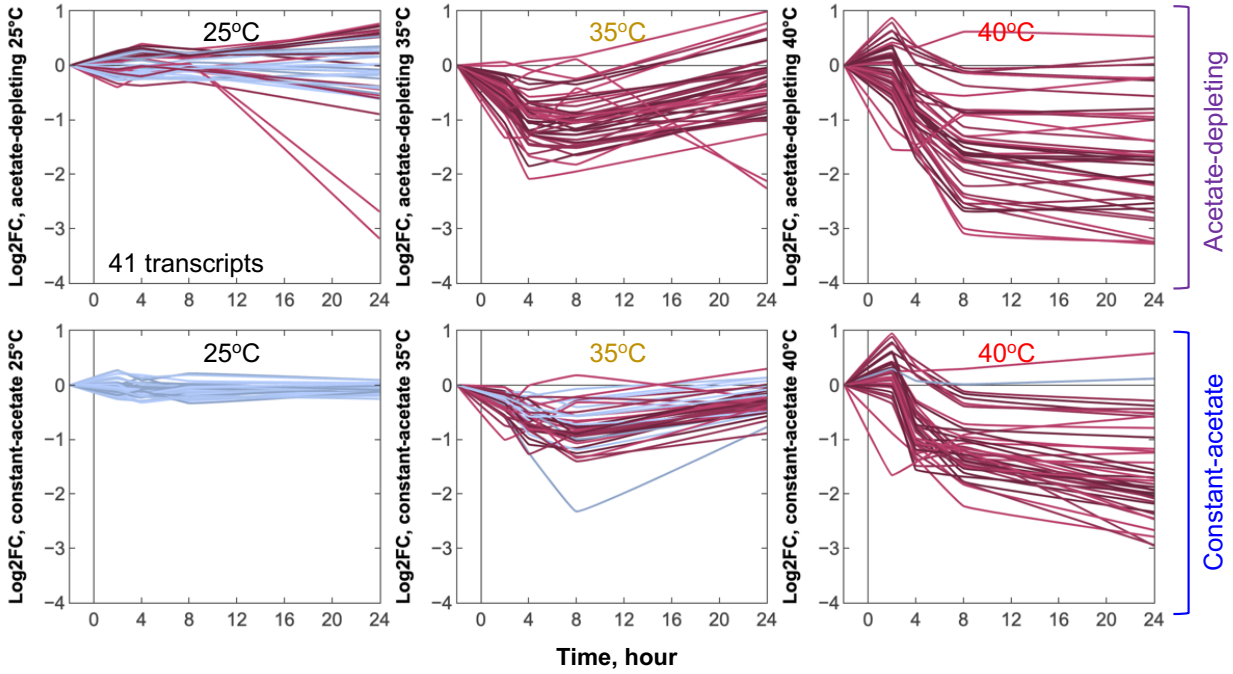

AH. Transcripts related to cell motility

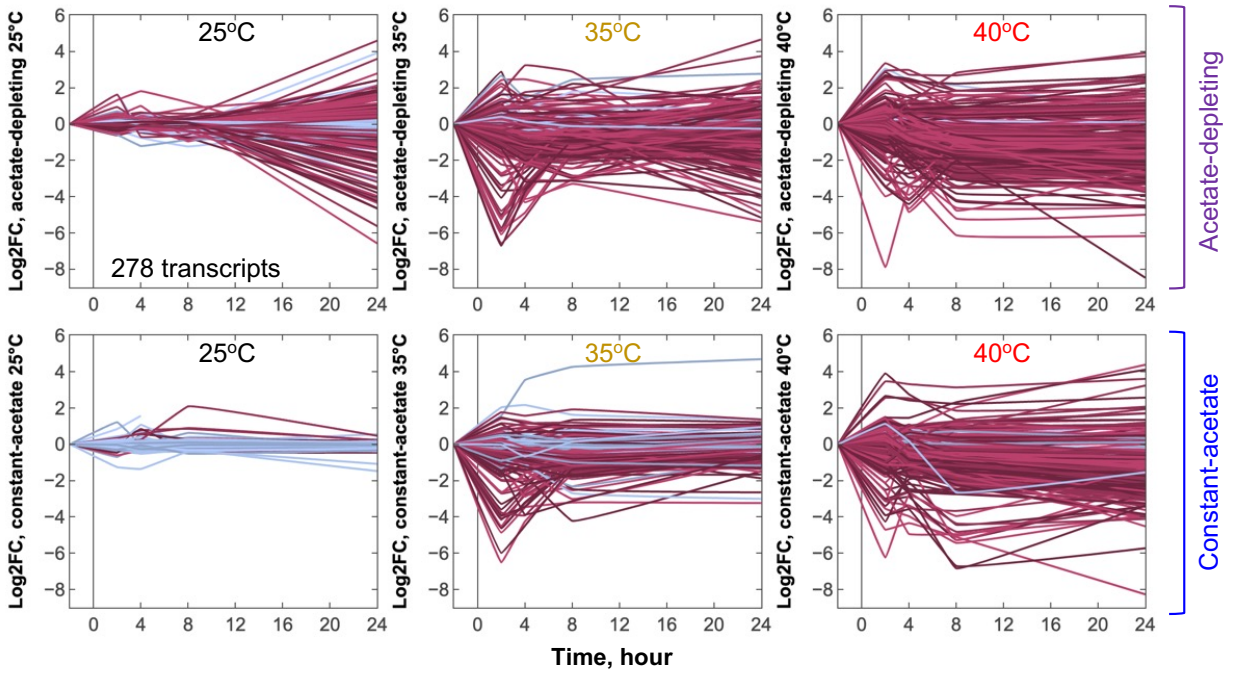

Supplemental Fig. 4. Log_2(fold change, FC) of mean normalized read counts of groups of transcripts based on MapMan function annotation or manual curation. Plots are Log_2FC of transcripts related to the indicated function groups under six different treatments, as compared to the pre-heat time points. RNA-seq data with normalized read counts were used for this analysis. Black vertical lines indicate the start of heat treatments under 35°C or 40°C or the equivalent time point at 25°C. Each line represents one unique transcript in the indicated function group. ANOVA test was applied to the time course (five time points) of one transcript for each condition. If a transcript differed significantly during the time course (or underwent a global significant change) of one condition, it is colored purple (ANOVA significant); blue lines had no significant changes during the time course. Different intensities of purple and blue colors were used to distinguish different transcripts. The total number of transcripts plotted in each function group is marked on the top left panel for each sub-figure. See the interactive figures with gene IDs and annotations in Supplemental Dataset 2.

Supplemental Fig. 5A

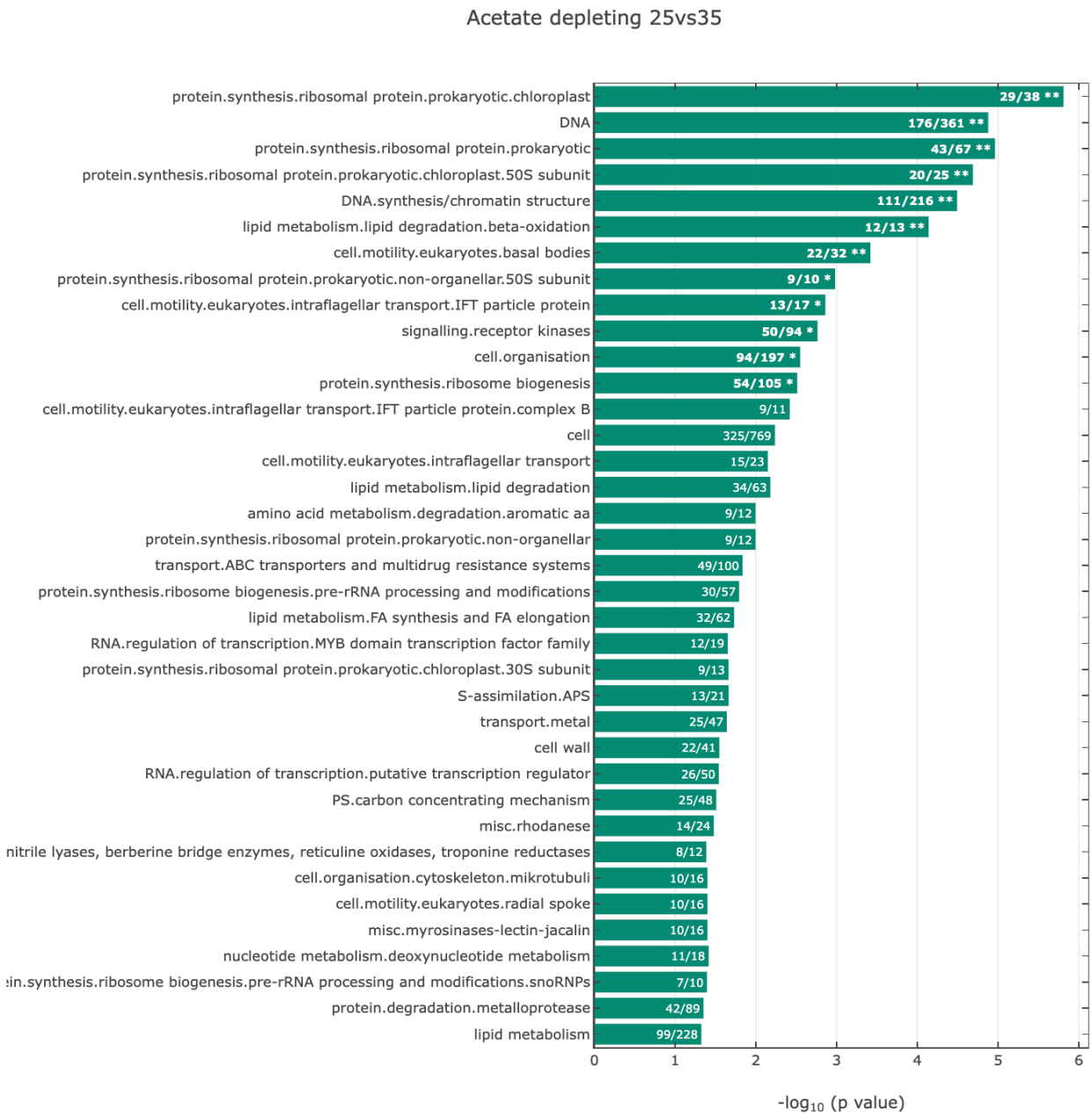

Supplemental Fig. 5B

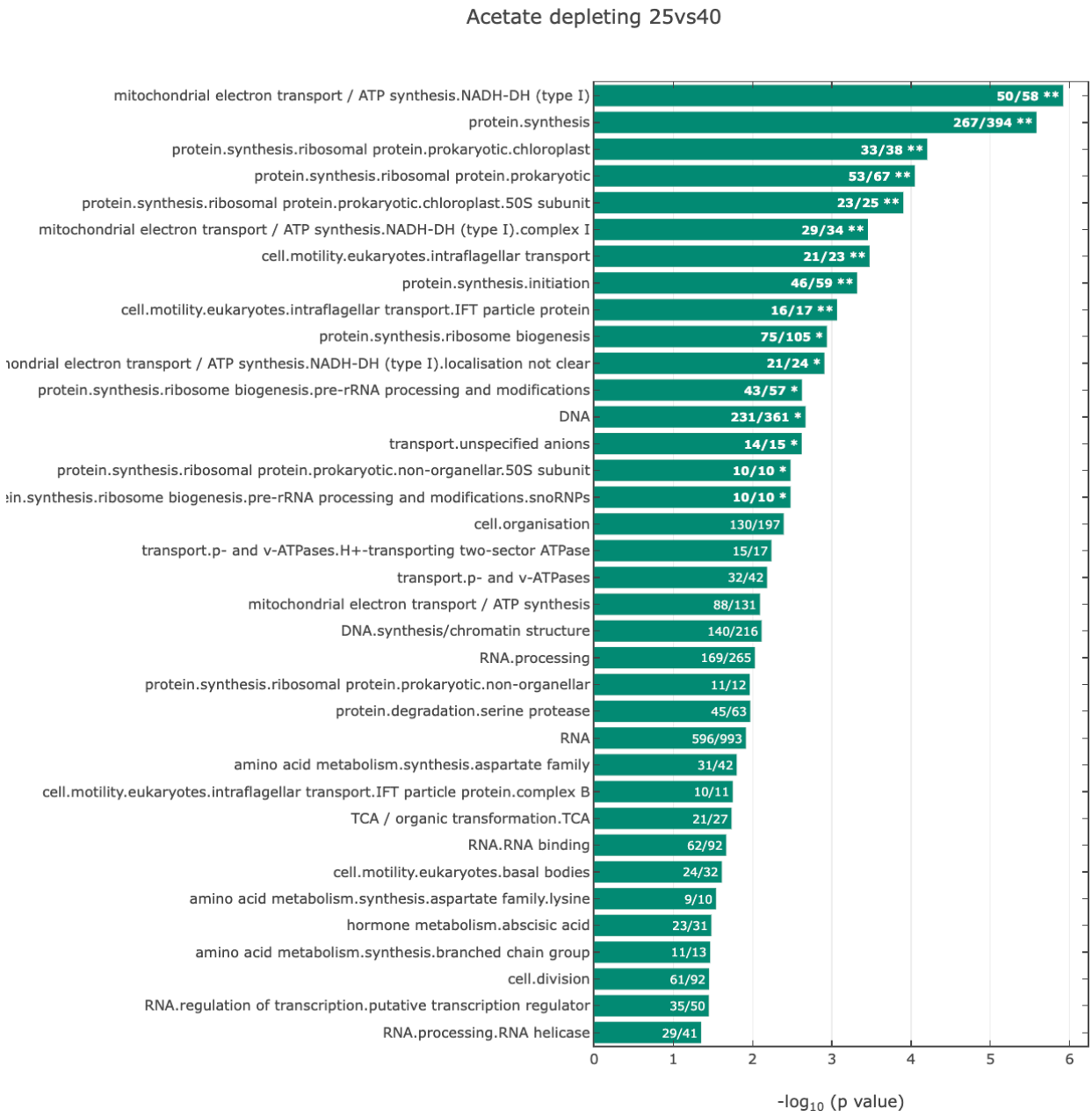

Supplemental Fig. 5C

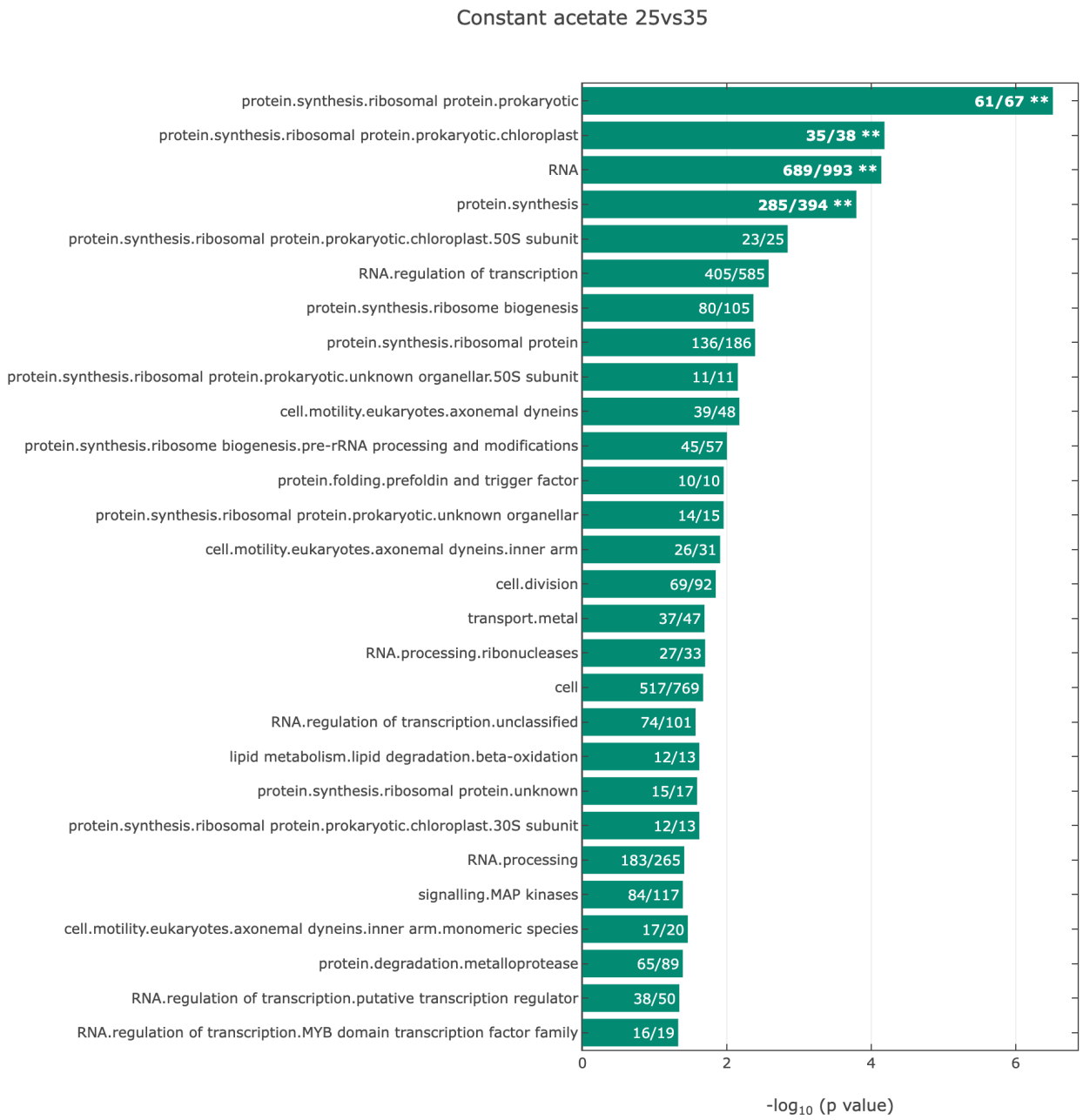

Supplemental Fig. 5D

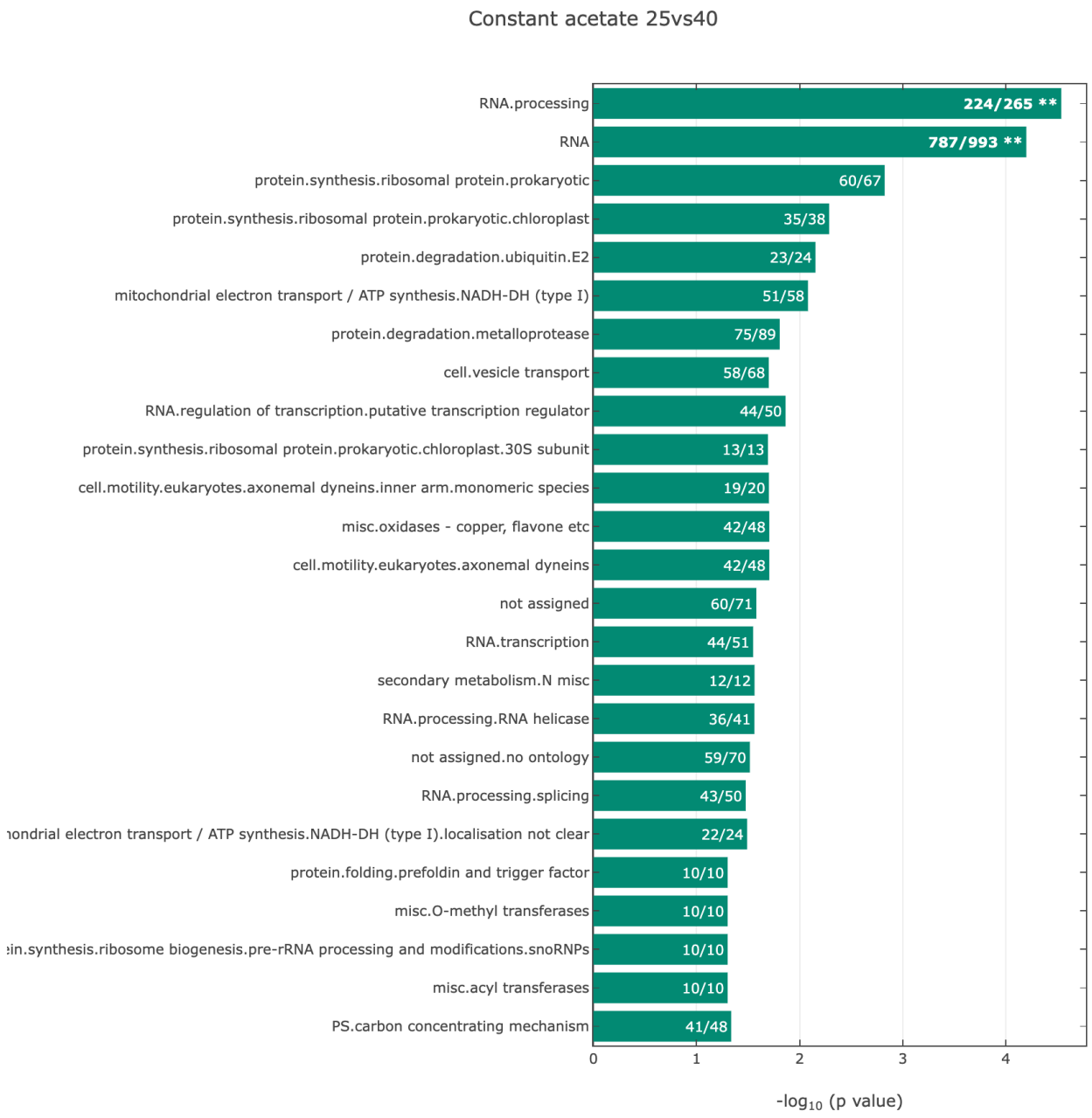

Supplemental Fig. 5E

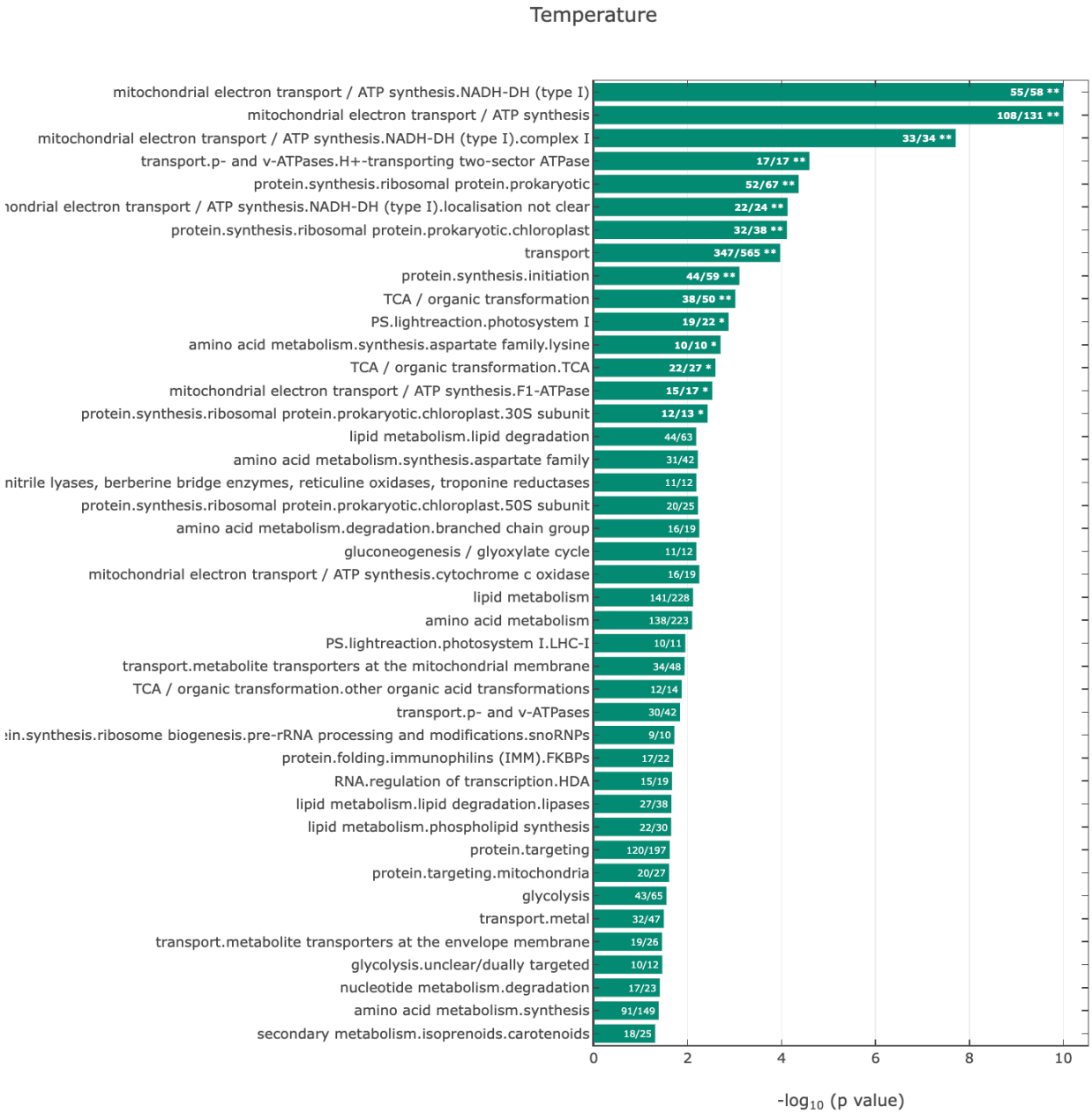

Supplemental Fig. 5F

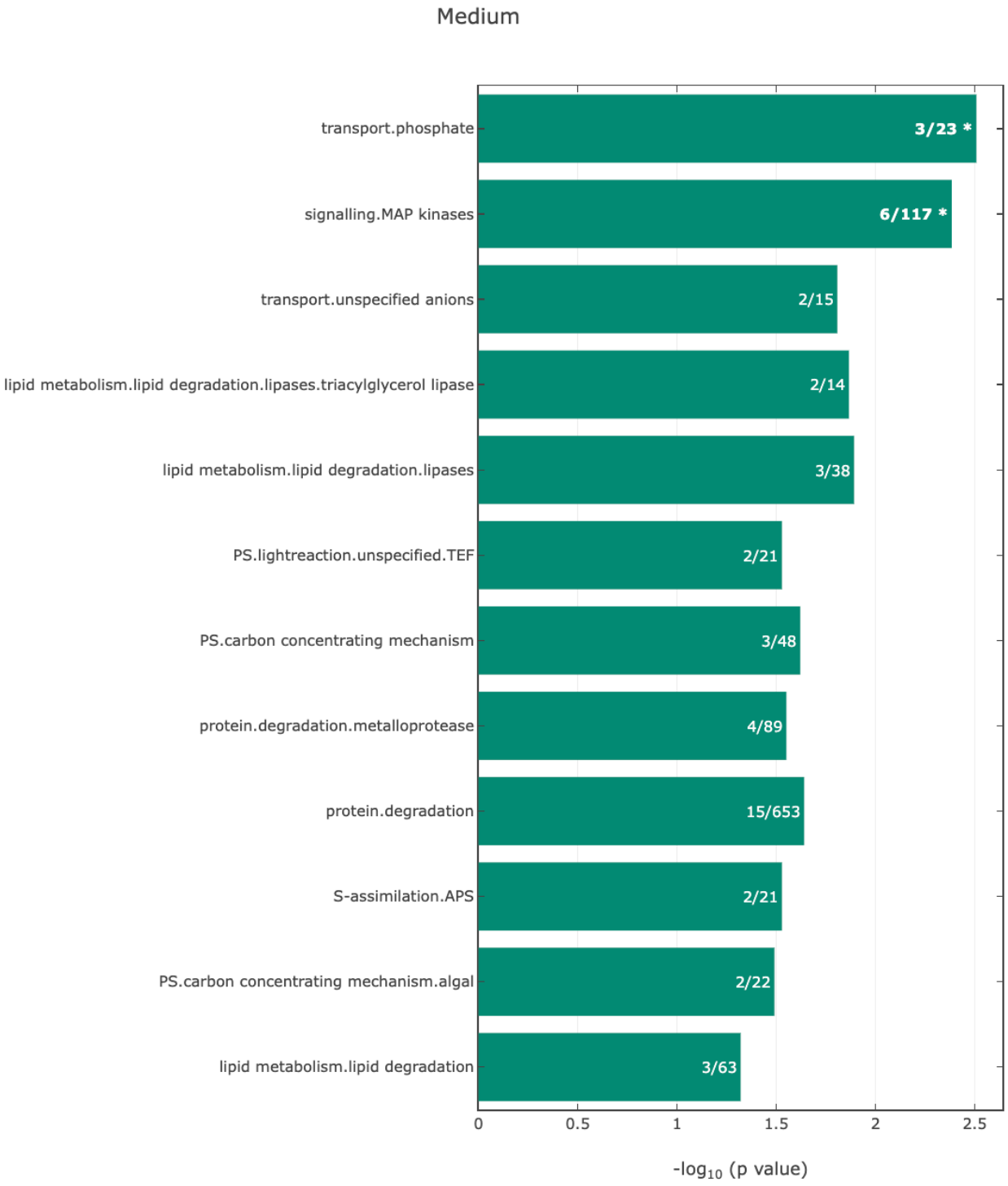

Supplemental Fig. 5G

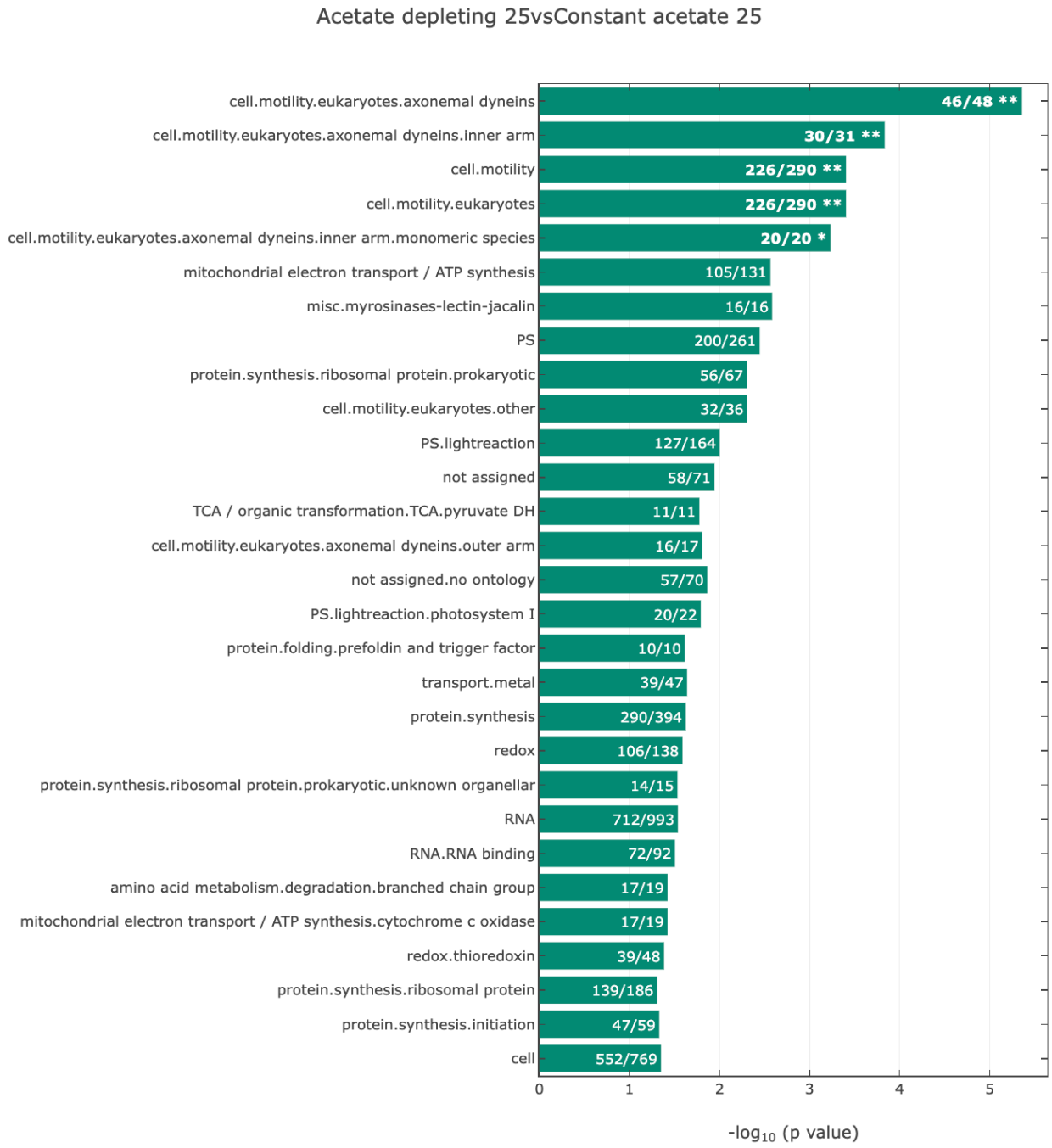

Supplemental Fig. 5. MapMan ontology enrichment revealed differentially regulated biological processes under different conditions. Ontology enrichment was performed for transcripts with significantly differential expression in the indicated comparisons using the extended MapMan ontology. The p values were calculated using a hypergeometric test. All functional sets with a p value less than 0.05 and more than 10 annotated transcripts

are shown. The ratio at the end of each bar indicates the number of significant transcripts between the two compared conditions vs detected transcripts in our RNA-seq data contained in the respective function bin. Multiple testing correction was performed by Benjamini & Hochberg FDR, * FDR < 0.1, ** FDR < 0.05. The bars are sorted based on the FDR p values, from top to bottom, from the small to big FDR values. **(A)** acetate-depleting 25°C vs acetate-depleting 35°C; **(B)** acetate-depleting 25°C vs acetate-depleting 40°C; **(C)** constant-acetate 25°C vs constant-acetate 35°C; **(D)** constant-acetate 25°C vs constant-acetate 40°C; **(E)** temperature effect: (constant-acetate 35°C and acetate-depleting 35°C) vs (constant-acetate 40°C and acetate-depleting 40°C); **(F)** medium effect: (constant-acetate 35°C and constant-acetate 40°C) vs (acetate-depleting 35°C and acetate-depleting 40°C); **(G)** acetate-depleting 25°C vs constant-acetate 25°C. See interactive figures and detailed enrichment analysis in Supplemental Dataset 3.

Supplemental Fig. 6

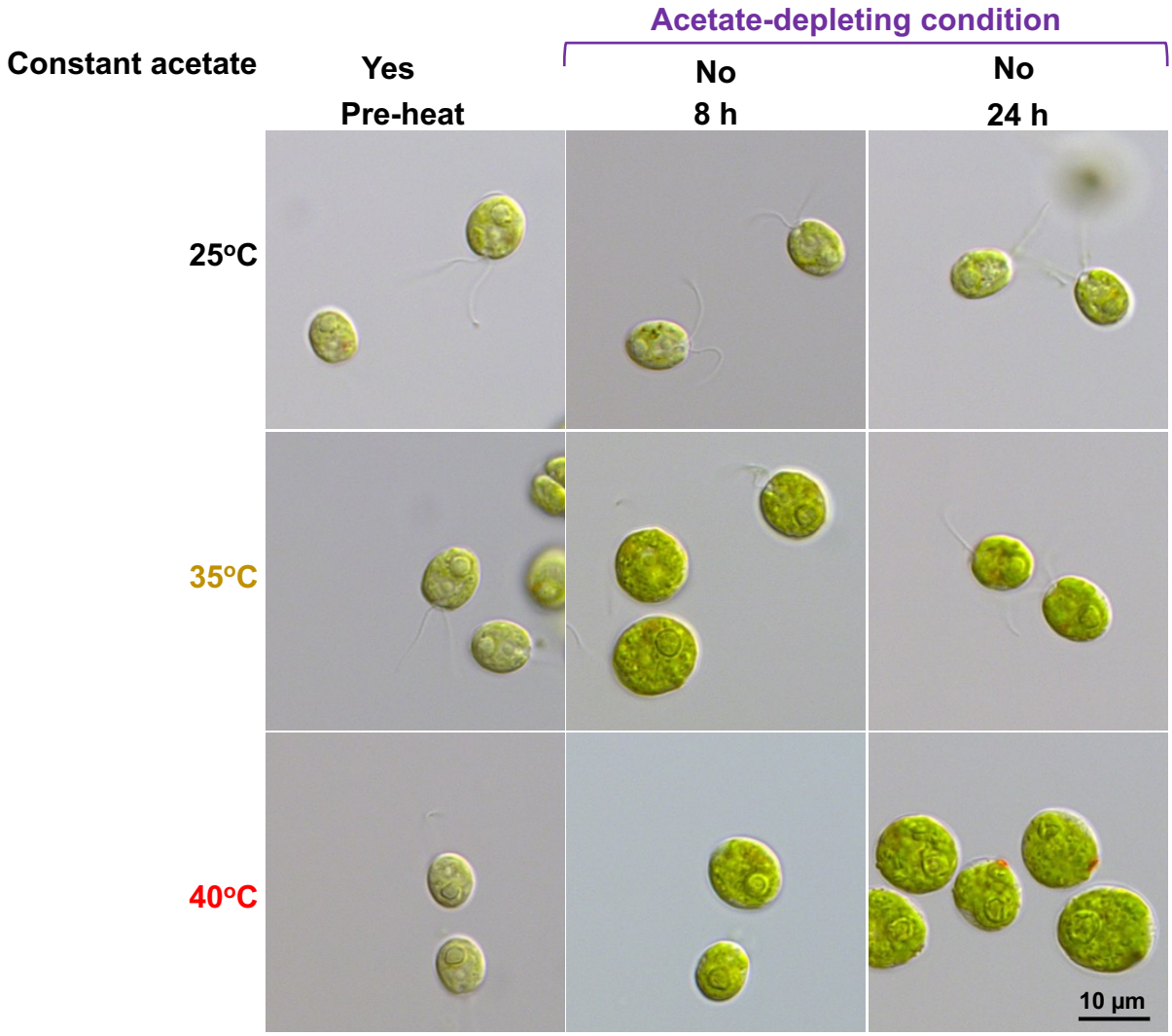

Supplemental Fig. 6. Chlamydomonas cells have different morphologies at different temperatures under the acetate-depleting condition. Light microscopic images of Chlamydomonas cells under the acetate-depleting condition. Images shown are representative results from at least three biological replicates. The algal cultivation and heat treatments were the same as in Fig. 1B.